NOTICE

The quality of this microform is heavily dependent upon the quality of the original thesis submitted for microfilming. Every effort has been made to ensure the highest quality of reproduction possible.

If pages are missing, contact the university which granted the degree.

Some pages may have indistinct print especially if the original pages were typed with a poor typewriter ribbon or if the university sent us an inferior photocopy.

Reproduction in full or in part of this microform is governed by the Canadian Copyright Act, R.S.C. 1970, c. C-30, and subsequent amendments.

AVIS

La qualité de cette microforme dépend grandement de la qualité de la thèse soumise au microfilmage. Nous avons tout fait pour assurer une qualité supérieure de reproduction.

S'il manque des pages, veuillez communiquer avec l'université qui a conféré le grade.

La qualité d'impression de certaines pages peut laisser à désirer, surtout si les pages originales ont été dactylographiées à l'aide d'un ruban usé ou si l'université nous a fait parvenir une photocopie de qualité inférieure.

La reproduction, même partielle, de cette microforme est soumise à la Loi canadienne sur le droit d'auteur, SRC 1970, c. C-30, et ses amendements subséquents.

The Structure Assignment of Isomeric Gas Phase Organic Ions and Neutrals

by

Marcia C. Blanchette

A Thesis
Presented to the University of Ottawa
in fulfillment of the
thesis requirement for the degree of
Master in Science
in
the Department of Chemistry
University of Ottawa

May 1987

ISBN 0-315-53767-1

to larry

Abstract

Structural isomerism in gas phase ions has received steadily increasing attention during the past ten years, and the gas phase chemistry of a number of stable ions of both familiar and unexpected structures has been studied. The two chief experimental methods currently available for structure investigations are (i) thermochemistry and (ii) dissociation characteristics. Advances in the latter field have considerably increased its applicability, investigation of the structure and stability of neutrals as well as ions is now possible.

The $[C_2H_3O_2]^+$ system has been thoroughly investigated via experiment and it is believed that five distinct isomeric species have been identified; the hydroxy-substituted oxiranyl (2) and acetyl (4) cations, $CH_2(O)CH-C^+-OH$ and $HO-CH_2-C^+=O$, the methoxycarbonyl cation (8), $CH_3O-C^+=O$, protonated glyoxal (10), $HO-C^+H-C(=O)H$, and the ion proposed to be generated by dissociative $CH_3\cdot$ loss from ethyl formate (11), $H_2C^+-O-C(=O)H$. For four of these isomeric species, experimental heats of formation have also been obtained; $\Delta Hf°[2]=590$ kJ mol^{-1}, $\Delta Hf°[4]=594$ kJ mol^{-1}, $\Delta Hf°[8]=527$ kJ mol^{-1} and $\Delta Hf°[11]\leq 602$ kJ mol^{-1}. These values have been compared to those obtained from high level ab initio molecular orbital theory calculations.

A thorough mass spectrometric investigation of the $[C_2H_5X]$ system is also presented. The unconventional isomers of the ethyl halide molecular ions, members of a class of ions in which the formal charge bearing site is separated from the radical site, have been found to be stable. The characteristic dissociations of these ions; $CH_3\overset{+}{X}CH_2\cdot$ (for X=Cl,Br), $CH_3\dot{C}H\overset{+}{X}H$ (for X=Cl,Br) and $\cdot CH_2CH_2\overset{+}{X}H$ (for X=F,Cl,Br), have been discussed in terms of their proposed structures. The latter species is presented for the first time.

An investigation of the neutral counterparts of these unconventional isomers has been carried out via the recently introduced dissociation technique of Neutralization-Reionization mass spectrometry. The neutral, $CH_3\overset{+-}{X}CH_2$, is proposed to be unstable. Contrary to expectations, the experimental results indicate that the unconventional cationic isomers $CH_3\dot{C}H\overset{+}{X}H$ and $\dot{C}H_2CH_2\overset{+}{X}H$, have neutral counterparts of significant stability.

Contents

FIGURES

TABLES

Chapter 1

INTRODUCTION AND FOCUS

1.1 Introduction

The basis of mass spectroscopy is the production of ions from neutral compounds and the examination of the subsequent decomposition of these ions. The techniques now available in this field however, have greatly expanded upon this basic function. Perhaps more than those of some disciplines, the roots of gas phase ion chemistry are found in technique development. It is only three decades since the usefulness of the mass spectrometer for the structural elucidation of organic compounds was fully recognised. The steadily increasing number of mass spectrometers available for research and their constant modifications have led to a rapid expansion of this relatively new discipline. Not only can the structure and thermochemistry of fast, isolated ions and their isomeric counterparts be probed, but recent advances have also enabled the generation and structural elucidation of certain novel neutral species.

As its name implies, a mass spectrometer measures mass (or strictly speaking mass-to-charge ratio) and gives no *direct* information on ion structures. In mass spectrometric terms, structure is defined as the arrangement of atoms only, how they are bound together in the ion or neutral, and not to the bond lengths and angles between atoms. Without further analysis of 'mass' selected ions little more than their elemental composition is available. For ions containing more than a very few atoms the number of possible corresponding isomeric structures makes positive structure assignment less than straight forward, and further analysis is required.

Structures are based on the indirect evidence of thermochemical arguments, decomposition products, and isotopic labelling. The experimentally obtained heats of formation and barriers to dissociation can reflect the stability, and characteristic pathways to dissociation of the ion.

These values may be compared with experimental values from similar systems or with those calculated theoretically. With the increasing precision of ab initio molecular orbital theory calculations, the latter comparisons have been given steadily increasing weight. The observed decomposition products, structure characteristic fragments of the precursor, may be considered on their own merits, or by comparison with the fragmentation pattern of other, reference, precursors. In either case, the analysis of isotopically labelled derivatives can also serve to underline the proposed structure.

Such interpretations for the structural assignment of gas-phase species may be considered little more than an exercise in curiosity. However, concrete structure assignment is necessary to properly assign heats of formation and to devise reaction mechanisms for gas-phase ions. In the early days of ion chemistry, structures and reaction mechanisms were proposed using analogies from condensed phase organic chemistry. Such analogies have been found to be unjustified; whole classes of ions, having no neutral counterpart, have been found to be stable species in the gas phase and thermodynamic properties of organic ions do not follow the same trends as for neutral organic molecules. The generation of a solid reference base, including the structure and thermochemistry of common and not so common gas-phase ions and neutrals, is essential for the continued expansion of the field of gas-phase ion chemistry.

1.2 The Focus

The focus of this thesis has been on the generation and structure elucidation of gas-phase isomeric species, via the wide and varied dissociative mass spectrometric techniques now available. Proposed structures, both conventional and unconventional, have been assigned based on the thermochemistry available, both experimental and theoretical, and the dissociative processes observed, for the ions and their labelled counterparts. The experimental chapters, 5 and 6, are preceded by three chapters which involve a basic history and introduction to mass spectrometry, an explanation of the thermochemical and dissociative

techniques utilized, and the applicability of these techniques to the question of structure.

Chapter 2 gives a brief outline of some of the major turning points in the history of mass spectrometry, and its advancement alongside that of the accompanying technology. The mass spectrometers used in this work, the VG ZAB-2F and the GEC-AEI MS-902S, have been described. Also described is the electron energy selector mass spectrometer, with which a number of ionization and appearance energies have been measured. Finally, some concepts which are basic to the understanding of mass spectra, have been introduced.

Chapter 3 introduces the thermochemical and dissociative techniques and the relevant underlying theory and assumptions. Over the last few years the latter has grown in scope to include, collision induced dissociative ionization, CIDI, and neutralization-reionization mass spectrometry, NRMS, along with the more established techniques of metastable ion, MI, collision induced dissociation, CID, and charge stripping, CS, mass spectra. These newer techniques have enabled the analysis of neutrals as well as ionic species via mass spectrometry.

The applicability of these techniques to the structural elucidation of isomeric gas-phase ionic species is discussed in chapter 4. Appended to chapter 4 is a brief summary of the dissociative mass spectrometric techniques, which may be quickly referred to when necessary.

Chapter 5 deals with the investigation of the $[C_2H_3O_2]^+$ isomeric system. Five unique isomeric species are proposed to have been generated. Assignment of their structures has been made on the basis of their metastable and collisionally induced dissociation mass spectra, and very recently published high level ab initio molecular orbital calculations. Comparison of the experimentally obtained heats of formation of these ions and the theoretically calculated threshold energies while not in very close agreement, are nevertheless, consistent.

In chapter 6 a thorough investigation of the isomeric radical cations of the ethylhalides is presented. The characteristic dissociations of these

ionic isomers are discussed in terms of their proposed structures, and their respective thermochemistry. These stable isomers are of unconventional structure, members of a class of ions in which the formal charge bearing site is separated from the radical site. Investigation of their neutral counterparts, via neutralization-reionization mass spectrometry has led to surprising results. Contrary to expectations, the experimental results indicate that not all the unconventional cationic isomers have unstable neutral counterparts.

Chapter 2

THE MASS SPECTROMETER

2.1 History

The advances in chemistry may be considered to be directly linked with the invention and technological improvements of instrumentation. A potent example of this is in the area of mass spectrometry. The knowledge gained from this analytical/research technique, based on concepts introduced around the turn of this century, has been paced by the parallel improvements in such areas as vacuum and electronics technology as well as the now indispensible computer.

The point by point history will not be dealt with here (a good overview may be found in (1)), but a few of the major turning points in the development of mass spectrometry will be presented.

The discovery of positively charged gaseous entities was made by E. Goldstein (2) in 1886. By 1902, W. Wien had shown that these rays of positive electrical charge could be deflected in a magnetic field (3). Upon the introduction of polyatomic molecules into the discharge tube of what was termed a parabola mass spectrograph, which incorporated a magnetic field, Thomson noted the formation of many parabolas, revealing the formation of a *variety* of positively charged fragments. These parabolas were recorded on a photographic plate, but due to differing sensitivities for the various ions, quantitative measurements were not possible. Therefore Thomson replaced his plate with a Wilson tilted electroscope and Faraday cylinder. By changing the magnetic field, he was then able to obtain a plot of the ion current as a function of the mass-to-charge (m/z) ratio. Thus it is Thomson who must be credited with the invention of the mass spectrometer although it was not until 1920 that F.W. Aston first introduced the term "mass spectrum".

By 1920 the early instruments were capable (although not simultaneously) of three types of measurements; precise mass determinations, measurement of relative ion abundances, and electron impact studies. The latter two are of most interest here. C.T. Knipp, in 1911, and later A.J. Dempster (4), in 1918, reported the construction of an electron bombardment ion source mass spectrometer, suitable, not for precise mass measurements, but for measuring the relative abundances of the ionic species and for studying electron impact processes in gases. Dempster based his construction (4) on the idea that a magnetic field alone would be sufficient to carry out a mass analysis if all the ions formed in the ion source possessed the same kinetic energy. He obtained such ions by causing them to be accelerated through a large, specific potential difference. The first apparatus constructed by Dempster *(fig 2.1)*, had a magnetic field of about 3000 gauss which was held constant. The mass spectrum was swept out by varying the accelerating potential (500-1800 electron volts), and the mass spectrum was therefore a plot of ion current versus accelerating potential. The relationship between the accelerating potential, $V_{acc.}$, and the mass, m, was given by;

$$m/z = B^2r^2/2V_{acc.} \qquad \textit{eq.(2.1)}$$

where B refers to the magnetic field strength, and r to the radius of curvature of the charged particle's path.

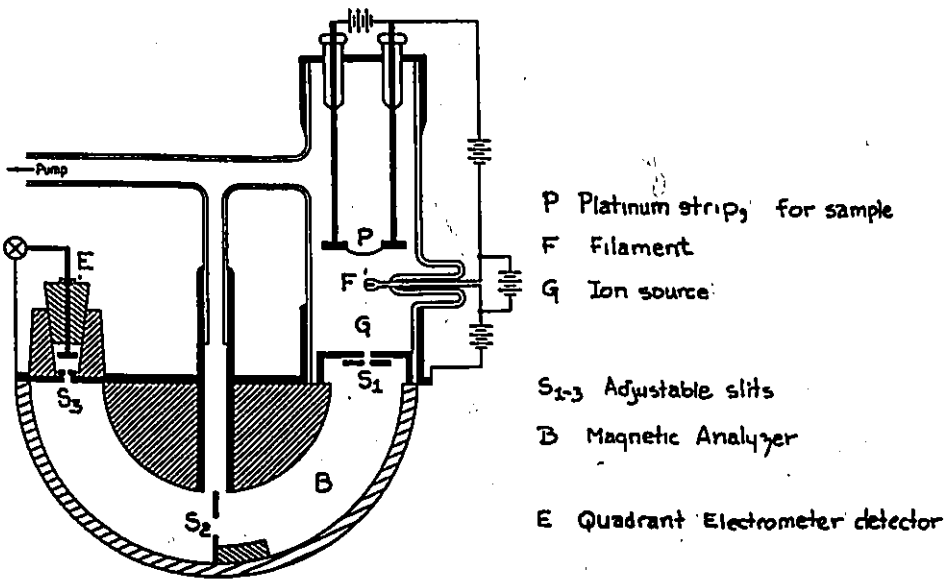

Figure 2.1 Dempster's first mass spectrometer

With the electronic developments of the 1920's and 1930's, more sophisticated equipment could be constructed. The parallel improvement in vacuum and electronics technology led eventually to an increasing interest in the field of mass spectrometry, with a fuller realization of its potentialities.

The first purely chemical application of mass spectrometry appears to have been made by Conrad in 1930 (5). By 1930 it was apparent that transitions between one electronic state and another, effected by electron impact, followed what has today become known as the Franck-Condon principle (6,7). Yet it was not until 1942 that the first commercial instrument, a 180° Dempster geometry unit, was built by Consolidated Engineering Corporation. The subsequent developments and discoveries that laid the ground work for mass spectrometry as a tool for the study of the structures and gas-phase ionic reaction mechanisms of organic compounds, took place chiefly in the laboratories of the petroleum industry. It was during this early period that the mass spectrometer was rightly characterized as a 'machine that almost doesn't quite work' (8). The manual for this instrument advised leaving a dime for the gremlin who was prone to short the high voltage.

The technological advances since then have not only allowed the general use of much higher ion acceleration voltages (typically 8-10 keV), but the electromagnets now available allow mass spectra to be generated by very quickly and successively sweeping the magnetic field. Also, with the most recent modifications, the incorporation of collision cells and ion beam deflectors, still wider applications have become available. The nomenclature has also advanced, for example in the eighth CEC users meeting in 1950 the terms 'pushers' and 'catchers' were formally replaced by 'repeller' and 'anode'.

Advances in mass spectrometry have also been closely linked to those of the computer, now an indispensable part of an analytical mass spectrometer. The first computer specifically designed for use in a mass spectrometer followed quickly on the heels of the first commercial analytical mass spectrometer. An analogue computer which solved a set of 12 simultaneous linear equations and reduced the clerical time per sample

by half (to 25 minutes) was installed in 1947 at the Whiting refinery in Indiana. Some seven years later the installation of the IBM Card-Programmed Calculator further reduced the calculating time to about three minutes. At present the capabilities of analytical mass spectrometers are, more often than not, given in terms of the power of the accompanying computer system.

Thus improved instrumentation has advanced the application of the mass spectrometer to a wide range of analytical and research problems, applications which Thomson had anticipated or recognised so many years before, when he suggested its use for the determination of atomic and molecular weights.

2.2 Instrument Description

For this thesis, three types of mass spectrometers have been used and a brief account of all three will be given. However, in the simplest terms, all mass spectrometers perform the same three essential functions; the formation and acceleration of ionic species, the separation of these ions with respect to mass and/or kinetic energy, and then their subsequent detection. Emphasis will be placed on the Vacuum Generators ZAB-2F, a reversed geometry, double focussing instrument, with which the majority of the experimental work was performed.

2.2.I VG ZAB-2F

Figure 2.2 is a schematic diagram showing the salient features of the Vacuum Generators ZAB-2F. The geometry is said to be reversed because the magnetic sector is placed before the electric sector. Forward geometry instruments are good for exact mass measurements, whereas those of reversed geometry are better suited for the investigation of ion dissociation mechanisms. The entire instrument is kept at a high vacuum of $< 10^{-8}$ torr, and where sample or collision gases are introduced to higher pressures, maximum differential pumping is utilized. Such reduced pressures are essential for back-ground interferences to be kept to a

minimum, and for the ions produced to have a sufficiently large mean free path to be considered lone entities (which thus avoid unwanted collisional relaxation or excitation). The sample is introduced into the ion source directly or indirectly by the appropriate inlet system. The septum injection inlet allows volatile liquids to diffuse slowly from a heated reservoir into the source, it is however not recommended for experiments requiring constant pressures.

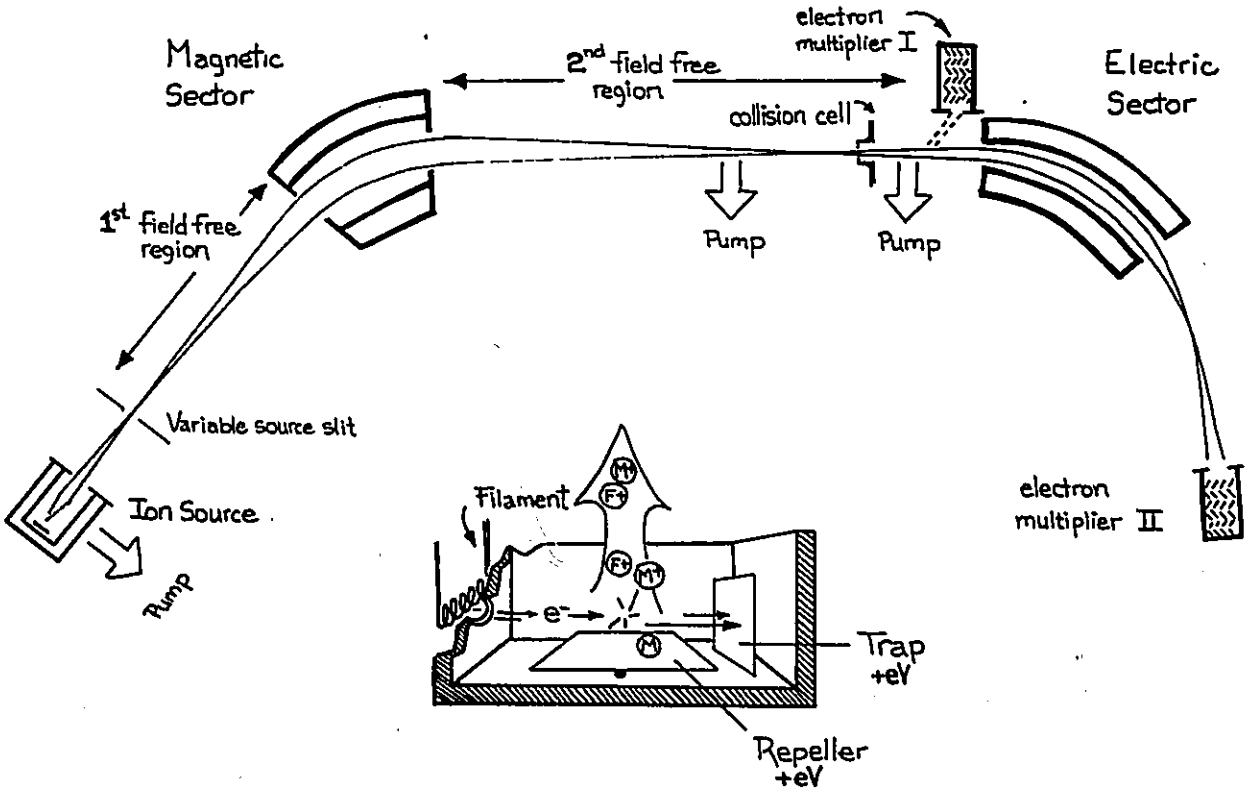

Figure 2.2 Schematic diagram of the unmodified Vacuum Generators ZAB-2F mass spectrometer; inset, the ion source block.

Constant sample pressures are better maintained by the inlet system involving a variable leak and capillary induced pressure gradient, whereby gases, liquids and volatile solids may be introduced. For non-volatile compounds, introduction into the source may be done directly by placing the sample in a glass ampule fixed to a probe tip which is inserted into the source housing. Finally, gaseous samples may be introduced directly into the ion source via gas lines attached to the ion source block.

Ionization of the sample molecules is achieved by passing a beam of electrons, emitted by a wire filament, across the ion source to the anode or trap. The energy (velocity) of the electron beam can be adjusted, but is usually ~70eV. The term -low electron energy- refers to a minimal electron energy with respect to an acceptable signal to noise ratio, and is necessarily arbitrary due to the relatively wide spread of electron energies emitted by the hot filament. A repeller plate having a small positive/negative potential pushes the cations/anions formed towards the source exit. As they leave, all ions will experience a large potential gradient, the accelerating voltage, V_{acc}, which is typically 8 keV. Thus all source generated ions with mass m and charge z will leave carrying the same kinetic energy of $z \cdot V_{acc}$, regardless of their mass. Thus,

$$\tfrac{1}{2}mv^2 = z \cdot V_{acc} \qquad \textit{eq. (2.2)}$$

where z=ne, or for singly charged ions z=e, and v is the velocity of the ion. For simplicity, unless otherwise stated, n is assumed to be one.

With this acquired kinetic energy, the ions travel through the first field free region towards the magnetic sector and are collimated by a series of paired focussing plates near the source exit. An electromagnet produces a magnetic field, B, and the ions experiencing this will follow a circular path, with radius r, through the magnet, given by *eq. (2.3)*.

$$mv^2/r = BzV \quad \text{or} \quad B = mv/zr \qquad \textit{eq. (2.3)}$$

Thus the magnet is a *momentum* analyzer, although it is most often referred to as a mass analyzer. For those ions generated in the source, *eq. (2.2)* may be substituted into *eq. (2.3)* to obtain;

$$m/z = (B^2r^2)/2V_{acc} \qquad \textit{eq. (2.4)}$$

Thus by varying B (via the current through the magnet coils), and maintaining a constant accelerating voltage, ions can be selected according to their mass to charge ratio, m/z. For an analysis of the source generated ions, a single focussing mass spectrum of the sample may be made by scanning the magnet current and detecting the relative intensities with respect to the mass-to-charge ratios with the first electron multiplier (*fig. 2.2*).

The area between the magnetic and electric sectors is referred to as the second field free region, and in the case of the VG ZAB-2F referred to here, it contains not only the standard original collision cell as supplied by the manufacturer, but also a second collision cell and an ion beam deflector electrode placed as depicted in *figure 2.3*. The newly installed collision cell is referred to as cell 1 since it is the first cell that the ion beam encounters.

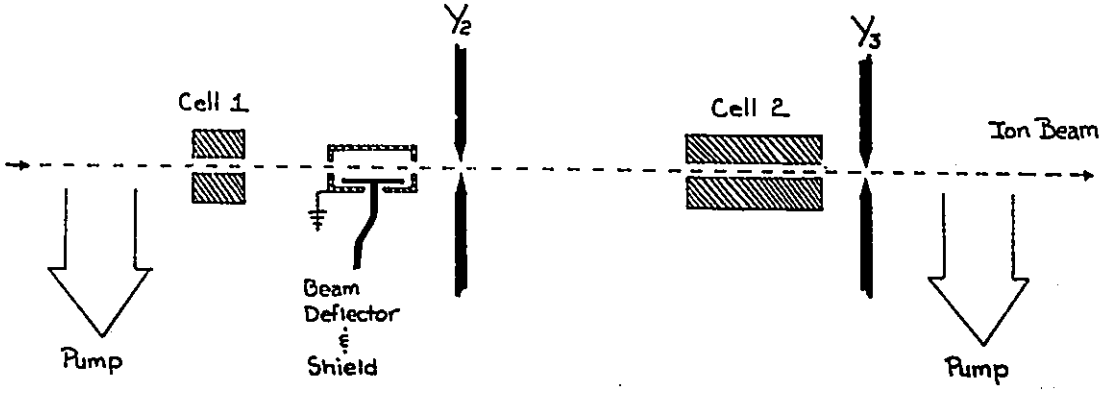

Figure 2.3 Schematic detail of the second field-free region of the modified VG ZAB-2F mass spectrometer.

Likewise the original cell is labelled cell 2. The collision gas cell 1 is ~10mm long, and was installed without moving the original cell (some 20mm long). The two cells were spaced ~10cm apart, center-to-center (9). Collision gas can be independently introduced to both cells. Pressures for the two cells are measured by the two ionization gauges mounted above the two diffusion pumps which are symmetrically located just upstream and downstream of the two cells. These pumps ensure a constant gas pressure within the cells and a good pressure gradient without. Both cells are electrically isolated and so may be floated at positive or negative potentials. The application of such voltages to cell 1 and cell 2 allow the separation of those processes occurring within and outside each cell and is illustrated in detail in the following chapter, in *figure 3.9*. The deflector electrode was installed midway between the two cells. Originally a simple, chargeable plate some 5mm from the center of the ion beam, the deflector plate is now enclosed in a grounded metal box. When charged, the electrode will deflect all ions out of the beam path, allowing only neutral species to enter cell 2. These modifications have radically increased the versatility of the instrument, allowing such experiments as Collision Induced Dissociative Ionization, CIDI, and

Neutralization-Reionization Mass Spectrometry, NRMS (which will be introduced and discussed at length in the next chapter), to be carried out. For a detailed description of these additions refer to (9).

The second sector, the electrostatic analyzer or ESA, consists of two curved plates (of radius R), between which an electric field, E, can be generated by applying a potential to them. Transmission of an ion through the ESA will occur when the centrifugal force on that ion equals the electric force;

$$mv^2/R = zE \qquad \textit{eq. (2.5)}$$

The electric sector, therefore, analyses with respect to the kinetic energy of an ion, and substituting in *eq. (2.2)*, leads to *eq. (2.6)*.

$$E = (2V_{acc}\ z)/R \qquad \textit{eq. (2.6)}$$

Thus for source generated ions, setting the electric field to match the accelerating potential ensures that all the ions mass selected by the magnet will be transmitted through the ESA. Detection of the ions after the electric sector, set to transmit ions at $z \cdot V_{acc}$, while scanning the magnetic field, will result in the double focussing mass spectrum of the sample introduced into the source. The advantage of a double focussing mass spectrometer is the added mass resolution acquired from the ESA, which focusses the small spread in kinetic energies of the ions. Further increases in mass and energy resolution are obtainable by narrowing the Y focussing slits, as discussed in chapter 3, however this also reduces the transmitted flux of ions.

The detectors, located before and after the ESA, are off-axis electron multipliers. The incoming ion beam is deflected onto a negatively charged conversion dynode, which liberates electrons. These in turn are accelerated across to the electron multiplier. The signal is then amplified via a series of electron emitting plates. For a review of the unmodified instrument refer to (10).

2.2.II GEC-AEI MS-902S

The MS-902S is a forward geometry mass spectrometer, that is, the electric sector precedes the magnet *(fig. 2.4)*. The modes of sample

introduction, ionization, and selection may be considered to be equivalent to those of the ZAB-2F. The ifferent ion source construction however results in a slightly shorter source residence time. Analysis of a system over varying time ranges, such as the times applicable to the ZAB-2F and the MS-902S, may yield valuable kinetic information (11). As well, this forward geometry instrument is able to measure the appearance energy (AE) of metastably generated ions produced in the first field free region. Ions are detected by a Daly fluorescence detector.

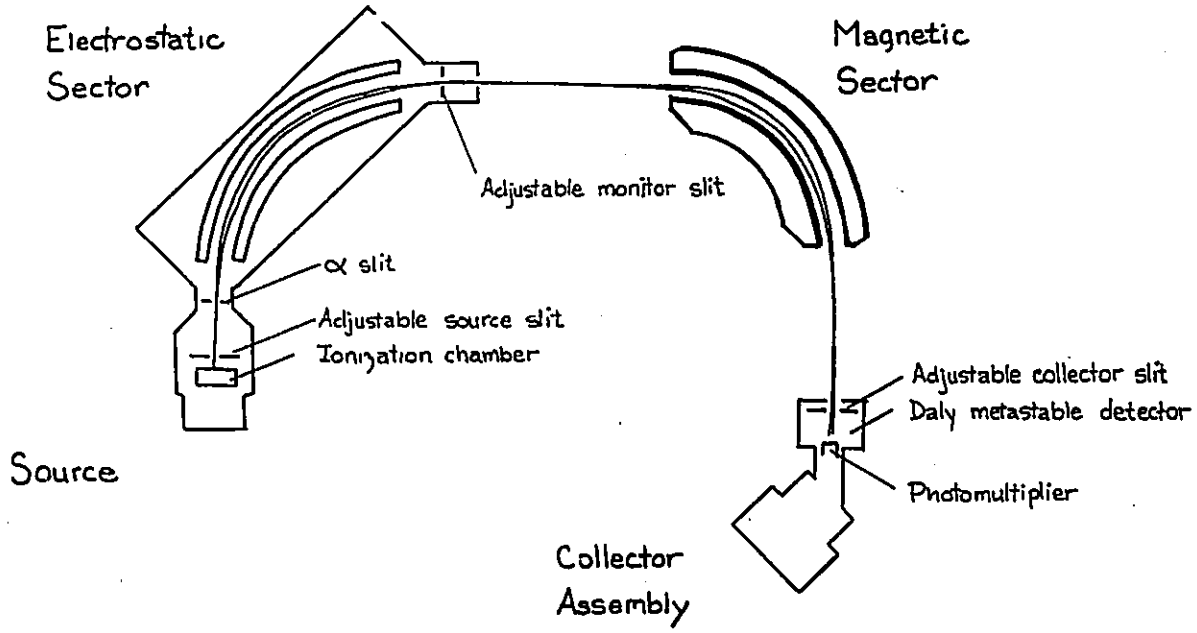

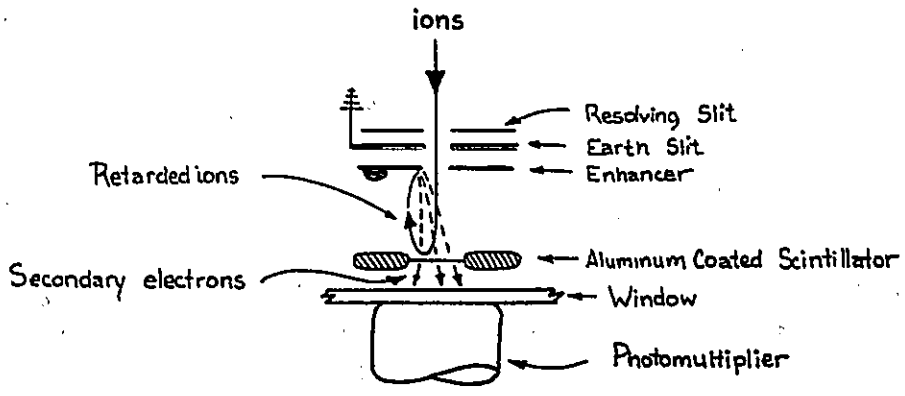

Figure 2.4 Schematic diagram, upper, representing the Kratos-AEI MS-902S mass spectrometer, equipped with a Daly fluorescence metastable ion detector, lower.

The advantage of this detector *(fig. 2.4)*, is that metastable ion signals may be enhanced, relative to source generated species.

2.2.III Electron Energy Selector Mass Spectrometer

The electrostatic energy selector quadrupole mass spectrometer, designed and built by F.P. Lossing and co-workers (12), has allowed the accurate measurement of adiabatic ionization and appearance energies (IE and AE). Simply, it contains an electron gun, a two stage hemispherical electron energy selector, a collimator, and a reaction chamber with an electron trap and ion collector *(fig 2.5)*, and final mass analysis is performed by a quadrupole mass analyzer.

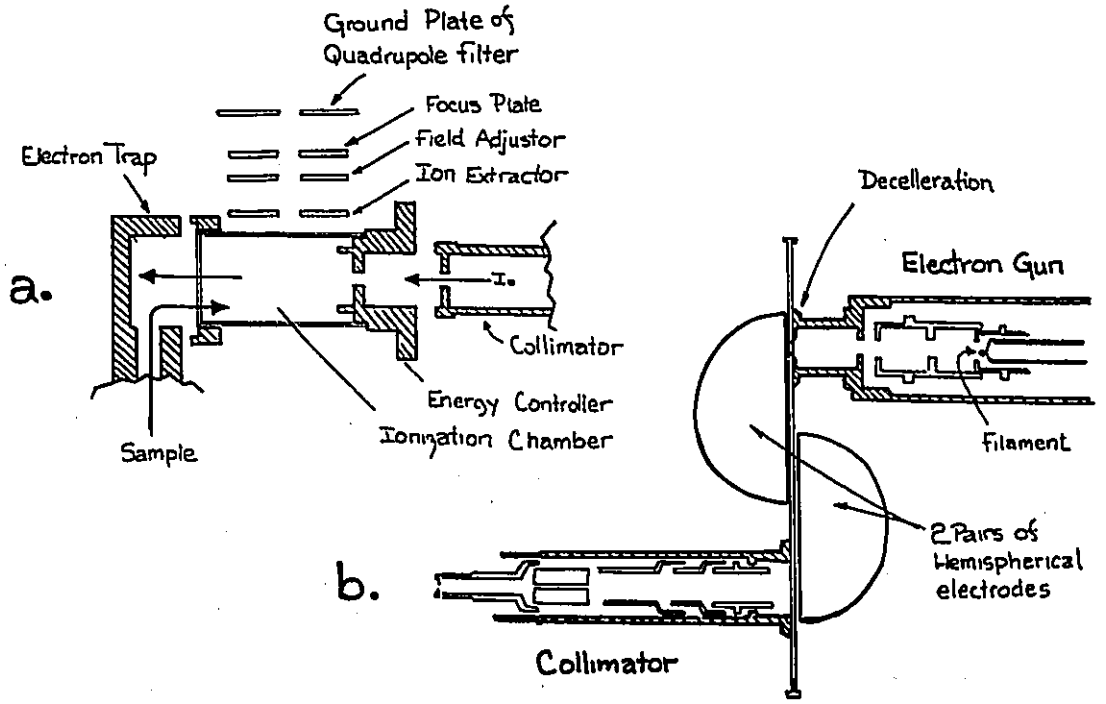

Figure 2.5 Schematic of a) the reaction chamber, and b) the two stage electron energy selector of the electron energy selector mass spectrometer.

The electron gun produces an essentially monoenergetic beam of electrons which is focussed through double hemispherical electron energy selector. The auxiliary electrode after the collimating lens is used to vary the energy of the electron beam from 5 to 30eV, at constant electric sector conditions. The lifetime of ions having reached the mass spectrometer's

detector is considerable, ~200μs. A calibration procedure utilizing H_2O as a reference compound corrects for the contact voltages within the system, and the adiabatic AE and IE values may be obtained with an accuracy of ±0.05eV.

2.3 Some Basic Concepts

Ionization of molecules achieved by impact with ~70eV electrons produces molecular ions having a wide range of internal energies. The majority of the ions formed will have excess internal energies of roughly 0-10eV, while only a small fraction of molecular ions will be formed with internal energies in excess of 10eV. This accounts for the fact that Electron Impact (EI) spectra change little as the electron energies are raised above 20eV. In section II only source generated molecular ions, which proceeded without dissociation through the ertire spectrometer to the detector, were discussed. Such ions are called 'stable' in mass spectrometric terms, because they contain insufficient excess internal energy to undergo dissociation in the time required to traverse the instrument, typically 20 μs. 'Unstable' would be the term applied to those molecular ions which are generated with sufficient excess internal energies to undergo dissociation inside the source *(figure 2.6)*.

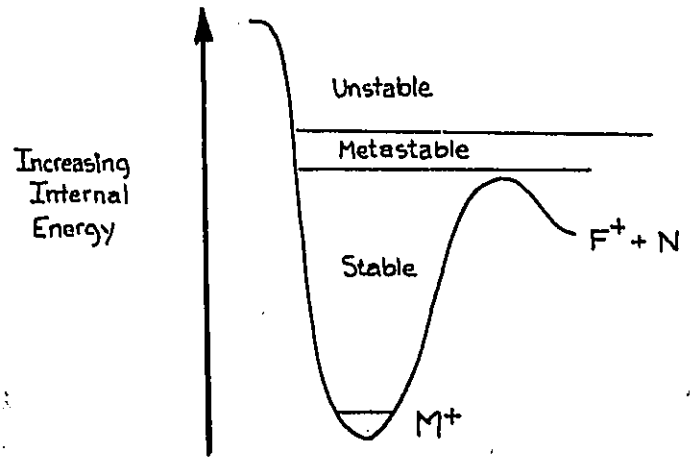

Figure 2.6 The stability of a molecular ion, $M^{+\cdot}$, as a function of its internal energy.

The excess energy may be sufficiently great to cause the newly formed molecular ions to dissociate into fragments which themselves may have enough energy to fragment further etc. Thus within the source, a complex mixture of ionic fragments will be formed through the competitive and consecutive reactions induced by the high internal energies given to the sample molecules. The fragments collectively make up the electron impact, (EI), mass spectrum of the molecule introduced into the source. (The spectrum is representative, but not always obviously characteristic of that molecule's neutral structure, for at these higher internal energies, complex rearrangements as well as dissociation may take place.) Source generated ions which undergo decomposition *in flight* between the source exit and the final detector are termed 'metastable'. These ions possess the narrow range of internal energies which correspond to dissociation rate constants specific for the time of flight between source exit and detector. This is simply represented in a k(E) versus E curve, *(fig. 2.7)*, illustrating the rate of dissociation as a function of excess internal energy.

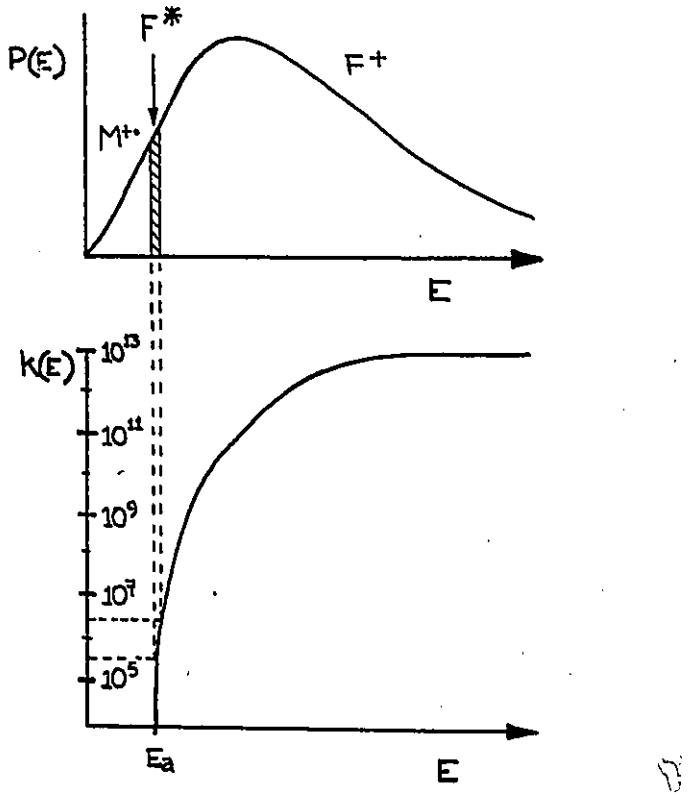

Figure 2.7 Schematic k(E) versus E curve, (lower part), and internal energy distribution, (upper part), where $M^{+\cdot}$ are 'stable' species, F^{*}, fragments from metastable $M^{+\cdot}$ ions, and F^{+}, fragments generated from 'unstable' $M^{+\cdot}$ ions.

2.3.I k(E) versus E curves

Near threshold, the rate constant, k, of a given decomposition process rises rapidly with increasing internal energy and levels off at higher energies, finally reaching a constant value at highest energies. This is to be expected because the shortest decomposition time of an excited ion should be of the order of one vibrational period, $\sim 10^{-13}$-10^{-14} s. Metastable ions decompose predominantly but not exclusively with rate constants between 5×10^5 and 5×10^6 s^{-1}, stable ions at lower rates, and nonstable, fragment producing ions at higher rates. Thus the terms 'stable', 'unstable', or 'metastable', are defined by the time scale of a given instrument, wherein a range of rate constants are involved in fragmentations. The time-scale of events applicable to the VG ZAB-2F mass spectrometer for a typical species of m/z=100 at 8keV accelerating voltage, is fully outlined in *figure 2.8* below.

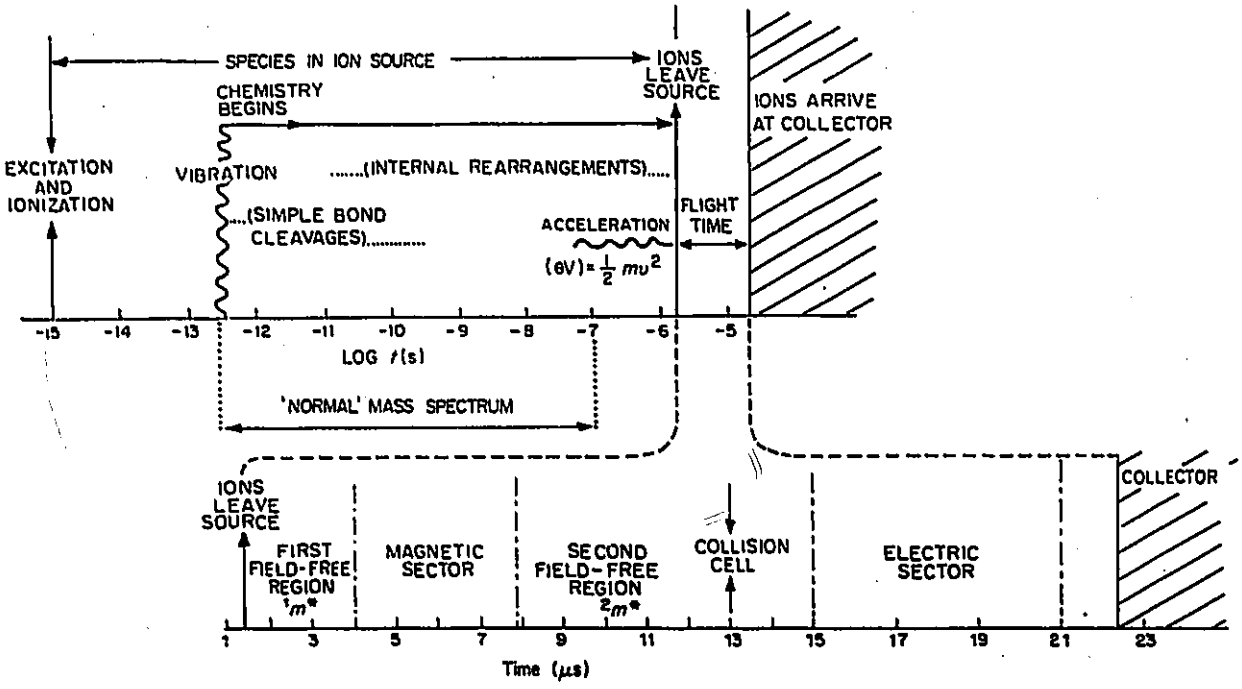

Figure 2.8 Time-scale of events for the mass spectrometer, based on an ion having a mass-to-charge ratio of 100, and acceleration voltage of 8keV. Reproduced from reference (13)

2.3.II Understanding Mass Spectra

Application of both kinetic and mechanistic theories have been considered in the interpretation of the relative abundances of molecular and fragment ions in the mass spectrum of a given molecule. The ultimate goal of any kinetic theory is to calculate the rate of reaction. However the Quasi-Equilibrium Theory, (QET) developed by Rosenstock et al. (14) in 1952, also offered a theoretical concept for understanding the fragmentation of gaseous ions, and enabling such phenomena as kinetic shifts (defined in chapter 3), and the dependence of the fragment intensities on energies of activation and on lifetime to be predicted and explained. The QET is based on the following assumptions (15-18).

(i) Ions generated represent isolated systems; thus the rate of a process is a function of the excitation energy only.

(ii) The time required for ionization by electron impact is short with respect to that for dissociation; the removal of an electron occurs within $\sim 10^{-16}$ s while the maximum rate of decomposition corresponds to one vibrational period and is of the order of $\sim 10^{-14}$ s.

(iii) The rate of dissociation is slow relative to the redistribution of the excitation energy over all degrees of freedom of the molecular ion's ground state; thus the rate of dissociation will be independent of the mode of ionization.

The mechanistic approach involves the rationalization of mass spectral behaviour by using generalizations about reaction mechanisms from physical organic chemistry. Accordingly the relative fragment ion abundances are determined by the following.

(i) The stability of the reaction products; those ions corresponding to dissociation processes which generate products of lowest total energy, $\Sigma \Delta H_f^\circ$, will preferentially be produced.

(ii) The strength of the bond cleaved.

The validity of this concept has been discussed in detail by R.W.A. Johnstone (19), however it is not always possible to extrapolate conventional views of bonding in neutral organic molecules to ions in the gas phase, where the existence of nonclassical structures, such as CH_5^+, are well known, and moreover an increasing number of other nonconventional species, such as ylid and distonic ions, which are fully described in chapter 6, are being discovered.

2.3.III Isomerization

Energised molecular and fragment ions are not limited to decomposition alone. A wide range of excess internal energies is transferred on ionization and so it is also possible for the molecular and fragment ions to rearrange to various isomeric structures, of classical or non-classical form. These isomerization reactions can greatly complicate the interpretation of mass spectra and thus some understanding of the parameters involved is necessary. The relative energy barriers for decomposition, (E_d), and isomerization, (E_i), are the parameters which principally determine whether and to what extent an ion A^+ rearranges to an isomeric ion B^+ at a given internal energy E. This is illustrated in *Figure 2.9.*

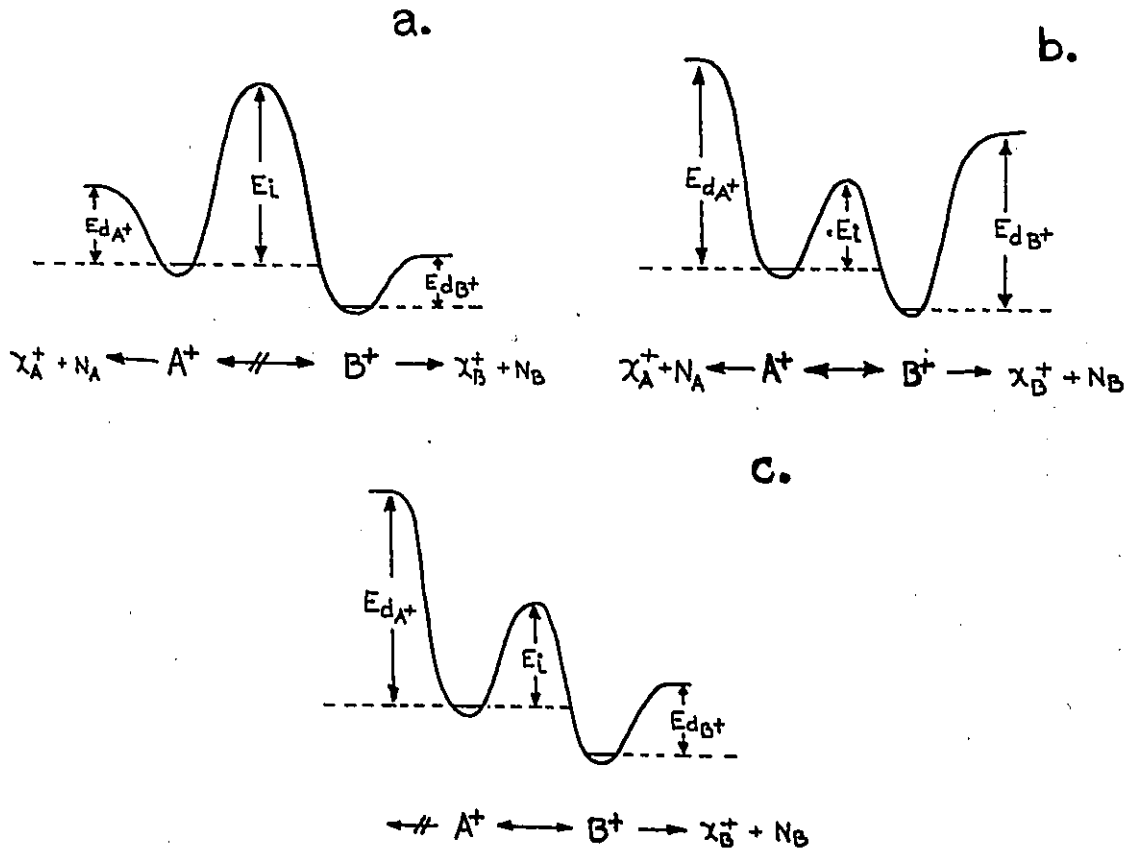

Figure 2.9 Schematic potential energy diagrams illustrating the possibility of isomerization between ions A^+ and B^+, versus their dissociation to $x_a^+ + N_a$ and $x_b^+ + N_b$ respectively.

In the case (a) where $E_i >> E_{dx}$, for all dissociations x, no isomerization is possible below the threshold energy for isomerization, and in general, even above this threshold, decompositions will be much faster

than isomerization (due to the greater density of states in the corresponding activated complexes). In (b) where $E_i << E_{dx}$, at internal energies above E_i, there will be a mixture of rapidly interconverting structures A^+ and B^+. At increased internal energies decomposition becomes possible, however having been preceded by a number of interconversions, the original placement of the atoms with respect to one another may have been altered several times resulting in partial or full randomization of the initial structure. Thus for (a), isomerization will not hinder the structural elucidation of A^+ and B^+, whereas for (b) the investigation of the decompositions of these ions will give no information unique to one *or* the other structure. Situations between these limiting cases are also possible, such as (c) where A^+ must isomerize to B^+ prior to fragmenting and thus both A^+ and B^+ will generate similar mass spectral results.

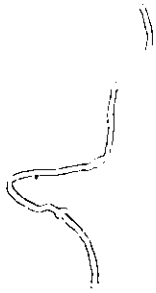

Chapter 3

EXPERIMENTAL ANALYSIS THERMOCHEMICAL AND DISSOCIATIVE TECHNIQUES

3.1 Introduction

Mass spectrometry has evolved into a powerful analytical technique since the early pioneer days, when ion structure assignments were predicted with one eye on the electron impact mass spectrum and the other on the corresponding system in solution. Not only do the present instruments possess a much greater degree of resolution, stability, and sensitivity, but their versatility has also improved dramatically. The accuracy of thermochemical measurements are now such that corresponding heats of formation, essential to firmly establish structural identity, may be confidently calculated. The increased versatility is reflected by the number of accepted experimental techniques now available to probe a system, over and above that of the initial dissociative technique, a 70 eV electron impact (EI) mass spectrum. These methods, applicable to the modified VG ZAB-2F, are all based on an examination of the decomposition, unimolecular or induced by collision, of the species of interest. In this chapter the experimental thermochemical and dissociative techniques will be described and discussed in terms of the relevant underlying theory and assumptions. The applicability of these techniques to the structural elucidation of isomeric gas phase ionic species will be enlarged upon in chapter 4.

3.2 Thermochemistry

Sound knowledge of gas phase ion thermochemistry, particularly heats of formation of isomeric organic ions, is essential to firmly establish the structures of ionic (and neutral) species. This is especially true when a whole system of isomeric species is involved. Heats of formation,

$\Delta H_f°$, may be considered ion specific; identical heats of formation can be taken to imply the presence of a single structure (barring any fortuitous agreement) and vice versa. Thus ion structures may be inferred from heat of formation data by comparison with the heats of formation of ions of known structure, or in many simple systems, with those heats of formation predicted from high level ab initio molecular orbital theory calculations.

Measurements of ionization and appearance energies are the experimental basis of ion thermochemistry. Through these values and the appropriate thermochemical data of the neutral species involved, the heats of formation for molecular and fragment ions may be calculated.

3.2.I Ionization Energy

The minimum energy required to remove an electron from the highest occupied orbital of a molecule is termed the first ionization energy, (IE). The heat of formation of a molecular ion, $M^+\cdot$ is then given by;

$$\Delta H_f°([M]^+\cdot) = IE(M^+\cdot) + \Delta H_f°(M) \qquad \textit{eq.(3.1)}$$

Thus, ideally, knowing the $\Delta H_f°$ of the neutral molecule, M, the IE value will allow the calculation of the $\Delta H_f°$ of the molecular ion (refer to *figure 3.1*). If the heat of formation of the neutral species is not contained in the general reference literature (20), it may be predicted via the additivity scheme of Benson (21), or via the use of new or provisional additivity terms (22,23). The accuracy of the ion's heat of formation depends directly on that of its neutral, as well as the experimentally determined ionization energy. IE values with a precision of ±0.05eV (i.e. ± 4 kJ mol^{-1}) can be achieved with specialised apparatus.

3.2.II Appearance Energy

The appearance energy, AE, of a fragment ion represents the minimum energy necessary to form this ion from a given neutral precursor. The heat of formation of a fragment ion, $A^+\cdot$, formed in the reaction,

$$M \rightarrow A^{+}\cdot + B + e^{-}$$

is given by;

$$\Delta H_f^\circ([A]^{+}\cdot) = AE(A^{+}\cdot) - \Delta H_f^\circ(B) + \Delta H_f^\circ(M) \qquad \textit{eq. (3.2)}$$

Alternatively, if $\Delta H_f^\circ[A]^{+}\cdot$ is known, $\Delta H_f^\circ(B)$ may be calculated. In some cases the structural identity of the neutral fragment, B cannot be disputed, for example H_2O, $CH_3\cdot$, or CH_4, however, where the possibility of the generation of isomeric neutral fragments exists (for instance $CH_3O\cdot$ versus $CH_2OH\cdot$), care must be taken to ensure that the appropriate ΔHf° value is employed when assessing $\Delta H_f^\circ[A]^{+}\cdot$. This will be discussed in more detail in the following chapter.

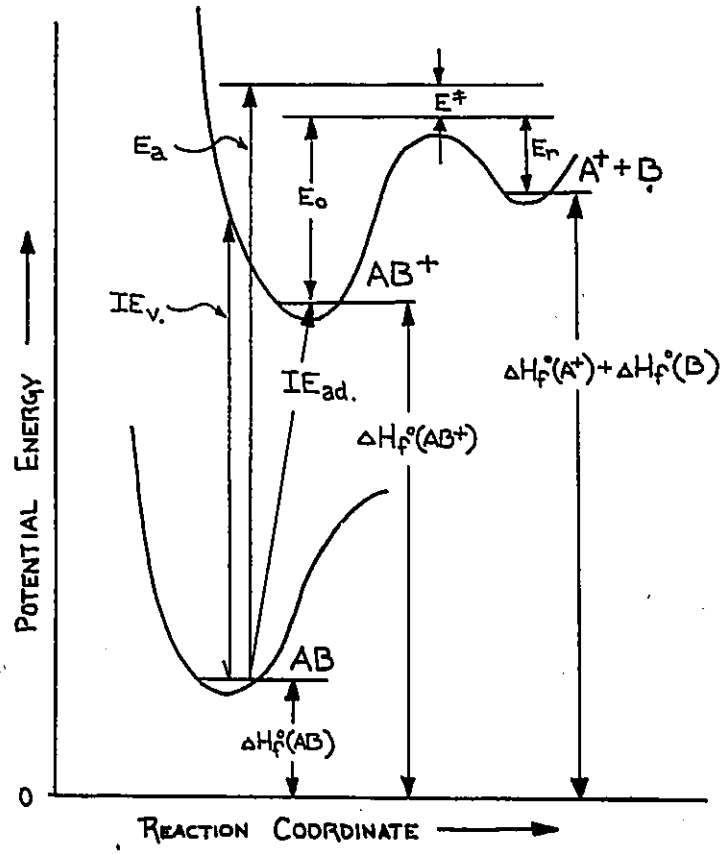

Figure 3.1 Schematic potential energy diagram illustrating the determination of heats of formation of gaseous organic ions.

3.2.III Experimental Considerations; Electron Impact Studies

IE values, of the molecular ion, $M^{+}\cdot$, and AE values of the appropriate fragment ion $A^{+}\cdot$ are obtained by recording the intensity of the ion signal as a function of the ionizing electrons' energy. The electron

energy corresponding to the onset or first observance of the ion of interest is then extrapolated from the curve. IE and AE values can only be measured with good accuracy, ±0.05 eV, with the aid of specialized apparatus such as photoionization mass spectrometers (24) or mass analyzers equipped with an energy-selected electron impact ion source, such as the instrument by Lossing, described earlier, in 2.2.II, (12). Acceptable IE values, ±0.1-0.2eV may be obtained using commercially available analytical mass spectrometers. Sufficient accuracy cannot be achieved on the VG ZAB-2F due to the appreciable spread in the energy of electrons emitted by the wire filament and because of poor design features in the electronics. The measurement of the AE of a metastably generated ion does not require highly specific electron energy control. Using the MS-902S mass spectrometer, reasonably accurate measurements of the threshold onset for the first field-free region generated daughter ion of interest is made together with that of a calibrant reaction whose metastable appearance energy is accurately known (25). Comparison of these thresholds in terms of measured electron energies allows the evaluation of the unknown AE.

The experimental difficulties associated with these measurements are due mainly to the problems of detecting small ion currents, of maintaining a minimal energy spread in the electron beam, and of calibrating the voltage scale. There are however more fundamental aspects to be considered when relating experimentally generated IE and AE values to ionic heats of formation.

3.2.IV Adiabatic versus Vertical Excitation Energy

Ionization energy measurements are usually reported as being adiabatic or vertical in nature. An adiabatic transition is a transition from the non-vibrationally excited electronic ground state of the molecule to the vibrational and electronic ground state of the molecular ion. This transition will give a minimum value for the ionization energy, and is therefore important in $\Delta H_f°$ calculations. Such adiabatic measurements are possible with the double hemispherical electron energy selecting mass spectrometer described in section 2.2.III. A vertical transition on the other hand will involve some amount of vibrational energy, (*figure 3.1*),

since it is defined as the energy required to remove an electron while holding the nuclei fixed in their equilibrium position. The time for the transfer of energy from an electron beam to a molecule is of the order of 10^{-16} s, several orders of magnitude faster than typical vibrational frequencies, 10^{-13} - 10^{-12} s. The most probable electron impact ionization process is that accomplished without changes in inter-nuclear separations and is labelled a vertical, or Franck-Condon type of process. How widely the vertical will vary from the adiabatic ionization energy for a given system, will depend on the differences in inter-nuclear positions in the molecule and in its corresponding ion. Thus the larger the nuclear separation between the two states, the larger will be the difference between the vertical and adiabatic ionization energies. The difference in IE between these two transitions is often insignificant, but can, in extreme cases, lead to errors in ionization energies of the order of 0.1-0.7eV (10-70 kJ mol^{-1}). A good example is the case of ethyl fluoride, which will be discussed in chapter 6. Thus, wherever possible, the adiabatic value of the ionization energy should be employed. The most complete collections of IE and AE observations are the two compilations from the National Bureau of Standards, (26,27). The earlier volume (27), includes calculated $\Delta H_f°$ values for a small number of ions for which the data are deemed reliable. The second makes no attempt to distinguish good from unsatisfactory values. Note also that vertical, as well as the thermodynamically more useful adiabatic IE values are reported in these volumes.

3.2.V Kinetic Shift

The difference between the experimentally obtained appearance and ionization energies cannot necessarily be equated with the activation energy, E_o. This difference, AE-IE, will be too large by the amount of the kinetic shift, the excess energy necessary to ensure that the rate of fragmentation in the ion source is such that a sufficient number of daughter ions are formed during the source residence time, (on the order of 10^{-6} s.). The magnitude of the kinetic shift is not only affected by the residence time of the ions in the source (a function of the instrument), it also depends upon the shape of the k(E) versus E curve for the

reaction. A unimolecular fragmentation reaction will have a significant kinetic shift when its rate constant, k(E), rises only slowly with increase in internal energy, $E^{\neq}$, and thus the measured appearance energy will lead only to an upper limit for $\Delta H_f°[ion]$. The absence of a metastable peak for a reaction indicates a rate constant which rises rapidly with increasing ion internal energy and thus has an appearance energy which may be used with some confidence. The error introduced into appearance energy measurements by the kinetic shift can be reduced by measuring the appearance energy of ions generated in the metastable time frame. Being of longer life time, metastable ions must necessarily have lower excess energy than those generated in the ion source. Thus the $\Delta H_f°$ value calculated from the AE of a metastably generated species must be less than or equal to the value calculated from that of a source generated species. Also, AE values of metastable species give $\Delta H_f°$ values specific to the product of a given reaction channel. To transmit a metastably generated daughter ion through electric and magnetic sectors the mass of its parent ion must be known. Therefore, the AE of a species C^+, generated metastably from A^+ and the AE of C^+ from a fragment B^+ thereof, may be differentiated.

$$A^+ \overset{*}{\rightarrow} C^+ + X \qquad \textit{eq. (3.3)}$$

$$A^+ \rightarrow B^+ + Y \overset{*}{\rightarrow} C^+ + Z \qquad \textit{eq. (3.4)}$$

Using AE measurements of metastable species does however have its drawbacks, not only are the number of reactants limited but the low intensity of some metastable peaks can give rise to sensitivity problems. Interfering collision induced reactions can also cause complications if the pressure in the field-free regions is not sufficiently low.

3.2.VI Reverse Activation Energy

The absence of a corresponding metastable peak does not in itself guarantee that a true heat of formation of the fragment ion is calculated. The accuracy of $\Delta H_f°[A]^+\cdot$ also depends upon the magnitude of the reverse activation energy *(figure 3.1)* for the reaction. There is considerable evidence that most simple bond cleavages have only small or no reverse activation energies, as the ion-free radical recombinations normally proceed without activation energy. Rearrangement reactions, however, may proceed with substantial reverse activation energy, (28).

3.2.VII Competitive Shift

The measurement of appearance energies may be further complicated if two (or more) reactions have k(E) versus E curves which intersect, such as competing rearrangement (r) and direct cleavage (d) reactions giving fragments A^+ and B^+ respectively as illustrated in *figure 3.2.* As a result of the competing reactions near threshold, the rise in the number of fragment ions $B^+\cdot$ with energy may be very slow such that the observed appearance energies will be erroneously high.

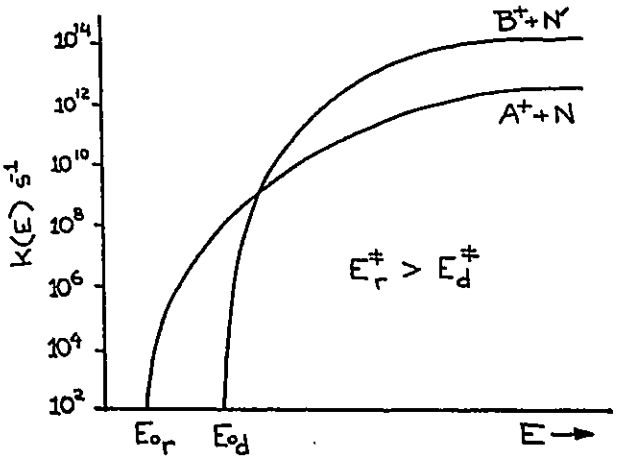

Figure 3.2 k(E) versus E curves for competing reactions involving rearrangement, (r), and direct bond cleavage, (d).

With all the problems described above, the IE and AE measurements will yield greater than the threshold value, resulting in calculated values of ΔH_f°[ion] which are too large.

3.2.VIII Isomeric Species

Ionization energy and appearance energy measurements are concerned with a peak onset with respect to electron or photon energies, thus it is of great importance to be sure that only a single reactant species will be monitored. The possibility of a mixture of isomeric product fragments at a given m/z value must also be considered. In this situation the AE threshold will correspond to the thermodynamically most stable isomer in the mixture. Considerations involved in thermochemical analyses of isomeric systems will be discussed at greater length in chapter 4.

3.3 Metastable Ions

Metastable ions are those which dissociate unimolecularly within the time taken to travel from the source exit to the detector; they have lifetimes in the range of 10^{-6} to 10^{-5} s. The resultant ionic fragments produce what are termed 'metastable' peaks. The origin of these metastable peaks was first correctly interpreted by Hipple and Condon (29) in 1945, although the parabolic experiments by Thomson some decades before had shown evidence of dissociations in flight (1).

The detection of stable ions, and fragments generated in the ion source, has been outlined in section 2.2.I. Detection of metastably generated fragment ions depends (intensity problems aside) upon where, within the instrument, the fragmentation occurs. Fragment ions generated within the magnetic or electric sector cannot be detected, the equations of motion, *eq. (2.4)* and *eq.(2.6)*, do not apply to mid-sector changes in mass. Fragmentations occurring after the electric sector will also go undetected, since no further energy or momentum analysis is made before detection. Only those fragments due to dissociations in the first or second field free-region, between the source and magnet and the magnet and ESA respectively, can be independently detected.

Consider the unimolecular reaction in *eq.(3.5)*, (note that, as in *eqs.(3.3)* and *(3.4)*, an asterix (*), is used to symbolize such metastable dissociation processes).

$$M_1^{+}\cdot \xrightarrow{*} A^{+}\cdot + N \qquad \textit{eq.(3.5)}$$

The fragmentation results in a distribution of the kinetic energy of $M_1^{+}\cdot$ between its products. The law of conservation of momentum has to be obeyed; thus the kinetic energy of the products generated between the sectors is given by,

$$\tfrac{1}{2}m_a v_a^2 = m_a/m_1 \cdot zV_{acc} \qquad \textit{eq.(3.6)}$$

$$\tfrac{1}{2}m_n v_n^2 = m_n/m_1 \cdot zV_{acc} \qquad \textit{eq.(3.7)}$$

Since the velocity of the particles is virtually the same, the kinetic energy of the products is a mass weighted fraction of the kinetic energy of the parent ion M_1^{+}. Thus the fragment $A^{+}\cdot$, produced via fragmentation

in the *second field-free region*, will be transmitted through the electric sector at an E value corresponding to $m_a/m_1 \cdot zV_{acc}$. Thus the mass of a product ion may be calculated from its kinetic energy. This is not only applicable to fragments of metastable ions, but for all fragments produced (unimolecularly or by collision) in the second field-free region from mass selected precursors.

Fragments A^+ produced before the magnet, in the *first field-free region*, will not be transmitted at a magnetic field B corresponding to an ion of mass m_a and kinetic energy of zV_{acc}, because they have only a fraction of that kinetic energy as seen in *eq.(3.6)*. These fragments will be transmitted by the magnet as a species possessing a full kinetic energy of zV_{acc} and an 'apparent' mass of m_a^2/m_1, and will then be transmitted through the ESA at an E corresponding to $m_a/m_1 \cdot zV_{acc}$. If these ions of apparent mass m_a^2/m_1 were to fragment before the electric sector, their fragments (m_f) will be transmitted by the ESA at a sector voltage equal to $[m_f/m_a \cdot m_a/m_1 \cdot zV_{acc}]$, or more simply, $[m_f/m_1 \cdot zV_{acc}]$ as illustrated in *figure 3.3*. Thus the production of unimolecularly generated ions in the first and second field-free region, and their possible decompositions between the sectors, may be independently detected.

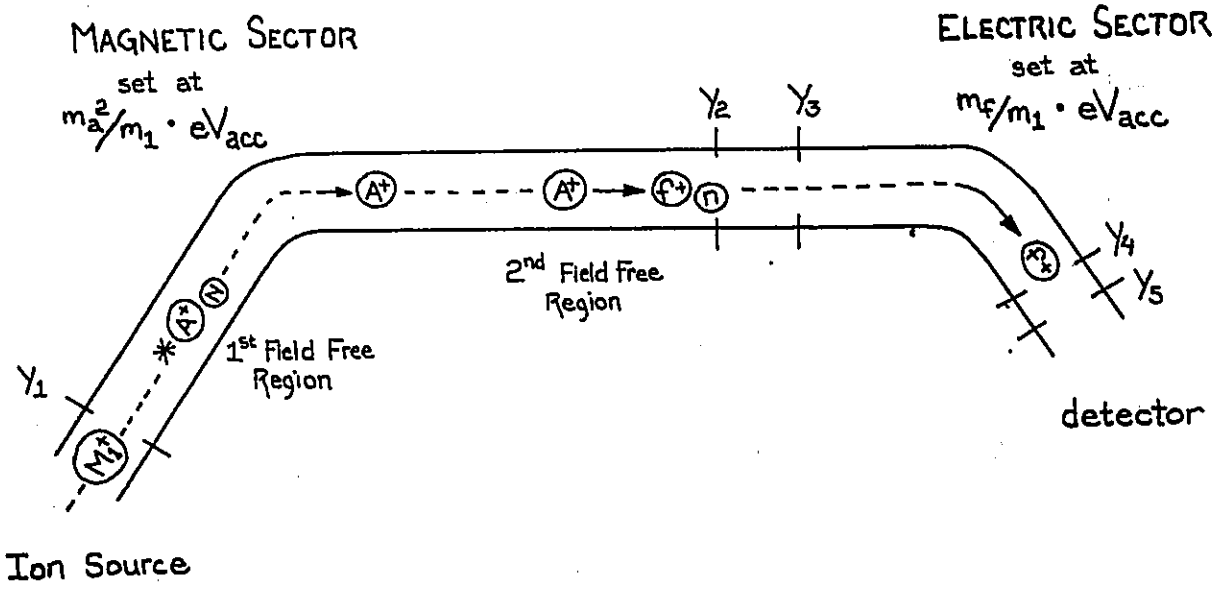

Figure 3.3 The metastable generation of A^+ from M_1^+ in the first field-free region which is then selected by the magnet via its 'apparent' mass. A^+, and the ionic fragments of those which dissociate in the second field-free region, are then detected.

Metastable ions allow precursor and daughter ions to be linked together and thus are extremely useful for the deduction of decomposition pathways of a given ion. Metastable ions recorded by scanning V_{acc}, link all precursor ions to a given daughter ion, while scanning of the electric sector, after mass selection by the magnet, links all daughter ions to a given precursor. Thus a flowchart of the low energy, competitive and consecutive fragmentations of a given system may be produced.

The general shape of a metastably generated peak may be very informative. For such peak shapes (beam intensity with respect to energy in volts) it is essential that they be recorded under conditions of good energy resolution (as well as stable instrumental conditions).

3.3.I RESOLUTION

The resolving power of a mass spectrometer may be considered in terms of energy as well as mass. However it is generally measured by the instrument's ability to separate two masses, M_1^+ and M_2^+, of any defined mass difference, Δm, and may be calculated by *eq. (3.8)*, where H is the height of the peaks and h, the height of the unresolved valley between them, as seen in *figure 3.4*.

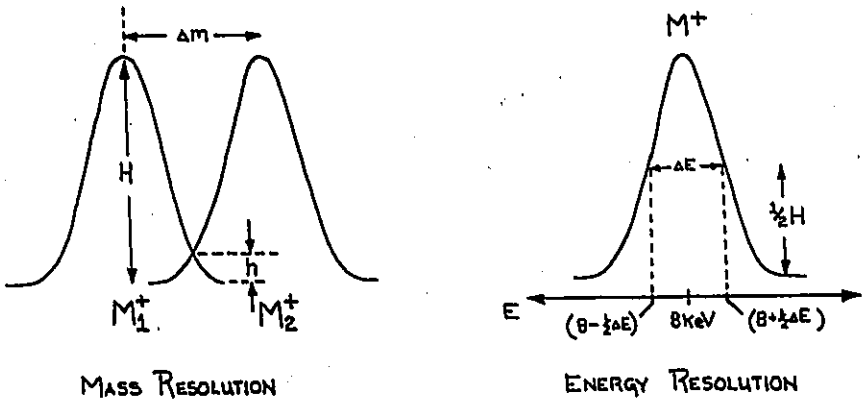

Figure 3.4 Measurements necessary for computing the mass and energy resolution achieved.

$$\text{thus:}\quad R = M_1^+/\Delta m \quad \text{when } (h/H)\cdot 100 \leq 10 \qquad \textit{eq. (3.8)}$$

Resolution in the ZAB-2F may be increased (at the cost of ion transmission) from its minimal value of ca 1000 by narrowing one or more of the variable focussing slits. In all there are five Y resolution slits, as observed in *figure 3.3*; one in the first field-free region, two between the sectors and another two between the electric sector and the detector. High mass resolution, obtained by

narrowing Y_1, Y_5, and sometimes Y_3, is particularly useful for observing constitutionally different ions having the same unit mass. For example, $[C_2H_3O_2]^+$ and $[C_3H_7O]^+$, having mass-to-charge ratios of 59.013303 and 59.049689 respectively, may be separated by a resolution of R≈16,000. High energy resolution is obtained in a similar fashion, again using Y_1 and Y_5. It is measured in terms of the recorded energy spread, ΔE, at half the height of the mass selected ion beam (*figure 3.4*). Values of ΔE>4 volts are usually acceptable.

Upon decomposition, part of the excess internal energy in the transition state of an ion, is released as kinetic energy, in what may be viewed as a spherically symmetrical distribution, from its centre of mass. The amount of kinetic energy released upon metastable decomposition dictates the shape of the metastable peak and can be readily detected as peak broadening since the ions' high translational energy causes substantial amplification of this translational energy spread. (This energy spread is not amplified for source generated fragment ions and thus is not detected as peak broadening.) The magnitude of the spread depends upon the reverse activation energy (E_r) as well as the kinetic shift ($E^{\neq}$) involved in the decomposition, as illustrated in *figure 3.5*.

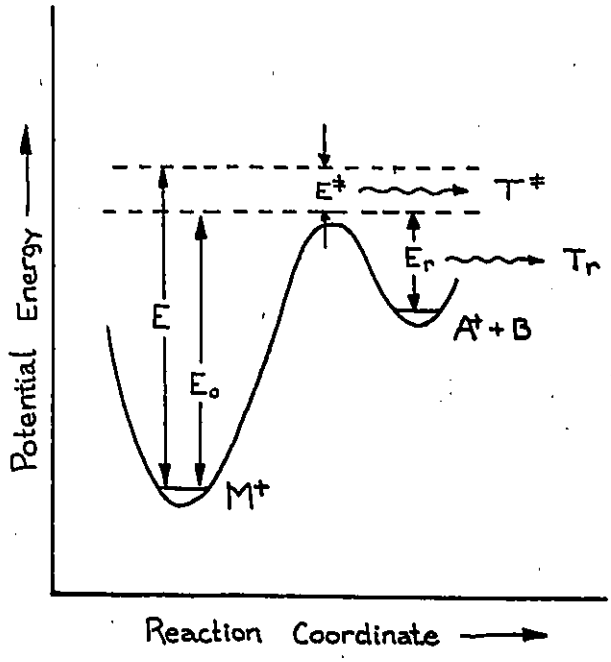

Figure 3.5 $T^{\neq}$ and T_r represent some fraction of the nonfixed kinetic energy shift, $E^{\neq}$, and the reverse activation energy, E_r. These contribute to the total kinetic energy release, T.

However because of an insufficient understanding of the process of energy partitioning, the total excess energy of the metastable ion (E_T) cannot be estimated from the measured kinetic energy releases, and no simple method exists for the simultaneous accurate evaluation of that kinetic energy distribution and the internal energy content. Thus T values (see below), useful for the comparison of one peak with another, lack any fundamental significance.

Under conditions of high energy resolution, the magnet is fixed to transmit the precursor, M_1^+, and the electric sector is scanned slowly through an energy range close to $[(m_a/m_m)\cdot zV_{acc}]$. The kinetic energy release, T is calculated from the measured width, ΔE_A, of the metastable peak, at a given fraction (usually 0.5) of the peak height. For the metastable process $M_1^+ \overset{*}{\rightarrow} A^+ + B$, the $T_{0.5}$ associated with the metastable formation of A^+ is given by the following relationship, (30) and is generally reported in units of meV.

$$T_{0.5} = \frac{(\Delta E_A)^2 \cdot (M_1)^2}{V_{acc} \cdot A \cdot B \cdot 16} \qquad \textit{eq. (3.9)}$$

Where ΔE_A is small and the spread in energies of the main beam, $\Delta E(M_1)$ is significant with respect to that of the metastable peak a correction to ΔE_A must first be made, using *equation 3.10* (31).

$$\Delta E_A(\text{corr.}) = \sqrt{[\Delta E_A]^2 - [\Delta E(M_1)]^2} \qquad \textit{eq. (3.10)}$$

Metastable peak shapes, which should also be recorded under conditions of good energy resolution, as seen in *figure 3.6*, fall into one of three categories. *Gaussian* type peaks may be represented as being roughly triangular in form. They are generally associated with small kinetic energy releases, $T_{0.5}$ typically no more than ~80meV. *Dished* and *flat-topped* peaks are associated with larger kinetic energy releases due to reverse activation energies, E_r, although the inverse statement is not necessarily true. The observed dish is produced by z-axial discrimination against the ion beam and will be instrument dependant. *Composite* peaks are the result of a combination of two or more metastable peaks, giving a more complex outline. A composite metastable peak indicates the involvement of more than one transition state and/or the production of more than one isomeric fragment ion.

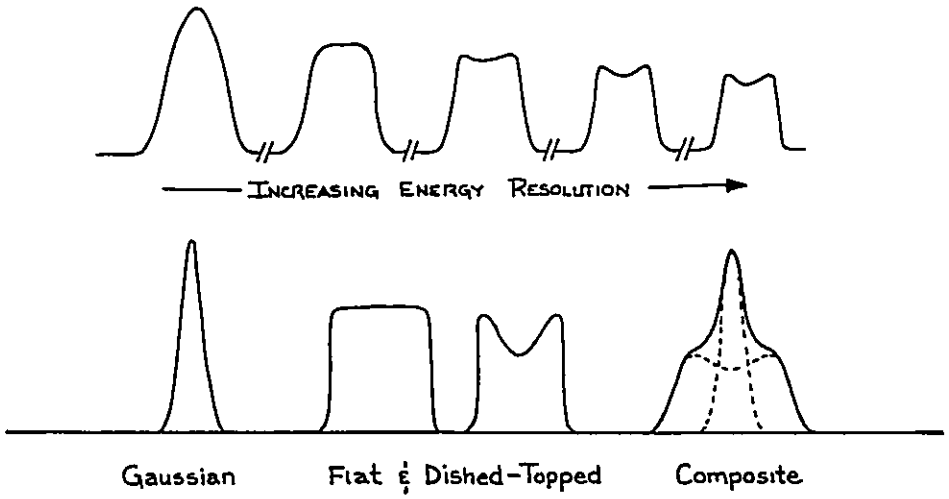

Figure 3.6 Common metastable peak shapes, and the dependance of these shapes on the energy resolution under which they are obtained.

3.4 Collision Induced Dissociation

Fragmentation of ions resulting from collision was first acknowledged by Smyth in 1925.(32). However the process was considered little more than a hindrance until 1968, when interest in collision induced dissociations was revived by Jennings (33), and by Haddon and McLafferty (34). Today, collision induced dissociation has become a very powerful technique for the elucidation of ion structures, and is the basis for several other methods for investigating beams of fast charged or neutral species.

When ions having a high translational energy (of the order of ~10^3 eV), collide with neutral atomic or molecular targets, a small fraction of the translational energy of the ion may be converted into internal excitation energy. This excitation may be considered essentially Franck-Condon in nature, provided no significant change in the internuclear distance of the ion can occur during the time of collision, and little deflection of the centre of mass of the ions results. For ions with translational energies $\geq 10^3$ eV the time of collisional interaction is sufficiently short, that 'collisional excitation' can take place vertically. The internal energy of the ion acquired by collisional excitation may be

sufficient to cause the ion to fragment,

$$M_1^+ + T \rightarrow M_1^{+*} \rightarrow A^+ + N \qquad \textit{eq. (3.11)}$$

a process known as *collision induced dissociation*, or CID. The collection of collision-induced fragments of a given precursor ion has been termed the *collision induced dissociation* or *CID mass spectrum*.

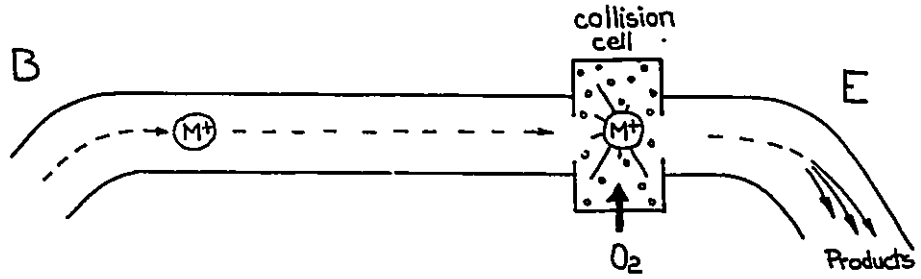

Figure 3.7 Schematic diagram for the generation of a CID mass spectrum of mass selected ions, M^+.

Collision-induced dissociation experiments on mass selected ions are now routinely carried out in a large range of mass spectrometers. Unlike the metastable ion or MI mass spectra, CID mass spectra primarily sample non-decomposing, lower energy species. The VG ZAB-2F allows a variety of CID experiments to be conducted. Collision gas may be introduced into the first field-free region as well as either of the collision gas cells in the second field-free region. For the most part however, the second collision gas cell is used. The precursor molecular or fragment ion of interest, $M_1^{+\cdot}$ is generated by impact with 70eV electrons in the source. The magnet is set to transmit the species with a mass-to-charge ratio $m/z=m_1$, and thus only $M_1^{+\cdot}$ enters the second field-free region. The collision gas cell in *figure 3.7* is pressurized with an inert target gas, typically helium or oxygen.

3.4.I Gas Pressure

Differential pumping by the diffusion pumps attached to the flight tube before and directly after the cell allows for a good pressure gradient, ensuring that the great majority of the collisional processes occur within the cell. The ionization gauge situated above the down-stream diffusion pump can give only relative pressures. Target gas pressures are therefore considered in terms of the ion beam's reduction in intensity, refer to *figure 3.8*. Although beam reduction involves the sum of scattering, fragmenta-

tion and other processes, it is a good indication of the relative importance of multiple collisions. At a beam reduction of 10%, some 95% of the ions undergoing collisions have but a single encounter, whereas at a 60% reduction, multiple collisions make up ~25% of the total. Although maximum yields of fragment ions are obtained at pressures corresponding to 40-80% beam reduction (35), collision gas pressures in this work were maintained at a 10% reduction, favoring single collisions and avoiding problems of interpretation which arise when multi-collision conditions are used.

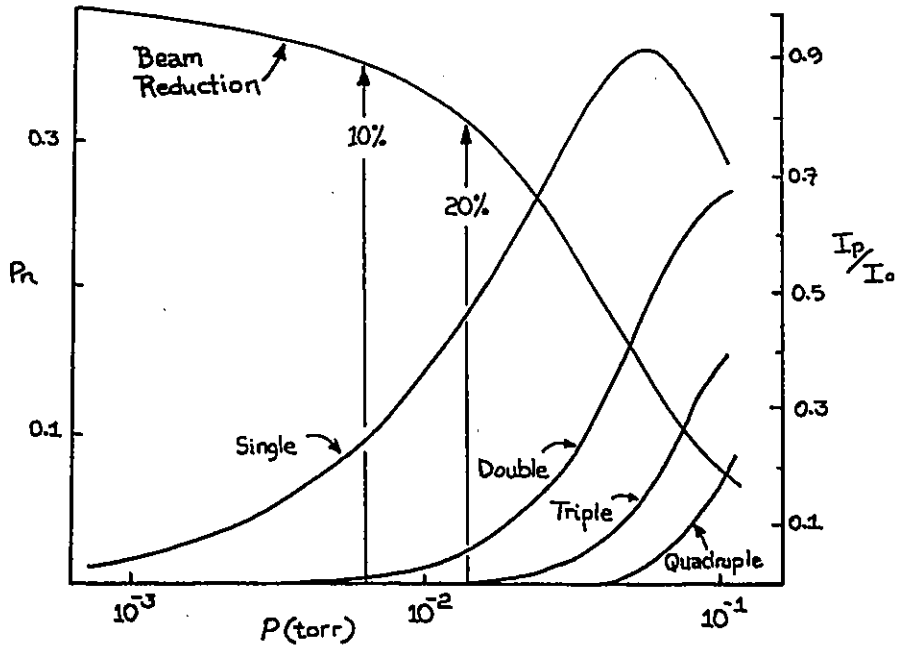

Figure 3.8 Total collision probability, (Pn), beam reduction, (Ip/Io), and the fraction of single and multiple collisional processes as a function of collision gas pressure, (P). Reproduced from reference (13).

3.4.II Collision Gas

The most frequently used collision gases are helium and oxygen, however nitrogen, hydrogen, xenon and others may also be utilized. Small targets are considered to deposit, on average, more energy into an ion than larger targets. Target gases fall mainly into two classes; "soft" agents (including O_2, NO, Cl_2, NO_2), providing a smaller degree of fragmentation and "hard" agents (including He, CH_4, SF_6, Xe), providing more, while N_2 is intermediate. It is also believed that in general, "soft" targets are capable of accepting an electron in an ionization process, a process that should have a lower energy requirement and produce an ionized species of lower average internal energy, (36). The choice of target gas, therefore, depends upon the information sought (37).

Upon collision with the target gas of choice, those ions which have gained sufficient internal excitation will rapidly dissociate. The percentage of these fragmentations which occur within the cell itself may be monitored via the technique described below, which is also a semi-quantitative means of separating collisional-induced and unimolecularly generated fragments of a given mass selected precursor ion.

3.4.III Cell Voltage

The percentage of fragmentations occurring within the cell itself may be monitored, because the cell, flanked by two grounded plates, is electrically isolated and may be raised to a preset voltage of up to ±5keV. For a voltage, -V, on the cell, the precursor ions, $M_1^{+\cdot}$, at V_{acc}, will have a translational energy of $(V_{acc}+V)$ after entering the cell. Collision-induced dissociation of $M_1^{+\cdot}$ to give A+ *within* the cell will produce A+ fragments detected at a translational energy of $[(A/M)\cdot(V_{acc}+V)-V]$, while those A+ produced *before* and *after* the cell will be detected at $[(A/M)\cdot V_{acc}]$ in translational energy, and are therefore unaffected by the cell voltage. An illustration is given in *figure 3.9* below. Separation of processes occurring within and without the cell can be linked to collision-induced and unimolecular processes respectively. Thus under CID conditions, where a peak is known to contain unimolecular contributions, that portion of the peak resulting from collision may be isolated. Despite the fact that the gas cell occupies <2% of the second field-free region, and that a good pressure gradient is maintained about the cell, such separations, although very informative, can only be considered semi-quantitative.

Detection of collision generated fragments from the second field-free region is performed by scanning the electric sector voltage. The resultant CID mass spectrum of the precursor, like that of its EI mass spectrum, will contain many peaks corresponding to consecutive and competitive dissociations, involving simple cleavage and/or rearrangement reactions. If the molecular ion of a compound does not undergo any complex time-dependent rearrangements, then the CID mass spectrum will be similar to the normal EI mass spectrum.

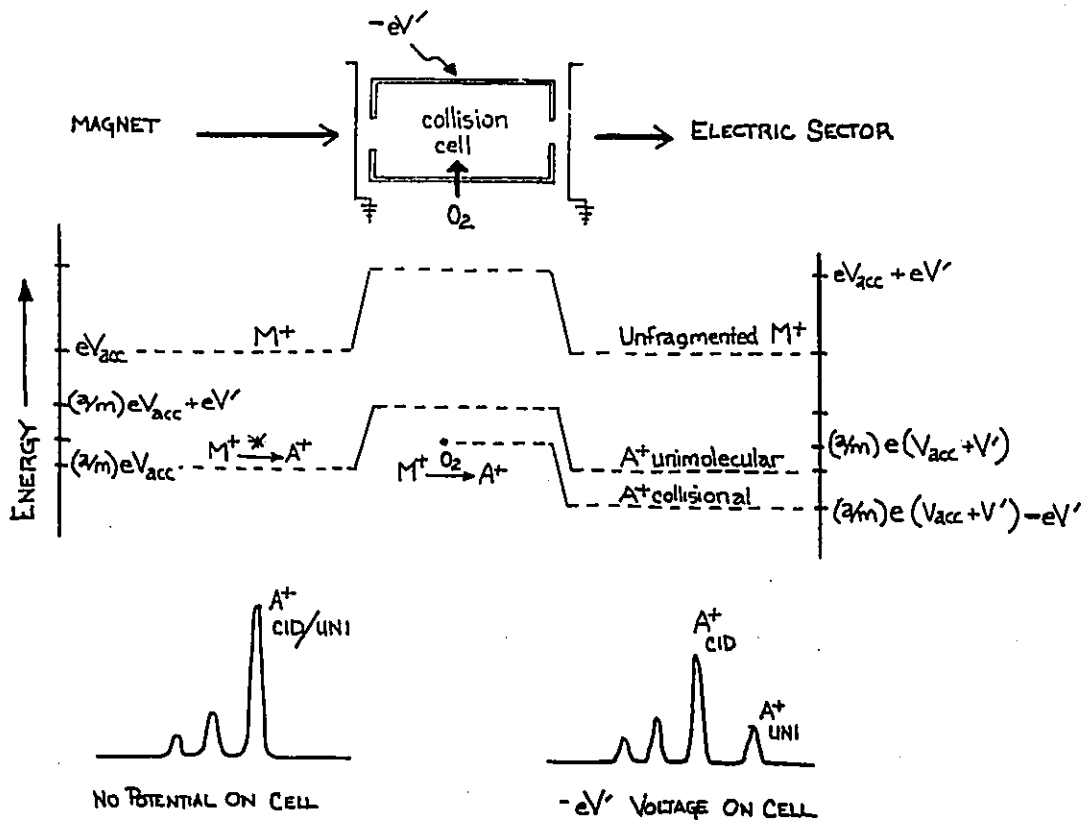

Figure 3.9 Separation of collisionally induced A^+ fragments from those A^+ generated prior to the cell, metastable M^+. Separation is achieved by floating the electrically isolated cell at some voltage, -eV'.

3.5 Charge Stripping

Collisional excitation of fast, mass selected precursors $M_1^{+\cdot}$, may be sufficient to cause the loss of an electron, resulting in a doubly charged species, M_1^{2+}.

$$M_1^+ + T \rightarrow M_1^{2+} + T + e^- \qquad \textit{eq. (3.12)}$$

This *charge stripping*, CS, process was first reported in 1972 by Beynon and co-workers (38) The signals resulting from CS may be easily differentiated from those of CID. They are greatly reduced in width, and appear at one half the electric sector voltage for transmission of their singly charged counterparts. Amplification of the CID mass spectrum is

usually necessary to detect charge stripping peaks because their intensity is in general far less than those from CID. The use of "soft" target gases, particularly O_2, resulting in less energized products, will increase the relative intensities of the CS peaks. As well, these target gases will yield more non-decomposing doubly charged parent ions relative to doubly charged fragments.(37)

3.6 Collision Induced Dissociative Ionization

Until very recently, mass spectrometric studies involved ionic species only, little or no attention being paid to the structure of the neutral products of ion fragmentation. In the majority of cases the neutral can exist in only one stable structural form, e.g. consider H_2O, CH_4, $CH_3\cdot$, however this may not be said of all cases, consider $CH_3CO\cdot$ versus $CH_2CHO\cdot$ (39), or HCN versus HNC (40).

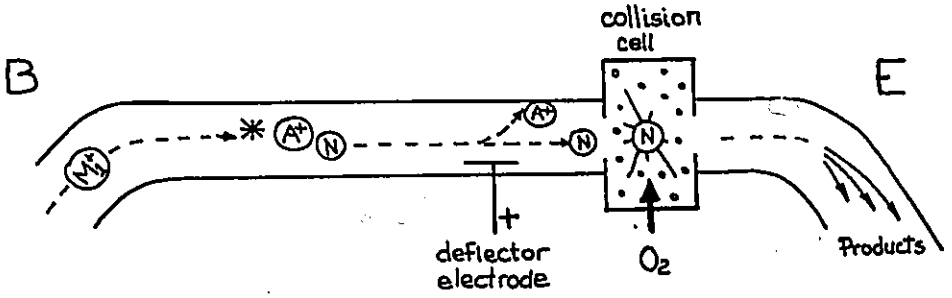

Figure 3.10 Schematic diagram for the generation of a CIDI mass spectrum of mass selected M_1^+ ions.

Consider the process;

$$M_1^+ \overset{*}{-} A^+ + N \qquad \textit{eq.(3.13)}$$

When a mass selected precursor fragments unimolecularly in the second field-free region, the recorded CID mass spectrum will consist of the ionic dissociation products of A+ and N as well as those of M_1^+, although the intensity of fragment ions from the latter will be 2-4 orders of magnitude greater. However, *elimination* of the *ion* flux prior to the

collision cell will result in the collision-induced dissociative ionization, or *CIDI mass spectrum* of the metastably generated neutral species alone:

$$N + T \rightarrow N^{+*} \xrightarrow{*} x_f^+ + y_f \qquad \textit{eq.(3.14)}$$

3.6.I Neutral Beam Isolation

In the first experiments (39,40), the neutral flux was isolated by floating the collision cell at a voltage, $+V_c$, such that $V_c > V_{acc}$, and the ion beam is repelled. However this restricted the acceleration voltage (to voltages which could safely be imposed on the collision cell, $\leq$ 5keV), and thus limited the sensitivity and resolution of the resulting mass spectrum. At present the charged and neutral species are separated by use of a beam deflector electrode, a description of which has been given in chapter 2.2. Its installation into the flight tube of the VG ZAB-2F was the first of two modifications (41) to this instrument. As seen in the schematic diagram in *figure 3.10*, the deflector is situated before the ionizing collision cell. A potential of ±500eV on the plate deflects ions sufficiently from the beam path to ensure that no ionic species, (M_1+ or A+) enter the collision cell, while the kinetic energy and direction of the neutral species is unaltered. The use of the deflector electrode allows CIDI spectra of neutrals generated unimolecularly from negative as well as positive precursors to be recorded (40,42). Also, maximum values of V_{acc} may be used, and the resolution is much improved.

Thus to record a CIDI mass spectrum of N, generated via *eq.(3.13)*, mass selected M_1^+ must generate a single, sufficiently intense metastable peak in the second field-free region corresponding to mass A^+. The deflector is charged and target gas, O_2 or He, is introduced into the cell to a pressure corresponding to 10% main beam reduction (see section 3.3.II). Scanning the electric sector mass analyses the ionic dissociation products, x_f, which are transmitted at an acceleration potential of $[(x_f/M_1) \cdot zV_{acc}]$, and thus a mass spectrum of a neutral species may be generated.

3.7 Neutralization–Reionization

The most recently introduced collisional technique combines neutralization and reionization in a tandem mass spectrometer for the generation

(as well as dissociative reionization) of novel neutral species. The early literature was concerned with ionization of atomic beams, and in 1967 Devienne (43) used the method for the reionization of neutrals formed by charge exchange (CE) of H_3^+ with 'residual gases'. Similarly, translational energy analyses of Ar^+ ions resulting from neutralization-reionization double collisions in a single focussing instrument were reported in 1977 (44). The term *Neutralization-Reionization* Mass Spectrometry or *NRMS* was introduced by Danis et al. (45) in 1983, with its application to the generation of fast polyatomic neutrals from their cationic counterparts (46).

3.7.I The Second Collision Cell

To generate NR mass spectra two collision cells separated by a deflector electrode are required in the second field-free region. The second modification of the VG ZAB-2F was the installation of a second, electrically isolated collision cell (9) (as described in 2.2), within the second field-free region, directly before the deflector electrode, as illustrated in *figure 2.3*. The newly installed collision cell is the first cell encountered by the ion beam and is therefore referred to as cell 1. In a similar fashion to the original cell, gas may be admitted and a relative cell pressure reading obtained from a second ionization gauge.

Ideally, an ionic beam undergoes collisional charge exchange with a target gas in cell 1 to generate the specific neutral of interest.

$$M_1^+ + T \rightarrow M_1 + T^+ \qquad \textit{eq. (3.15)}$$

Then, as in CIDI experiments, the remaining ionic species are electrostatically deflected out of the beam path.

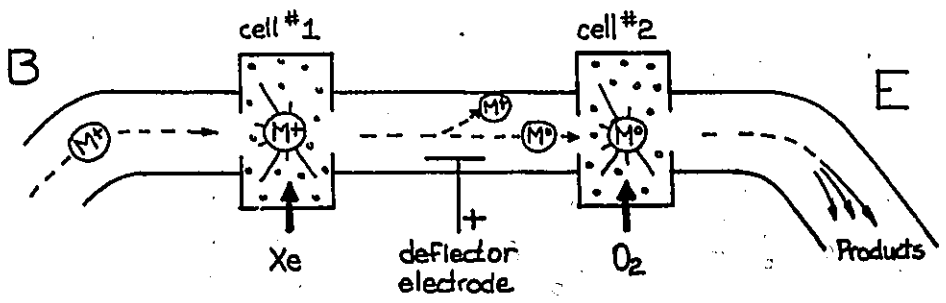

Figure 3.11 Schematic diagram for the generation of a NR mass spectrum of mass selected M^+ ions.

The neutral species alone enter the second collision cell to be collisionally reionized. In practice however, the neutrals reaching cell 2 may be of mixed origin.

3.7.II Origin of Neutrals

The corresponding neutral of the mass selected, multikilovolt ion [ABC+], will be generated by charge exchange, but neutral fragments will also be formed by metastable $[ABC]^{+*}$ dissociations, its collisionally induced dissociation, and/or dissociation of the neutrals resulting from these processes.

$$ABC^+ + T \rightarrow ABC + T^+ \qquad \textit{eq.(3.16)}$$

$$ABC^+ + T \rightarrow AB + C^+ + T \qquad \textit{eq.(3.17)}$$

$$ABC^{+*} \rightarrow AB + C^+ \qquad \textit{eq.(3.18)}$$

The relative contribution of the neutrals generated unimolecularly before the first collision cell, *eq.(3.18)*, is dependant upon the number and intensity of the unimolecular processes of the precursor and may be isolated (semi-quantitatively) by floating the cell at a voltage similarly to the technique described in section 3.3.III. The relative importance of neutralization, *eq.(3.16)*, versus fragmentation, *eq.(3.17)*, depends markedly on the target (and its pressure) used in cell 1, thus although contributions from these latter two processes are not separable, the choice of target may favour one over the other.

3.7.III Neutralization & Reionization Targets

Resonant charge exchange was initially considered to be a necessary criterion for efficient neutralization. Such experiments made the use of alkali metal vapors, allowing a wide range of ionization energies to be sampled, attractive in the neutralization process (45,47). Resonant exchange between target and ion species is however, not necessary, the optimum efficiency for CE being observed for processes which are endothermic by a few volts (13). The very high ionization energy, IE, of He (24.6eV) (26) makes it a very inefficient neutralization agent (47), whereas Xe (12.1eV), (27) has been found to yield good neutral fluxes, without appreciable contributions from collisionally generated neutral fragments (48), and so has become the neutralization gas of choice.

The pressure of the neutralization gas should be maintained in the single collision regime, to minimize subsequent fragmentations. Such pressures will not give the maximum flux of neutrals (a condition advised by McLafferty (47)), but however, will ensure that those neutrals formed are not themselves subjected to collision

induced fragmentation. Such complications can make structure elucidation difficult.

Reionization target species giving a high yield of charge exchange and fragmentation processes are also necessary. Helium and oxygen have become the gases of choice, both giving good fluxes of reionized species and their dissociation products. The superiority of O_2 as a reionization target for fast neutrals has been linked to its capability for effecting inverse neutralization:

$$M_1 + T \rightarrow M_1^+ + T^- \qquad eq.(3.19)$$

producing O_2^- and O^- (36).

Thus the following steps must be taken to achieve a NR mass spectrum of M_1^+. M_1^+ ions are generated in the source by electron impact and mass selected via the magnet into the second field-free region. The ions travel through the first collision cell containing a pressure of Xe gas corresponding to ≥90% transmission of the M_1+ beam. The deflector electrode, at a voltage of +1700eV (49) allows only the fast neutrals (generated by charge exchange, and as well unimolecular and/or collision induced dissociations) to enter cell 2. Collision with a similar pressure of O_2 imparts sufficient energy for reionization as well as subsequent dissociation to occur. The resultant ionic fragments are analyzed by the electric sector and detected by the multiplier to produce a NRMS of M_1^+.

Optimising the sensitivity in a NR mass spectrum is of extreme importance, since the double process of neutralization and subsequent reionization reduces the flux of detected resultant ionic fragments, often by orders of magnitude with respect to CID mass spectra. Reduction may be due to scattering, as well as incomplete neutralization. In this work, signal averaging was in most cases unnecessary; however for species whose ion source generated flux was weak, where charge stripping peaks were of interest, or for high resolution NRMS experiments, signal averaging was utilized (50) with satisfactory results.

Chapter 4

STRUCTURAL ELUCIDATION APPLICATION OF THE TECHNIQUES

4.1 Introduction

The exact mass and thus the atomic composition of an ion, obtained via high resolution EI mass spectrometry, may in a few cases be sufficient to deduce its structure. However the increasing number of isomeric structures (classical and nonclassical) which are possible for quite small ionic species (say up to 6-7 atoms), together with their possible interconversions, can greatly complicate the structural elucidation of gaseous organic species. Thus to ensure successful structure assignment the thermochemical properties and dissociative characteristics are analyzed as completely as possible. In most of the techniques presently employed for ion structure determination, described in the preceding chapter, the unknown ion's structure is established *by comparison*. If an unknown ion fragment, $A^{+}\cdot$, yields thermochemical and dissociation characteristics very closely similar to those of a known ion, $B^{+}\cdot$, then the structure of $A^{+}\cdot$ is concluded to be identical with that of $B^{+}\cdot$. However reference ions of known structure are not always available. To this end comparisons are made employing as wide a range of analytical techniques as possible. The correct structure of the ion is then inferred from all the available information. It must be kept in mind that ions of different lifetime and internal energy are being sampled by the various techniques. Thus whether all the techniques will give information on the *same* ionic structure will depend on the ions relative thresholds for isomerization and decomposition. Appended to this chapter is a summary of each mode of analysis considered here, a brief description of the experiment and to what it may be applie..

4.2 Thermochemistry

Ionization and appearance energy measurements establish energy levels for the molecular and ion fragments as outlined in chapter 3. Calculated ionic heats of formation obtained from IE values will be specific for the ion having *at least initially* the same structure as the neutral molecule.

The AE of a fragment ion provides an upper limit for the heat of formation of that ion, the excess energy being dependant on the kinetic shift and energy of the reverse reaction as seen in *figure 3.5*. Consider the fragmentation of Benzonitrile,

$$[C_6H_5CN]^{+\cdot} \rightarrow [C_6H_4]^{+\cdot} + HCN \qquad \textit{eq.(4.1)}$$

Due to the unusually large kinetic shift involved in this reaction, the reduction of the mean fragmentation rate constant, from 10^5 to 10^4 s^{-1}, caused the measured AE to be reduced by ~0.3eV (51). Thus where an ion fragment is produced both in the source and metastable time frame, indicating a possibly significant kinetic shift (section 3.2.V), the AE of the ion of both origins should be measured. The lower AE, indicating reduced excess energy of the ion fragment, should then be used. Measurement of the metastably generated ion also serves to define and isolate the specific reaction channel, because ion source species may be a mixture or have multiple origins. Consider Oxalic acid which generates both $[C(OH)_2]^{+\cdot}$ and $[HCOOH]^{+\cdot}$ on electron impact in the ion source. $\Delta H_f°[C(OH)_2]^{+\cdot}$ could only be obtained by measuring the AE of the *metastable* ion, since no $[HCOOH]^{+\cdot}$ is produced metastably, (52).

$$[COOH]_2^{+\cdot} \xrightarrow{*} [C(OH)_2]^{+\cdot} + CO_2 \qquad \textit{eq.(4.2)}$$

Where the species with a mass-to-charge ratio of interest, consists of a mixture of isomers as in the above example, the AE experiments will yield the $\Delta H_f°$ for the thermodynamically most stable isomer in the mixture. Thus great care must be taken to ensure purity of sample and ion flux, since trace contaminants which produce a more stable ion will yield an uncharacteristically low AE and thus $\Delta H_f°$ for the ion.

Once the heat of formation has been obtained for an ion of known mass and composition, it is sometimes possible to assign a structure based on the

extensive literature concerning ion enthalpies. The experimentally derived heat of formation of an ion may also be compared with isomeric 'reference' ions of known structure and heat of formation. They may be compared with *estimated* ionic heats of formation based on correlations involving homologous series (53); the relation between ionization energies and ion size (54), the effect of group substitution on a charge bearing site (55), and the correlation of the heterolytic bond strength $D(R^+-H^-)$ with ion structure and size (56). In the case of relatively small ionic species, the $\Delta H_f°$ measured experimentally may be compared with those obtained by ab initio molecular orbital theory calculations.

However, thermochemical data alone are rarely sufficient for confident structure assignments. Distinct isomeric species may have $\Delta H_f°$ values which are the same, within experimental error. For example the measured $\Delta H_f°[CH_3CH_2Cl]^+\cdot \approx \Delta H_f°[CH_3CHClH]^+\cdot$ (57). Likewise, ions generated with similar structure but within a different internal energy range may yield different 'apparent' heats of formation. The added information derived from the unimolecular and collision-induced dissociation characteristics may strengthen the tentative assignment, point to a more logical choice of structures, or reveal complications which make more detailed analyses necessary.

Consider the fragmentation of ionized aniline,

$$[C_6H_5NH_2]^+\cdot \rightarrow [C_5H_6]^+\cdot + [H,N,C] \qquad \textit{eq.(4.3)}$$

The AE of $[C_5H_6]^+\cdot$ was found by Baer and Carney (58) and Lifshitz et al. (59) to lie ca. 0.8eV above the calculated threshold for ionized cyclopentadiene plus HCN. Lifshitz et al. (59) proposed that this apparent excess energy could be accounted for if the neutral product were hydrogen isocyanide, HNC, because $\Delta H_f°[HNC]$ is 0.6±0.1 eV greater than $\Delta H_f°[HCN]$ (60). This argument, based on the thermochemistry, was substantiated when the technique of collision-induced dissociative ionization, CIDI, was applied to the neutral product (39), and the results were consistent with the structure HNC.

In another example, taken from the present work, the thermochemical analysis of the $[C_2H_5F]^+\cdot$ fragment ion from methyl fluoroacetate was

less helpful. The measured (adiabatic) AE of $[C_2H_5F]^{+\cdot}$ generated from FCH_2COOCH_3 resulted in a $\Delta H_f^{\circ}[C_2H_5F]^{+\cdot}$ of 873 kj mol^{-1}, some 63 kcals mol^{-1} below that of the ΔH_f° of 936 kj mol^{-1} calculated from the (vertical) IE of ethylfluoride. This discrepancy was initially credited to the formation of a more stable ylid ion, $[CH_3FCH_2]^{+\cdot}$. The dissociation characteristics of this 'new' ion however corresponded *exactly* to those of ionized ethylfluoride. The discrepancy in the appearance energies was explained when the *adiabatic* ionization energy of ethylfluoride was measured and found to be some 0.65eV below that of the vertical value.

4.3 Metastable Dissociations

Metastable ions, M_1^{+*}, restricted by definition to those ions which decompose within a limited time-scale of 10^{-6}-10^{-5}s, possess a narrow range of relatively high internal energies as illustrated in *figure 4.1.* Thus, of all source generated M_1^+ ions, those capable of undergoing metastable decompositions are the most likely to undergo rearrangement to another structure prior to fragmentation. Metastable peaks are therefore often characteristic not of the *ground state*, ionization-threshold structure of the precursor ion, but rather of the *reacting configuration* (RC) resulting from rearrangement of the original ion. Metastable ion mass spectra are therefore more useful for comparative analysis than for structure elucidation, and thus, without additional information, species generating closely similar metastable peak intensities, shapes, and kinetic energy releases are concluded to have the same reacting configurations rather than the same ground state structures.

4.3.I The Metastable Peak Abundance Ratio

The first semi-quantitative relationship between metastable peak intensities and the structure of a fragmenting ion was proposed in 1966 by Shannon and McLafferty (61), following a related study by Rosenstock et al. (62). The *'metastable peak abundance ratio test'* was based on the premise that when two (or more) competing fragmentations from the same ion give reasonably intense metastable peaks, then the *ratio* of the

abundances (measured under carefully controlled experimental conditions) may be used as a criterion for ion structure. Simply, dissociation to give the same m/z peaks, with closely similar intensity ratios, is good circumstantial evidence that the reacting configurations of the two precursor species must be the same. These peak abundances may be measured in terms of peak height or area. Under conditions of low energy resolution peak heights should be used, while peak areas will result in more representative values under high resolution. In either case, comparisons must be made under equivalent resolution conditions.

The difficulty with this test lies in deciding what constitutes a significant variation in the ratios and thus non-equivalence of the RC structures. The ratio can be very sensitive to experimental conditions such as ion lifetimes and ionizing electron energies as will be discussed below. Also, small impurities in the precursor ion flux, as seen in the case of $[C_2H_3O_2]^+\cdot$ (refer to chapter 5), may alter the ratio or introduce a false metastable peak to the MI mass spectrum.

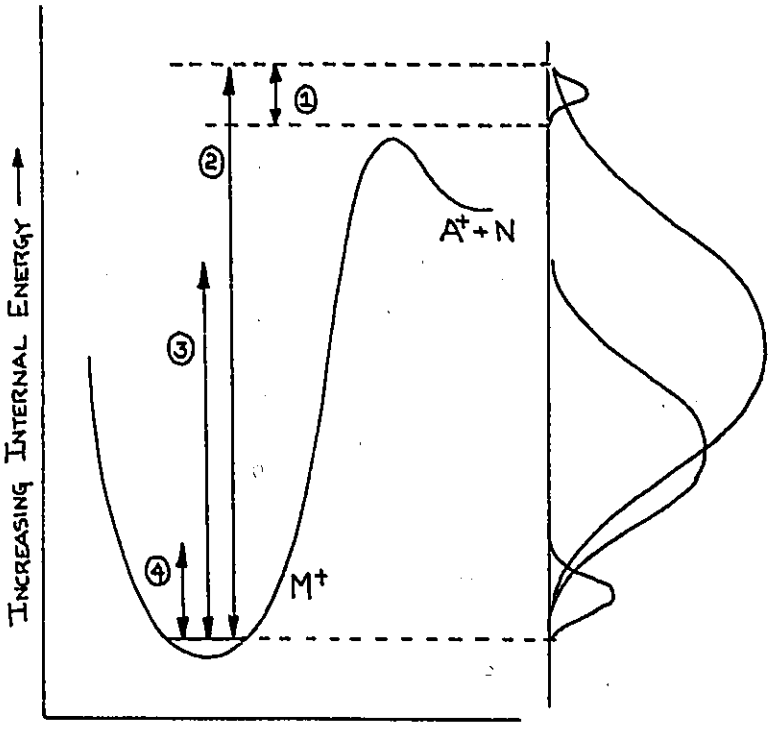

Figure 4.1 The range of internal energies of M+ sampled by experiment. 1. MI mass spectrum, sampling metastable M+ ions. 2. CID mass spectrum of source generated M+. 3. CID mass spectrum of M^+ under conditions of lower electron energy &/or translational energy. 4. CID mass spectrum of M+ species generated metastably.*

4.3.II Metastable Peak Shapes

Comparison may also be made of the metastable peak shapes. Equal shapes, under conditions of high energy resolution, point to similar RC species or mixture of species, while differences may indicate variation in experimental conditions and/or differences in the structure of the precursor's RC, or of the resultant fragments. Metastable peak shapes are classified into three broad categories, introduced in chapter 3.2, Gaussian, flat or dished-topped, and composite. The number of components in a composite metastable peak, indicates the number of transition states involved. They most frequently result from the combination of two separate peaks (37), Gaussian and/or dished or flat-topped. Thus a composite peak may indicate two transition states and/or two isomeric or isobaric daughter ions. The unequivocal classification of a composite metastable peak is difficult but isotopic labelling, AE measurements, and varying the electron energy and ion lifetimes may enable the separate processes to be identified. In many cases, however, their origin remains unexplained.

For example, the intense metastable peak for the loss of $CH_3\cdot$ from ionized 1-methyl cyclopentene is composite, composed of two Gaussian peaks. Careful analysis showed that the $[C_5H_7]^+$ daughter ion, the stable cyclopentenium ion, was generated by both a low energy process, the specific loss of the exocyclic methyl group, and a higher energy process, involving complete hydrogen scrambling prior to methyl loss (63). A composite shape may however, also indicate that the metastable peak has an unusually large cross-section for collisional activation. Collision gives rise to peaks of Gaussian type which are relatively broad, typically 50 V at half height. Gaussian type metastable peaks are usually less than 20 volts at half height, although the half height widths of metastable ions may range from less than 1 volt to greater than 100 volts. The possibility of collisional contributions may be tested for in the following ways. Careful comparison of the peak height increase with introduction of collision gas into the collision cell; the CID component should increase in direct proportion to the pressure while the unimolecularly generated species will not be affected. Applying a voltage to the cell (refer to *figure 3.9*) will cause the peak to be divided into two

peaks of nonequivalent shapes if collisional activation is taking place and assuming that the background pressure is largest in the cell region, even under MI conditions.

The use of $T_{0.5}$ values to characterize the reacting configuration structure of metastably fragmenting ions was proposed in 1973 by Jones et al. (64) who suggested that fragmenting ions having the same RC should show similar $T_{0.5}$ values. It has been concluded that the effect of ion preparation on the shape and T value of a metastable peak which unequivocally arises from a single reacting configuration will be small (65). Thus differences in the kinetic energy release, under similar experimental conditions, are indicative of non-equivalent processes, or mixture of processes.

4.3.III Ion Lifetimes

Comparisons may also be made *within* a system via the effects of changing ion lifetime, ionization energy, and isotopic labelling. By making measurements in the first and second field-free region of the VG ZAB-2F mass spectrometer, metastable ions of lifetimes 1-2μs and 10-15μs respectively are sampled. The abundance ratio may be affected if the dissociation rate constants vary quite differently with excess internal energy, i.e. if the k(E) versus E curves for the competing unimolecular fragmentation processes have markedly different slopes. Consider the metastable reactions of $[C_3H_7O]^+$ ions derived from diethyl ether,

$$[C_3H_7O]^+ \overset{*}{\rightarrow} C_2H_4 + CH_2OH^+ \qquad \textit{eq.(4.4)}$$
$$\overset{*}{\rightarrow} H_2O + [C_3H_5]^+ \qquad \textit{eq.(4.5)}$$

where the variation of the ratio, m_1^*/m_2^*, with reaction time is quite clear; a value of 3.6 was recorded in the first field-free region of the MS-902S mass spectrometer, and 16.0 and 16.7 in the second field-free regions of the MS-902S and VG ZAB-2F mass spectrometers respectively (65,66). A lower measured kinetic energy release with increased lifetime may also result if the dissociation process involves a significant kinetic shift. On the other hand, the unexpected composite nature of a metastable peak may be revealed by a marked increase (with increased lifetimes) in $T_{0.5}$ (51,67).

4.3.IV Ionizing Electron Energy

Reduced ionizing electron energies may also result in an abundance ratio change since the dissociation process of lowest activation energy will be increasingly favored. For composite metastable peaks, this may in turn affect their shape and measured $T_{0.5}$ value. Such is the case for $[C_3H_3O]^+$ ions generated from [CH≡CCH$_2$OH]. At normal electron energies the composite metastable peak corresponding to $[C_3H_3O]^+ \xrightarrow{*} CO + [C_2H_3]^+$ is relatively narrow (20 V at half height) but skirted, resulting from dissociation of two isomers, (a) [CH$_2$CHCO] and (b) [CH≡CCHOH] (68). At reduced ionizing electron energy, the broader component from fragmentation of (b) is reduced, changing the shape and reducing the T value of the metastable peak.

Finally, the time-honored method of isotopic labelling of the metastable precursor may give valuable insight into the (rearrangement/cleavage) dissociation mechanism, as well as to what extent the atoms change their position within the ion, before fragmenting in the metastable time frame.

4.4 Collision Induced Dissociation

As discussed above, unimolecular dissociations result from precursor ions with internal energies sufficient to fragment within the 10^{-6}-10^{-5} s time-scale. These dissociations correspond necessarily to processes having the lowest barriers to dissociation, and thus only a limited number of fragment peaks are produced. The relatively high excess internal energies that they possess, as seen in *figure 4.1*, cause these metastable ions to be the most susceptible to rearrangement prior to dissociation. Thus MI mass spectra, while often structure specific, are less often structure *characteristic*. Causing the ion to collide with a neutral atom or molecule can add a substantial amount of energy to the stable source generated ion, energy which may be sufficient to cause fast subsequent ion decomposition. The potential of collision-induced fragmentation of precursor ions for ion structure work was first recognised by McLafferty and co-workers (69,70) in 1973. As can be seen from *figure 4.1*, the precursor ions which suffer collisional activation are

those species which have internal energies ranging from zero up to the lowest threshold for decomposition. Note that the upper limit *includes* the narrow range of internal energies corresponding to metastable precursors. Those ions however, with lower internal energies are much less likely to have undergone rearrangement prior to collision-induced dissociation. The much greater internal energy content of those same ions just *after* collision will ensure fast decomposition over a wide range of pathways. These induced decompositions will include many bond cleavages directly generating structure characteristic fragments.

4.4.I Structure Characteristic CID Mass Spectra

Structure assignment may be based on comparison, i.e., if the CID spectra of species M_1^+ and M_2^+ are the same, then so are the structures of M_1^+ and M_2^+. However CID mass spectra are more versatile, for the initial structure of the precursor may be elucidated from the large number of characteristic fragment peaks produced by direct bond cleavages. Consider for example the use of collision-induced dissociation in the investigation of stable $[C_2H_6O]^+\cdot$ isomers (71). Representative bar graphs of the partial CID spectra of five known isomers are given in *figure 4.2.* The first two $[C_2H_6O]+\cdot$ species investigated, for which a stable neutral counterpart exists, were the molecular ions of ethanol and dimethylether, a) $CH_3CH_2OH^{+}\cdot$ and b) $CH_3OCH_3^{+}\cdot$ respectively (72). Their CID spectra are unique; that of ionized ethanol possessing m/z=14,15 and 31, indicates clearly the presence of CH_2, CH_3, and CH_2OH, while that of ionized dimethylether, generating little other than m/z=15 and 29, points to CH_3 and CHO from the unstable CH_3O fragments. 1,3-propanediol, via CH_2O loss, was concluded (72) to yield a π-bonded complex of a water molecule to an ethylene ion, represented simply as c) $CH_2CH_2OH_2^{+}\cdot$. The dominance of m/z=14 and 28 as well as the presence of m/z=18 indicated the lack of a CH_3 unit. The major generation of $[C_2H_4]^+\cdot$ by easy water loss, and the presence of H_2O were all consistent with this assignment. Methoxyacetic acid is believed to generate d) $CH_3O(H)CH_2^{+}\cdot$ by CO_2 loss. Correction for isobaric ion interferences and ^{13}C contributions must be made to its CID mass spectra (71). The lack of m/z=26 and 27 indicate no C-C bond, while the presence of m/z=31 shows the likely presence of a CH_2OH group. Lactic acid was concluded (71) to generate the isomer

$CH_3CHOH_2^{+\cdot}$ via loss of CO_2. Thus the CID spectra indicated not only that unique isomers were formed, but also something of their structure.

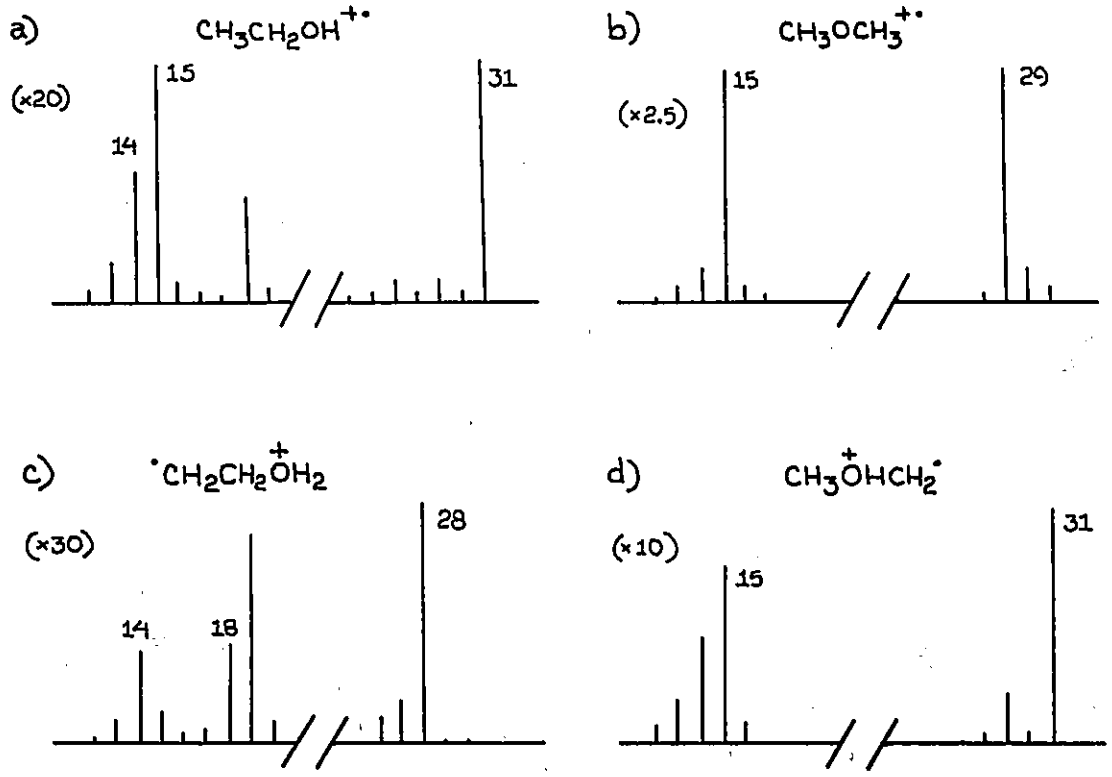

Figure 4.2 Partial collision induced dissociation mass spectra of isomeric $[C_2H_6O]^{+\cdot}$ ions represented as bar graphs. Refer to text.

CID mass spectra will be specific for each of a given series of isomeric ions *provided* that the following three criteria are met.

(i) The isomeric ions do not freely interconvert at energies below that for the lowest energy decomposition.

When CID (and MI) spectra are identical; as in the $[C_7H_{11}]^+$ system, where the m/z=95 CID spectrum from 2-iodonorbornane, and 2,4-octadiene were indistinguishable (73), isomerization to a common ion or mixture of ions has occurred prior to dissociation. The generation of ion specific (non-equal) spectra may however, still be possible by lowering the range of internal energy possessed by the ions below that of the barrier to isomerization. The generation of CID spectra from ions possessing relatively low internal energy is possible, but in all cases the intens-

ities of the peaks are strongly reduced and at least a minimum signal-to-noise ratio must be maintained. The simplest way of varying internal energy is by lowering the ionizing electrons' energy (74). Lowering the translational energy of a mass-selected ion also narrows and reduces the range of collisionally derived internal energy (75). The mass-selected ions generated metastably in the first field-free region however, possess internal energies within the lowest achievable range. Thus with a sufficiently lo internal energy range, the interconversion of the ions may be reduced and the resultant CID spectra will no longer be indistinguishable.

(ii) There are sufficient significant, non-isobaric fragmentations to render the spectrum clearly characteristic.

In most isomeric systems, as for example that of $[C_2H_6O]^{+\cdot}$ above, the spectra are clearly characteristic. However for isomeric ionic hydrocarbons, these characteristic spectral differences are often very minor. The CID spectra for the benzyl and tropyl ion are considered to be structure specific only in the ratio of the peak intensities of m/z 74:77 (76), very minor peaks in the CID mass spectrum.

(iii) The collisionally activated ions do not undergo very fast rearrangements prior to dissociating.

The elimination or reduction of such a post collision rearrangement while maintaining CID conditions is not possible. The high internal energies obtained on collision however, are expected, in the large majority of cases, to enhance the kinetically favored bond cleavages, not the thermodynamically favored rearrangements.

4.4.II Comparing The Spectra

In analyses of isomeric ions, comparison of the CID spectra of the species in question with those from reference ions of known structure is necessary. With the exclusion of metastable processes, whose intensities are often quite dependant on the internal energy distribution, the peak intensities in a CID spectrum are generally held to be independent of the initial internal energy of the precursor, due in part to the large excess of energy obtained in the collision process. This ensures reproducibility and enables direct comparisons of ions whose different

mode of formation/ionization may have generated ions of quite different internal energy distributions. Comparison of the CID and EI mass spectra is also possible for molecular ions. As in the case of ethyl fluoride for example, in *figure 4.3*, the similarities are quite obvious, leading to the conclusion that (i) and (iii) above are upheld. For fragment ions, comparison of the normal CID and those CID mass spectra generated from lower internal energy species is also possible. Similar resultant spectra indicate the presence of a single ion structure and the absence of isomerization, within the energy range sampled.

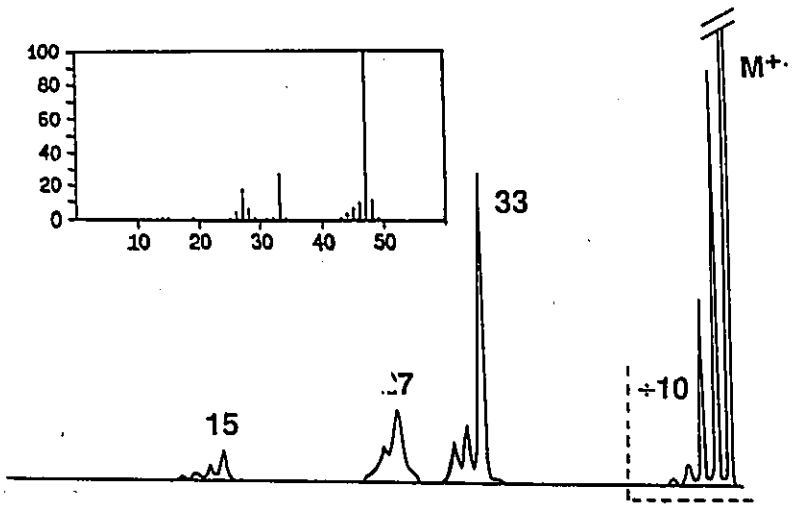

Figure 4.3 The EI and CID mass spectra of ethyl fluoride, illustrating very similar fragment peak patterns.

4.4.III Isotopic Labelling

Isotopic labelling can further probe the possibility of atom scrambling and precursor isomerization prior to dissociation. CID mass spectra of labelled and unlabelled species may however, only be qualitatively compared, because of the operation of isotope effects of unknown magnitude. Consider for example the following collisionally induced dissociations of the molecular ion of ethanol.

$$CH_3CH_2OH^{\ddagger +}\cdot \rightarrow CH_3CH_2^{+} + OH\cdot \qquad \textit{eq. (4.6)}$$

$$\rightarrow CH_3\cdot + {}^{+}CH_2OH \qquad \textit{eq. (4.7)}$$

If the CID mass spectrum of the labelled species, $CH_2CH_2OD^{+\cdot}$, showed only $CH_2CH_2^+$, m/z=29, and $^+CH_2OD$, m/z=32, it could be concluded that neither rearrangement nor atom scrambling occurred prior to dissociation. On the other hand formation of both $C_2H_4D^+$ and $^+CH_2OD$ may have resulted from scrambling, while formation of only $C_2H_4D^+$ and $^+CH_2OH$ would have indicated a specific rearrangement of the initial structure.

Thus the technique of CID mass spectra, via comparison or direct interpretation, is a very powerful method for structural elucidation. It is limited to some extent by the potential energy surface of the system involved, i.e. how the barriers to isomerization(s) and dissociation(s) are related as discussed in section 2.3.III.

4.5 Charge Stripping

Charge stripping, CS, is a technique which may be used only if the doubly charged species of the precursor of interest are sufficiently stable to be observed under optimal CID conditions, and provided that they are not obscured by singly charged fragment ions of the same m/z ratios. CS mass spectra have been found crucial in the identification of the two isomeric $C_3H_6^{+\cdot}$ ions from propene and cyclopropane, whose CID mass spectra are very closely similar (77). It was considered that the charge stripping spectra arose predominantly from ions of lower average internal energy (and hence structure retaining) as discussed in (78). More recently, in the investigation of the norbornyl cation in the $[C_7H_{11}]^+$ system, the charge stripping mass spectra alone generated structure specific characteristics, apart from just one peak in the CID (75) experiment. In the case of ionized methyl chloride and its ylid isomer, $CH_2ClH^{+\cdot}$, the CS mass spectra are very distinctive (79) and have been the basis of arguments for and against rearrangement (48,80). If the CS mass spectra are identical then the reacting configurations must be the same and vice versa.

4.6 Collision Induced Dissociative Ionization

The technique of collision induced dissociative ionization, CIDI, isolates and analyses the neutral fragments accompanying unimolecular decompositions of mass selected precursors. Assuming the neutral species do not isomerize prior to collision or directly thereafter, their CIDI mass spectrum will reflect their structure. These neutrals, as well as the accompanying metastably generated ionic fragments, will in general, possess little internal energy, thus, for relatively stable species, rearrangement is very unlikely prior to collision. The highly excited species produced by collision are capable of isomerizing at such high internal energies. However, even if isomerization and dissociation are both energetically feasible, direct dissociation is often just as fast or faster than isomerization. The structure characteristic CIDI mass spectra may be compared with isomeric ionic analogues.

4.6.I The Neutral Fragment

Although not a direct technique for the structural elucidation of isomeric ionic species, a CIDI mass spectrum may nevertheless prove informative. Consider the metastable dissociation,

$$[M_1^+] \xrightarrow{*} A^+ + N \qquad eq.(4.8)$$

The heat of formation of A^+, calculated from the following equation introduced in chapter 3.2,

$$AE = \Delta H_r = \Delta H_f^\circ[A^+] + \Delta H_f^\circ[N] - \Delta H_f^\circ[M_1] \qquad eq.(4.9)$$

is dependant on the heat of formation of the accompanying neutral. Knowing the correct structure of N will ensure that the appropriate $\Delta H_f^\circ[N]$ is used. For the metastable dissociation of aniline, assignment of the correct neutral structure, (HNC not HCN), lent considerable strength to the measured appearance energy of the ionic fragment (39,59). As well the structure of the neutral may reflect the reacting configuration of the precursor ion, M_1^+. In the case of methyl acetate, the detailed mechanism proposed for its metastable fragmentation (81,82) was based on $[CH_3O\cdot]$ as the structure of the unimolecularly generated

neutral. CIDI of the neutral showed that its structure was, surprisingly, chiefly [$\cdot CH_2OH$] (39).

4.6.II The Neutral Molecule

Indirect analysis of molecular ions, $M_1^{+\cdot}$, is possible by CIDI, if the proton bound dimer, $[(M_1)_2H]^+$, generated under conditions of high ion source pressure, is capable of unimolecular dissociation in the second field free region as follows:

$$[(M_1)_2H]^+ \xrightarrow{*} M_1H^+ + M_1 \qquad \textit{eq.(4.10)}$$

The subsequent collision induced dissociation of the neutrals thus results in the analysis of M_1 species of near threshold internal energies. Thus where potential isomerization of a molecular ion is possible, comparison of its CID mass spectrum and the spectrum obtained from collision induced dissociation of the fast neutrals obtained via *eq.(4.10)* should be made. Non-isomerization may be concluded where very similar spectra are obtained. Such similarity has been observed between the CID mass spectrum of acetic acid, and the CIDI mass spectrum of its proton bound dimer (9).

4.7 Neutralization-Reionization

Neutralization-reionization mass spectrometry is the most recently introduced procedure for the structural analysis of isomeric systems. It is, as well, the most complex technique, involving the two steps of collisional neutralization followed by collisional reionization and dissociation. At present the mechanisms involved are far from completely understood.

Charge exchange (CE) between atoms has been studied extensively (83) and the occurrence of CE between organic ions and target species is well known (84), although no reports have considered the resultant internal energies of the neutrals produced. The stability of the neutral, and thus the NR mass spectrum of its corresponding ionic species, will depend

on how this internal energy relates to energy barriers for dissociation and/or isomerization. The neutralization target is chosen to ensure that the CE process is slightly endothermic (as discussed in chapter 3.7) with the intention of producing a good flux of high velocity neutral species having *low* internal energies and thus experimentally useful lifetimes, i.e. >1μs. It is, however, difficult to distinguish whether the generation of a structure specific NRMS, as for the benzene molecular ion (9), results from little excess internal energy being imparted on collisional neutralization or the relatively high stability of the neutral.

4.7.I Generation of the Neutral

Interpretation is also complicated by the various origins of the neutral species within the undeflected neutral beam. They may be generated by both collisional and unimolecular dissociation as well as those from charge exchange (and possible subsequent fragments of these neutrals will result in still others). This is well illustrated in the NRMS of the acetyl cation (9) which is dominated by CO^+, m/z=28, produced via the following four processes.

a) $[CH_3CO]^+ \xrightarrow{*} CH_3^+ + [CO] \xrightarrow{He} [CO]^+\cdot$

b) $[CH_3CO]^+ \xrightarrow{Xe} CH_3^+ + [CO] \xrightarrow{He} [CO]^+\cdot$

c) $[CH_3CO]^+ \xrightarrow{Xe} [CH_3CO]\cdot \xrightarrow{*} CH_3\cdot + [CO] \xrightarrow{He} [CO]^+\cdot$

d) $[CH_3CO]^+ \xrightarrow{Xe} [CH_3CO]\cdot \xrightarrow{He} [CH_3CO]^+ \xrightarrow{*} [CO]^+\cdot$

The contribution of neutral fragments from the unimolecular dissociation of ionic precursors prior to cell 1, process (a), may be semi-quantitatively separated from NR spectra by placing a sufficient voltage on cell 1 (similar to the separation of collisional and unimolecular processes using cell 2 as outlined in *figure 3.9*). For the shorter cell 1, the separation is less specific since only ~80% of collision induced processes occur within the gas cell (9), and thus a comparison of separation for peaks with and without contributions from (a) should be made. Separation is advisable when comparing NRMS of isomeric species or the NRMS, CID, or EI mass spectra of a single species, since, as discussed earlier, metastable processes may be significantly dependant on the internal energy distributions, while the reproducibility of collision-induced processes has proven to be far less affected.

4.7.II Structure and Stability

Despite difficulties in direct interpretation, the NRMS of a compound whose *molecular ion* does not readily undergo extensive isomerization may be expected to be similar to the normal EI mass spectrum thereof. Excitation of the neutral via 70eV electron impact in the source and via the target gas O_2 in the collision cell, are comparable. The vertical excitation process predominates and a wide range of internal energy is deposited. The NRMS of M_1^+ may also be compared with the CIDI mass spectrum of the metastably generated M_1° neutral. This is only possible, however, where a proton bound dimer, $[(M_1)_2H]^+$, formed in the ion source, fragments metastably to give the neutral, M_1. For fragment precursor ions the possibility of isomerization may be probed by comparison of the NR and the CID mass spectra.

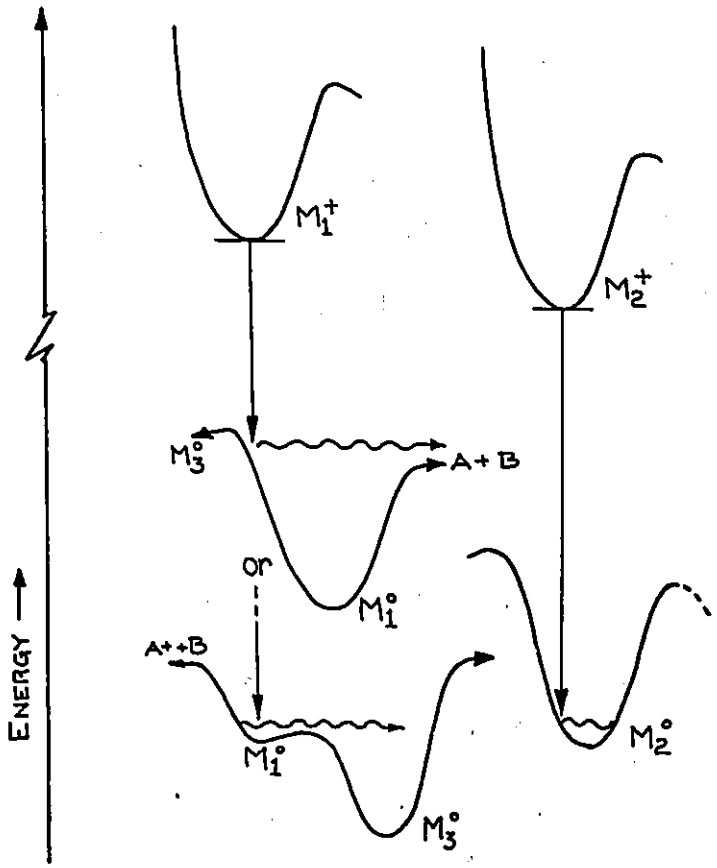

Figure 4.4 Vertical neutralization of M_1^+ and M_2^+. M_1^+ produces an unstable neutral, M_1°, which will isomerize to M_3° &/or dissociate to A + B. M_2^+ produces a stable neutral, M_2°.

In the case of both benzene and acetic acid molecular ions (9), the close similarities of the EI, CID, CIDI (in the case of acetic acid where dimer formation was possible), and NR mass spectra, indicated that the ionic and neutral species did not undergo any major rearrangements. Thus the neutral and ionic species are of much the same structure and stable on the mass spectrometric time scale. Significant dissimilarities may result when vertical neutralization does not lead to the formation of stable neutrals as illustrated in *figure 4.4*. The lack of a recovered ion, M_1^+, and other high m/z fragments, such as $[M-1]^+$, $[M-2]^+$, may indicate the rapid decomposition of an unstable neutral, as for acetyl in process (c) above. The resultant NRMS of such neutrals may nonetheless generate structure specific peaks through the reionization of their dissociation products. Conversely, dissimilarity of the NRMS and CID, in the presence of 'recovered ions', may well indicate that M_1° is reactive, rapidly rearranging to some more stable isomeric neutral, M_3°.

NRMS may become a particularly useful technique to produce and study unstable and reactive neutrals whose parent ions are stable. Ideally, the stable parent ion is generated *uniquely* and then neutralized; the neutral or its products of fragmentation are subsequently excited by collision causing dissociative reionization. Whether a particular neutral is indeed likely to be analyzed by NRMS will depend on the energy of the vertically neutralized species with respect to that of the transition structure for subsequent rearrangement or fragmentation. Consider the chloronium ylide, CH_2ClH, and its isomer, methyl chloride, CH_3Cl. Both the ylid and conventional molecular ions are stable within the mass spectrometric time scale, however, the neutral ylide was found, by theoretical calculation, to be located in only a very shallow potential well of ~1 kJ mol^{-1} (85,86). Thus it was predicted that the ylide should not survive the neutralization experiment but dissociate to $:CH_2$ + HCl and/or $CH_2Cl\cdot$ + $H\cdot$. The observation of 'recovered ions' believed initially to be $CH_2ClH^{\cdot+}$ (45), have since been credited with the interference of source generated $CH_3Cl^{\cdot+}$ ions (87).

Neutralization of an ion may also provide additional structural information in making a given structure characteristic dissociation pathway more

definitive. In the gaseous protonation of alkyl benzenes, the site of protonation could not be defined from conventional CID spectra. The dissociation of the corresponding neutral isomers were considered to be more selective (45). An extreme example of this intensified selectivity has been discovered in the $[C_7H_5X]$ isomeric system and will be introduced in chapter 6.

Appendix

Below is a brief summary of the dissociative mass spectrometric techniques which have been defined and discussed in terms of isomeric gas phase ion analysis in chapters 3 and 4 respectively. They will be applied to the analysis of two isomeric systems in chapters 5 and 6.

Metastable Ions - MI

The MI mass spectrum records the fragment ions, produced unimolecularly in the first or second field-free regions, from source generated metastable ions, M_1^{+*}.

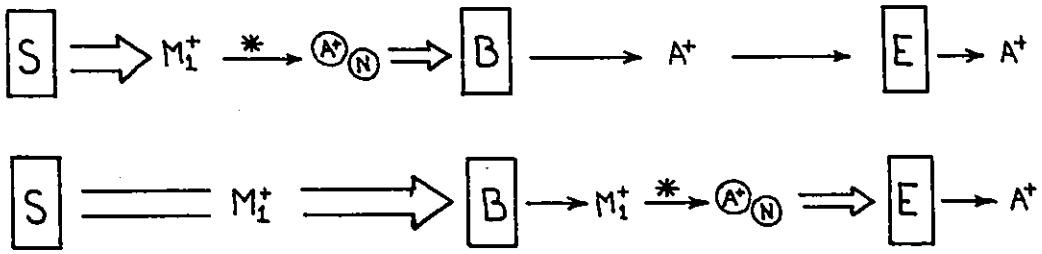

The M_1^{+*} sampled, fall into a narrow range of internal energies near the energy for M_1^+ dissociation, and have lifetimes of 10^{-6}-10^{-5} s. These species sampled by MI are the most energetic M_1^+ and thus most likely to have undergone some rearrangement process prior to dissociation.

Peak shapes and kinetic energy releases, $T_{0.5}$, may be compared under conditions of high resolution. Where more than one metastable peak is generated, their relative intensities may also be compared.

Collision Induced Dissociation - CID

Scanning the electric sector records the fragment ions produced by collisional excitation and rapid subsequent dissociation of source generated ions, M_1^+, in the second field-free region. In the majority of cases, CID spectra are more intense than MI, CS, CIDI, and NR mass spectra.

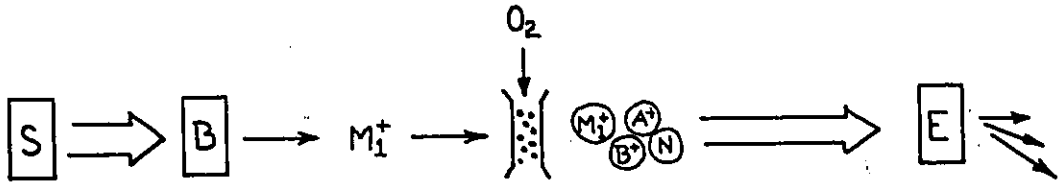

The M_1^+ sampled via CID fall within a wide range of internal energies, from the ionization threshold of M_1^+ to the high internal energies possessed by metastable species. The average internal energy content may be reduced by lowering the electron energy and/or translational energy. Alternatively, first field-free region metastably generated M_1^+ have the lowest obtainable average internal energy. The lifetimes of these ions are of the order of 10^{-5} s.

Comparison of CID spectra may be made (excluding metastable processes) as well as direct interpretation of the peaks with respect to ion structure.

Charge Stripping - CS

CS and CID mass spectra are obtained in a similar fashion, but the characteristically narrow, doubly charged CS peaks will be seen at one half of the accelerating potential. "Soft" target species, such as O_2, are recommended for higher yields. Not all ions however, generate a measurable CS and as well interference from more intense singly charged species is possible.

The M_1^+ ions sampled are of similar lifetimes as those undergoing fragmentation due to collision, but their internal energies are in general somewhat lower. Comparison of the relative intensities of the doubly charged ions may be made under conditions of equal resolution.

Collision Induced Dissociative Ionization - CIDI

The neutrals generated unimolecularly, in the second field-free region, from source generated M_1^{+*} are isolated by placing a voltage on the deflector electrode. Collisional excitation results in rapid dissociation and ionization, and resultant fragment ions of the neutral are analyzed by the electric sector.

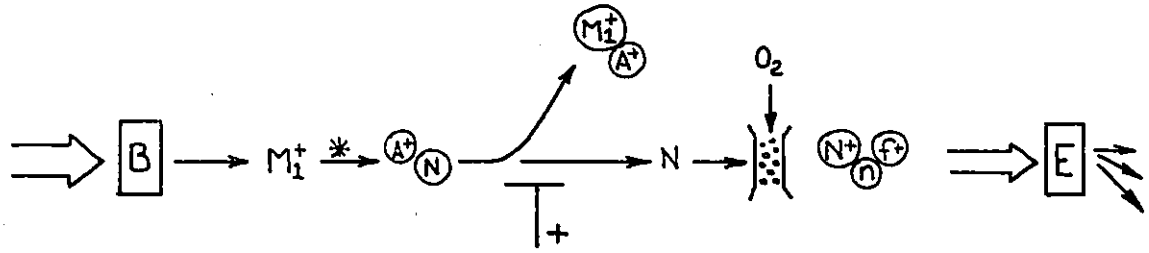

The neutrals possess little internal energy prior to collision, and their lifetimes are of the order of a few microseconds.

CIDI mass spectra, characterizing the structure of the neutral, may be compared with CID spectra of the corresponding ions and/or interpreted directly. Unimolecular dissociation of a source generated dimer, $[(M_1)_2H]^+$, giving $M_1°$ in the second field-free region allows the analysis of low internal energy $M_1°$ by CIDI.

Neutralization Reionization Mass Spectra - NRMS

NRMS are obtained by; colliding mass selected, source generated ions, M_1^+ with a target gas such as Xenon, to induce neutralization via charge exchange, then deflecting all ionic species from the beam path, and finally collisionally exciting the isolated neutrals producing rapid subsequent dissociation and/or reionization.

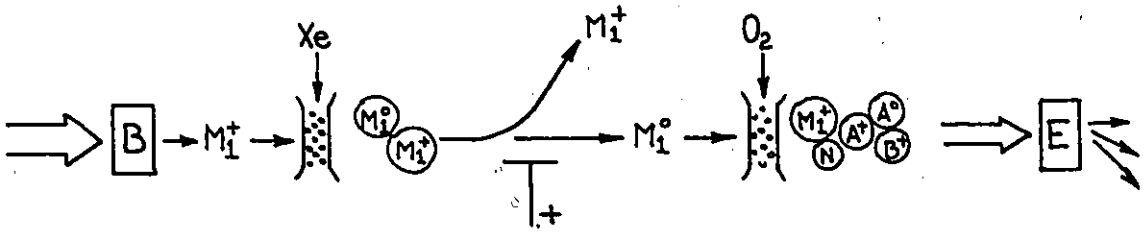

The M_1^+ species are of similar internal energy content and lifetime as those analyzed by their CID mass spectra. However, unlike CID, NRMS will reflect the stability and structure of the neutral M_1. As well as producing structure characteristic ionic fragments, the NRMS may be compared (excluding metastable processes) with the CID and EI (in the case of a molecular ion) mass spectra of M_1^+.

Chapter 5

THE $CH_3O-C^+=O$ ION AND ITS ISOMERS

5.1 Introduction

The subject matter of this chapter forms part of collaborative research involving the Department of Theoretical Chemistry at the University of Utrecht, and the Mass Spectrometry Laboratories at the Universities of Ottawa and Utrecht, and has been published in the Journal of the American Chemistry Society, 108, 7589, (1986).

Structural isomerism in gas-phase ions has received steadily increasing attention during the past 10 years, and the gas-phase chemistry of a number of stable ions of both familiar, e.g., $CH_3-C^+=O$ (88,89) and unexpected structure has been carefully studied. While conventional ions, such as $CH_3OH^{\neg+}\cdot$, may be known to be stable (and as such are confidently assigned in normal, EI mass spectra), the stability of ions of unconventional form, e.g., $CH_2OH_2^{\neg+}\cdot$ (90a,b), $CH_2CH_2OH_2^{\neg+}\cdot$ (91,92), and $CH_2=CH-O\cdot\cdot H\cdot\cdot OH_2^{\neg+}\cdot$ (93), must often be predicted by theoretical calculations. The structure and heat of formation of the simpler ions (say up to 6 or 7 atoms), can now be calculated via high level ab initio molecular orbital theory calculations with considerable accuracy. These predicted structures and energies, coupled with the experimental thermochemical data and dissociation characteristics, obtained via the mass spectrometric techniques already introduced, have enabled unconventional structures to be assigned with increasing confidence.

The $[C_2H_3O_2]^+$ system has been thoroughly investigated via experiment and it is believed that five distinct isomeric species have been identified. The structural assignment of these isomers has been based mainly on their respective dissociation characteristics. For four of these isomeric species, experimental heats of formation have also been obtained. High

level ab initio molecular orbital theory calculations have predicted the structure and relative stability of eleven isomeric ions of this $[C_2H_3O_2]^{+\cdot}$ system (94). The experimental mass spectrometric investigation, is outlined herein and where applicable, interpretation in terms of the theoretical calculations have been made.

The ions $CH_3\text{-}C{=}O^{+}$ and $HO\text{-}C{=}O^{+}$ and their isomers have been studied in considerable detail (75,88,89,95,96), however the closely related $CH_3O\text{-}C{=}O^{+}$ ion and its $[C_2H_3O_2]^{+}$ isomers have received little attention. Of the stable isomeric ions predicted by theory, only two such ions have been reported as characterized, albeit incompletely, by experiment. The first, the methoxycarbonyl cation, $CH_3O\text{-}C{=}O^{+}$, is frequently observed in the mass spectra of oxygen-containing compounds, corresponding to a mass-to-charge ratio of 59. The collision induced dissociation, CID, mass spectrum of this species has been reported (97), and m/z=59 is the base peak in the electron impact, EI, mass spectrum of methyl trifluoroacetate (98). Based on the assumption that it is $CH_3O\text{-}C{=}O^{+}$ which is generated by simple cleavage from simple methyl carboxylates via *equation (5.1)*,

$$RCOOCH_3 \rightarrow R\cdot + C(=O)OCH_3^{+} + e^- \qquad \textit{eq.(5.1)}$$

appearance energy, AE, measurements of the m/z=59 ion would then be expected to yield a consistent heat of formation, ΔH_f°, for this ion. Surprisingly, however, such a series of measurements by Briggs and Shannon (99) for $R{=}CH_3$, CH_3O, $NCCH_2$, $ClCH_2$, Cl, yielded ΔH_f° values ranging from 556 to 640 kJ mol^{-1}, and thus the heat of formation of this ion was not firmly established.

Dissociative ionization of ICH_2COOH has been proposed to yield a second $[C_2H_3O_2]^{+}$ isomer by $I\cdot$ loss, CH_2COOH^{+}. Its CID has also been reported (97), but no further characterization was made. The acyloxy cation, $CH_3\text{-}COO^{+}$, has been investigated theoretically and by experiment, but for the latter, only indirectly, since it is not a stable gas-phase species. The mass spectrum of the $[C_2H_3O_2]^{+}$ ions, obtained by collision induced charge reversal of acetate anions, $CH_3\text{-}COO^{-}$,

$$CH_3\text{-}COO^{-} \xrightarrow{He} CH_3\text{-}COO^{+} + 2e^- \qquad \textit{eq.(5.2)}$$

was interpreted in terms of the formation of transient acyloxy cations, in either a singlet or a triplet state (97). These ions undergo complete

dissociation in the energy manifold and time frame (~0.1μs) associated with the charge reversal experiment (37). Theoretical calculations (100,101) have indicated that the ion may isomerize into the energetically more favorable cyclic dioxyryl form,

eq. (5.3)

The decomposition to the fragments CH_3^+ and CO_2 from either of these species was nevertheless, calculated to be exothermic. The reactive acyloxy cation therefore, has not been considered among the proposed, stable $[C_2H_3O_2]^+$ isomers.

High level ab initio molecular orbital theory calculations have been carried out by P.J.A. Ruttink and R. Postma at the Department of Theoretical Chemistry, University of Utrecht, as part of a continuing collaborative investigation of the structure and gas phase chemistry of stable ions. From these calculations eleven isomeric $[C_2H_3O_2]^+$ ion structures (*figure 5.1*) and their relative energies (Table 5-1) have been predicted (94). These include the hydroxy-substituted oxiranyl and acetyl cations 2 and 4, two carbon monoxide hydrogen bridged species, 6 and 7, protonated glyoxal, 10, and the ion 11, which has earlier been proposed to be generated (102) by direct cleavage of $CH_3\cdot$ from ethylformate.

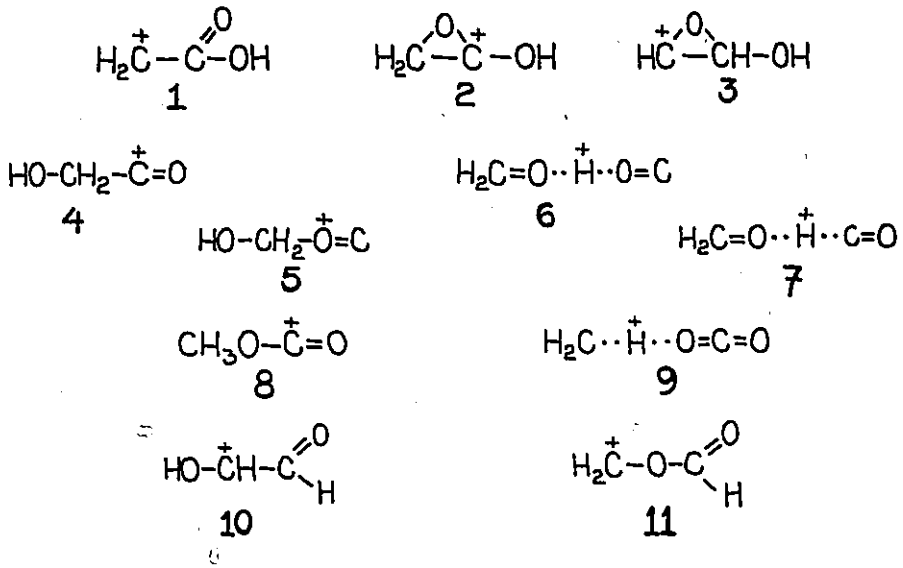

Figure 5.1 Eleven proposed stable isomeric forms of the $[C_2H_3O_2]^+$ ionic system, (94).

Briefly, standard LCAO-MO-SCF calculations were performed with the program GAMESS (103), employing restricted Hartree-Fock (RHF) procedures (104,105). Geometries were determined with gradient optimization procedures. Standard STO-3G (106a), 4-31G (106b), and 6-31G* (106c) basis sets were used. However, at the SCF level or with small basis sets, problems arose with respect to the relationship between small cyclic ions and their ring-opened counterparts, e.g., for the isomeric ions of $[C_2H_3O]^+$ (89) and $[C_2H_2O]^{+\cdot}$ (107). In the investigation of the $[C_2H_3O_2]^+$ system it was found that the SCF local minimum for 1 and 3 disappeared when electron correlation was included. Thus correlated wave functions in the geometry optimization were used via the CASSCF procedure (108) as implemented in the program GAMESS. CASSCF stands for the Complete Active Space Self Consistent Field procedure, and in view of the expense of such calculations the small STO-3G basis set was used. The procedure used to combine the effects of correlation and basis set extension for geometry optimization and total energy calculations for the ions is detailed in reference (94).

TABLE 5-1 Calculated Relative Energies for Stable Isomers in the $[C_2H_3O_2]^+$ Potential Energy Surface, and their corresponding enthalpies.

Structure	Relative Energy[1]	Absolute Energy[2]
1	[3]	
2	86 kJ mol^{-1}	590 kJ mol^{-1}
3	[3]	
4	15 kJ mol^{-1}	519 kJ mol^{-1}
5	[4]	
6	3 kJ mol^{-1}	507 kJ mol^{-1}
7	[4]	
8	0 kJ mol^{-1}	504 kJ mol^{-1}
9	114 kJ mol^{-1}	618 kJ mol^{-1}
10	47 kJ mol^{-1}	552 kJ mol^{-1}
11	39 kJ mol^{-1}	544 kJ mol^{-1}

[1]Calculated as described in ref 94 [2]Based on the experimentally derived enthalpy of 590 kJ mol^{-1} for 2 [3]No local minimum at CASSCF4/STO-3G level of theory [4]Not pursued at higher levels of theory

5.2 Results and Discussion

5.2.I Ions 1 and 2

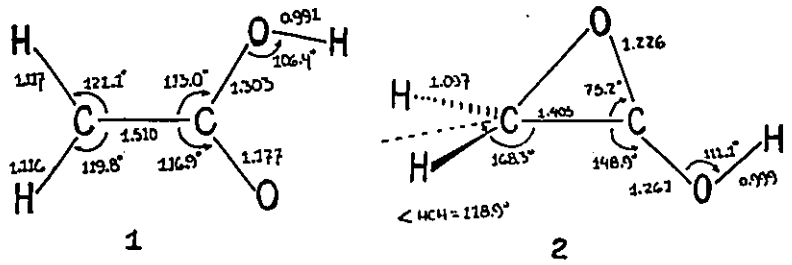

Figure 5.2 Geometry optimised structures of ions 1 and 2, as obtained via CASSCF4/STO-3G and corrected for correlation effects. (94).

The m/z=59 $[C_2H_3O_2]^+$ ions observed in the mass spectrum of ICH_2COOH may reasonably be proposed to have structure 1, resulting from the simple direct I-C bond cleavage,

$$I\text{-}CH_2C(=O)OH \rightarrow I\cdot + {}^{+}CH_2C(=O)OH \qquad eq.(5.4)$$

or structure 2,

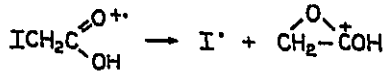

eq.(5.5)

However, of the two proposed structures, ion 1 was not found to correspond to a local minimum on the potential energy surface at the higher level of calculation. (Similar observations have been reported for the $[C_2H_3O]^+$ system (88,109). All precursor molecules $R\text{-}CH_2C(=O)H$, which could, by direct bond cleavage yield the formylmethyl cation, $CH_2C(=O)H^{\urcorner +}$, are found instead to generate the oxiranyl cation, $\overbrace{CH_2\text{-}\overset{+}{C}H\text{-}O}$. Ab initio calculations by Radom et al. (89), concluded that the formylmethyl ion was not a minimum on the $[C_2H_3O]^+$ potential energy surface, while its isomer, the oxiranyl ion did correspond to a local minimum.)

The dissociation processes observed for this ion are in keeping with the assigned structure, 2. Only one process is observed in the metastable time scale, namely the loss of CO. The intense peak at m/z=31, corresponding to $CH_2OH^{\urcorner +}$ is broad and dished and the $T_{0.5}$ value is measured to be 1230meV, the magnitude of which points to a considerable reverse activation energy associated with the fragmentation. The AE for this

metastable process, m/z=59 * m/z=31, was measured to be 13.2eV, leading to a transition state energy of 816 kJ mol^{-1}. The sum of the heats of formation of the products on the other hand, ($\Delta H_f°[CH_2OH]^+$ + [CO]) results in 596 kJ mol^{-1}. Thus an energy barrier of ~226 kJ mol^{-1} exists for dissociation of **2** into CH_2OH^+ and CO, while the reverse activation energy is some 816-596 = 220 kJ mol^{-1}, illustrated in *figure 5.3*.

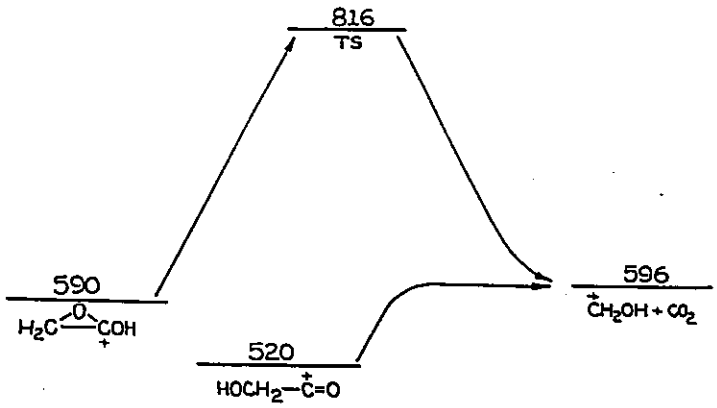

Figure 5.3 Energy diagram for the fragmentation of ion 2, refer to text.

An earlier publication (97) reported the generation of m/z=15, not m/z=31 as the (only) metastable process ($\Sigma\Delta H_f°$[products]=702 kJ mol^{-1} (26)), however the present observations recorded both here and in Utrecht, from samples of different origins are in excellent agreement and indicate no such process.

The CID mass spectrum is illustrated in *figure 5.4*, and, in keeping with the proposed structure, shows dominant peaks at m/z=14, 29 and 45, corresponding to the structural units CH_2, CHO and C(=O)H respectively. Also noteworthy is the intensity of m/z=30, indicative of CH_2O, specifically in keeping with the structure of **2** but not **1**.

The AE of m/z=59, the base peak in the EI of iodoacetic acid, was measured to be 10.86eV. Together with $\Delta H_f°[ICH_2COOH]$=-351 kJ mol^{-1} (110), and $\Delta H_f°[I]\cdot$=107 kJ mol^{-1} (26), the heat of formation of the $[C_2H_3O_2]^+$ ion produced is calculated to be 590 kJ mol^{-1}.

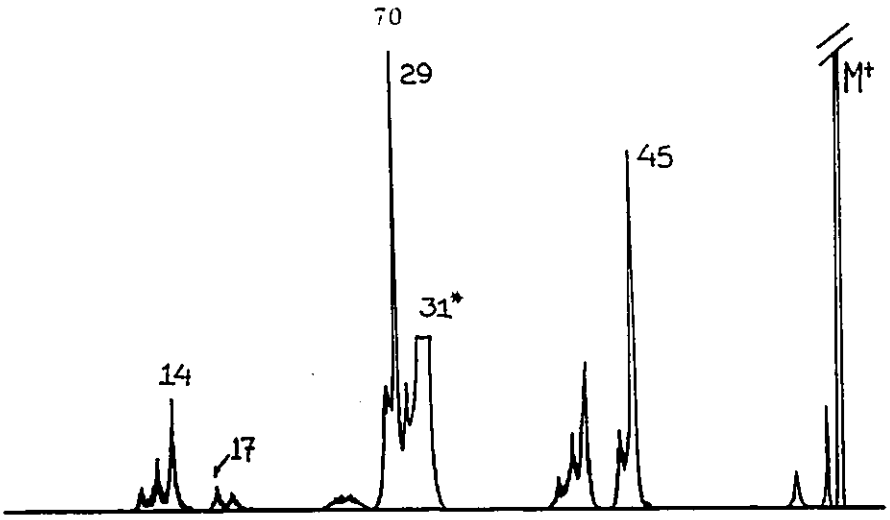

Figure 5.4 The CID mass spectrum of the mass selected m/z=59 ion. 2. obtained by electron impact induced loss of I· from iodoacetic acid.

The loss of I· is also weakly metastable, and generates a Gaussian type metastable peak with a kinetic energy release measured from the width at half-height corresponding to a $T_{0.5}$ of only 6meV. This minor kinetic energy release associated with the process indicates that the dissociation does not involve a reverse energy barrier of any significance and that the resulting $\Delta H_f°[C_2H_3O_2]^+$ value therefore, corresponds to product formation at or near its thermochemical threshold.

An estimate of the heat of formation of ion 2 can also be made by considering the general stabilizing effect of OH substitution at a charge-bearing site, for 2 may be considered as a hydroxy-substituted oxiranyl cation. The effect of OH substitution can be estimated from $\Delta H_f°[CH_2CH_2]^+\cdot$=1067 kJ mol^{-1} (26) and $\Delta H_f°[CH_2CH\text{-}OH]^+\cdot$=757 kJ mol^{-1} (23) without a size adjustment necessary (55), showing a net stabilization of 1067-757 =310 kJ mol^{-1}. From the oxiranyl cation, whose heat of formation is well-established by both theoretical calculation and experiment (88) to be 900 kJ mol^{-1}, $\Delta H_f°$[2]=900-310=590 kJ mol^{-1}, in excellent agreement with that obtained by AE measurement.

Based on the above results, it is therefore proposed that the $[C_2H_3O_2]^+$ ion generated from iodoacetic acid is ion 2 and that it is produced at its thermochemical threshold. This is important, for without threshold energies, direct comparisons with theory become difficult. The thermo-

chemistry of the $[C_2H_3O_2]^+$ ions, as alluded to in the introduction, has not proven straightforward to establish by experiment, the heats of formation often being upper limits only. Some reference point is required to correlate the theoretically determined relative energies of the predicted ionic isomers with the m/z=59 ions obtained by experiment. The $[C_2H_3O_2]^+$ species generated from iodoacetic acid, has become this reference point. The measured and estimated value of 590 kJ mol^{-1} for its heat of formation will be used hereafter as the reference point for the heats of formation of the remaining ions from their relative energies given in Table 5.1.

5.2.II Ions 4 and 6

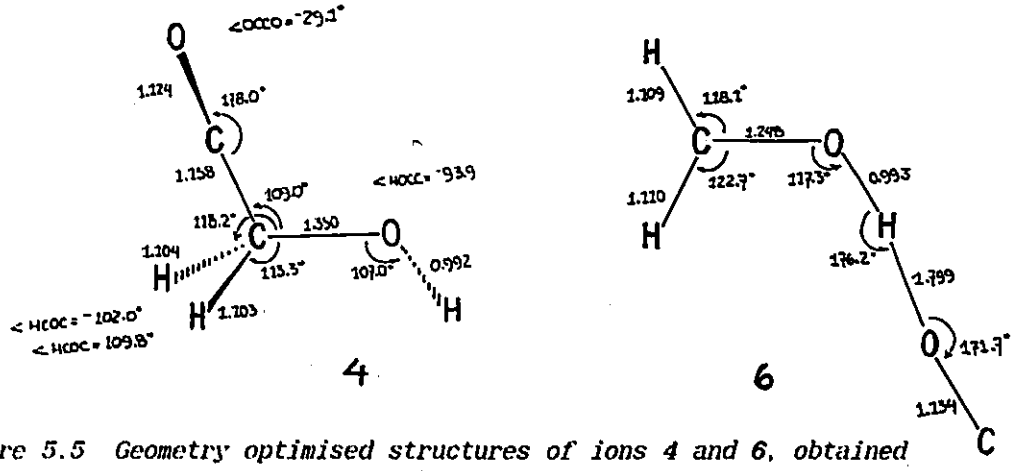

Figure 5.5 Geometry optimised structures of ions 4 and 6, obtained at the CASSCF/STO-3G level, (94).

The EI mass spectrum 1,3-dihydroxyacetone shows a m/z=59 peak which corresponds to some 2% of the base peak, m/z=31, and may have a structure represented by either 4 or 6. Ion 4 may be generated by $CH_2OH\cdot$ loss from 1,3-dihydroxyacetone if the dissociation reaction involves a direct bond cleavage from the unrearranged molecular ion,

$$HOCH_2C(=O)CH_2OH \rightarrow HOCH_2C{=}O^{+} + {\cdot}CH_2OH \qquad \textit{eq. (5.7)}$$

Also, the $CH_2OH\cdot$ loss from this molecular ion may occur after rearrangement, via an internal hydrogen bond shift and C-C bond fission, into the hydrogen-bridged radical, generating either 4 or 6,

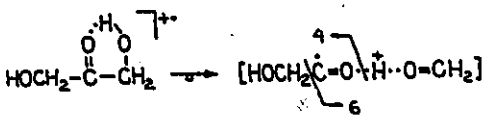

eq. (5.8)

From the relative energies in Table 5.1, and the experimentally obtained $\Delta H_f°$[2] of 590 kJ mol^{-1}, the heat of formation of ions 4 and 6 are calculated to be 519 and 507 kJ mol^{-1} respectively. As for the hydroxy-substituted oxiranyl ion, 2, an estimate of $\Delta H_f°$[4] may be made via an OH substitution in the acetyl cation on the noncharge-bearing C-atom. With the heat of formation of the acetyl cation set at 653 kJ mol^{-1} (111), and the stabilizing effect of OH on a noncharge-bearing site of ca. 151 kJ mol^{-1} (112), $\Delta H_f°$[4] is then ≈ 653-151 ≈ 502 kJ mol^{-1}, again in excellent agreement with the theoretical value.

The dissociation characteristics observed for the $[C_2H_3O_2]^+$ ion generated by 1,3-dihydroxyacetone are not unreasonable for either isomer 4 or 6. The MI mass spectrum consists of a single narrow Gaussian peak at m/z=31, CH_2OH^+, with a $T_{0.5}$=6meV, and thus no significant reverse energy barrier is involved. This may well be expected since direct bond cleavages, as in 4 and 6, often proceed at threshold, while rearrangement prior to fragmentation often leads to an energy barrier, as strikingly observed for m/z=31 loss from ion 2.

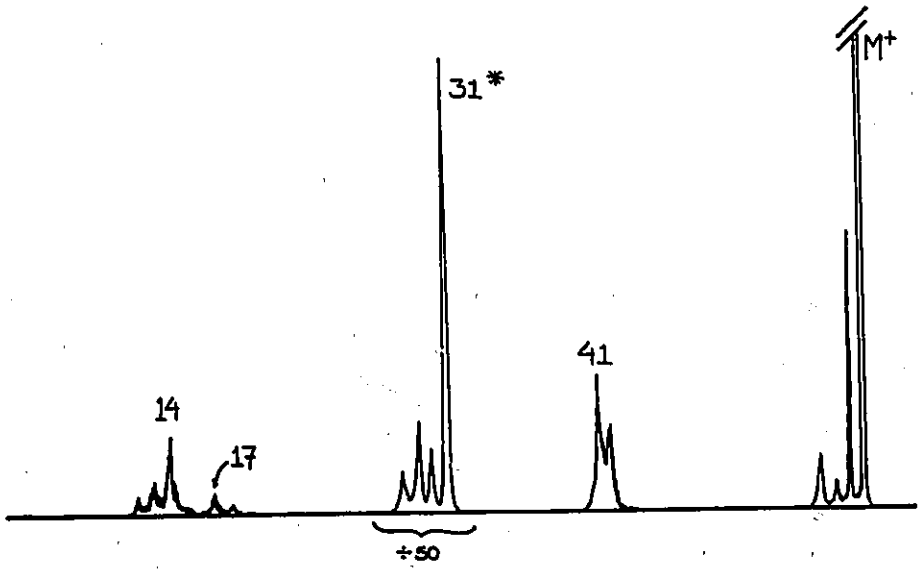

Figure 5.6 The CID mass spectrum of mass selected m/z=59 ion, 4, generated from dihydroxy acetone on electron impact excitation.

The CID mass spectrum, illustrated in *figure 5.6* is also dominated by m/z=31; however the minor peaks at m/z=41 and 42 indicate the presence of a C-C-O structural unit, compatible with the generation of ions of structure 4, and inconsistent with that of 6.

The appearance energy measured for m/z=59 was 11.24eV, (an average of several measurements). With $\Delta H_f°$[1,3-dihydroxyacetone]=-515 kJ mol^{-1} by additivity, and $\Delta H_f°[CH_2OH]$ 26 kJ mol^{-1}, the heat of formation of the $[C_2H_3O_2]^+$ ion is calculated to be 594 kJ mol^{-1}, some 85 kJ mol^{-1} above the estimated and computationally derived values for either ion **4** or **6**. This measured heat of formation is near that for threshold dissociation to m/z=31 as observed in *figure 5.2*, and ions of such energy may well explain the relatively low intensity of m/z=59 and large abundance of m/z=31 in the EI of their precursor, as well as the abundance of m/z=31 in the dissociation spectra of mass selected m/z=59.

The MI and CID mass spectra of the ion generated from 1,3-dihydroxyacetone yield information on both the structure and stability of the ion. The structure of the ion, as indicated by its collisional fragmentation, is consistent with that associated with the ionic structure **4**. It is stable, even at internal energies corresponding to metastable dissociations, with respect to isomerization to the hydroxy-substituted oxiranyl cation, **2**. The reason for the failure to observe the generation of the ions at the expected threshold energy is, however, not known and therefore a firm structure assignment cannot be made at present.

5.2.III Ions 8 and 9

As shown by the optimised geometries of these ions (see *figure 5.7* below), **9** may be considered as a methylene/CO_2 hydrogen-bridged ion. Such unconventional -C··H··O- ionic species have recently been considered experimentally (113) and theoretically (92,114,115), theory showing that at least for the systems studied, [ethylene/H_2O], [propene/H_2O], and [ketene/H_2O], the barriers for interconversion between the conventional and hydrogen bridged species are low. The conventional ion **8**, may be generated from a variety of methylcarboxylates assuming direct bond cleavage, as represented by the general *equation (5.1)*. A number of these potential precursors, listed in Table 5-2, have been investigated. All generate m/z=59 species which have been proposed to be of the conventional structure, **8** (97), and whose MI and CID mass spectra are indistinguishable.

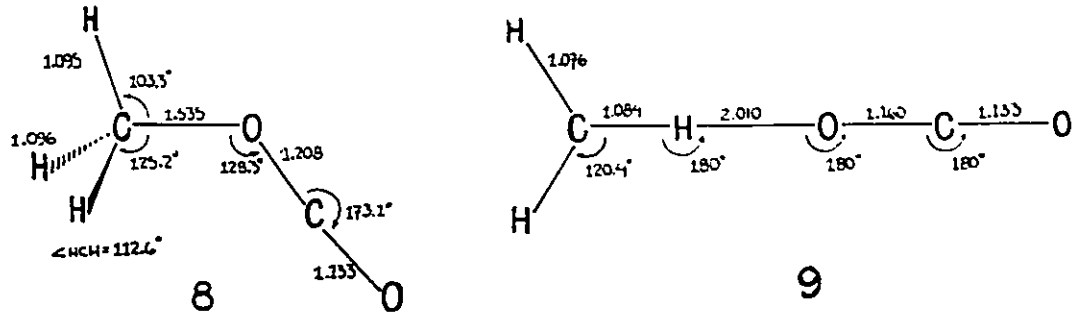

Figure 5.7 Geometry optimised structures 8 and 9: 8 at the CASSCF1-/STO-3G level with correlation corrections at the SCF/STO-3G level, 9 as 8, but with additional optimization of angles and distances associated with the H-bridge at the SCF/6-31G level (94).*

The MI mass spectra of these $[C_2H_3O_2]^+$ ions contain only one peak, that at m/z=15, from loss of CO_2. Of the eleven stable isomers predicted by theory, only the structures 8 and 9 possess a CH_3 group. The narrow profile of this metastable peak indicates that its generation is by direct cleavage, not rearrangement, thus ruling out the other nine isomers. The peak is of Gaussian shape with a very small $T_{0.5}$ value of 0.2meV, indicating that the dissociation has no reverse energy barrier. The threshold for this fragmentation, the reaction of lowest energy requirement, corresponds therefore, to the sum of the product energies, $\Sigma\Delta H_f°$[products]=702 kJ mol^{-1} (26). The CID mass spectrum, illustrated in *figure 5.8*, is in good agreement with that reported earlier (97), except for the presence of a broad peak at m/z=30 which overlaps m/z=29 in the present work. The fragments corresponding to m/z=15, 28 and 44 may be expected by direct cleavage, while m/z=45 and 29 may be explained by the interconversion of ion 8 to 9, or a 1,4 hydrogen shift prior to dissociation. The presence of m/z=56 on the other hand, via loss of three hydrogen atoms, cannot result directly from a hydrogen bridged species. The absence of m/z=31 both in the MI and CID, is striking and sets this isomer apart from either ion 2 or 4. A considerable energy barrier must exist for the generation of CH_2OH^+. The energy for the observed generation of both m/z=44 and 45 are some 400 kJ mol^{-1} above the threshold energy of 596 kJ mol^{-1} for m/z=31 ($\Delta H_f°[CH_2]$ + $[HOCO]^+$ =983 kJ mol^{-1} and $\Delta H_f°[CH_3]\cdot$ + $[CO_2]^+$ =1067 kJ mol^{-1}), and yet these fragment ions are present in the CID mass spectrum.

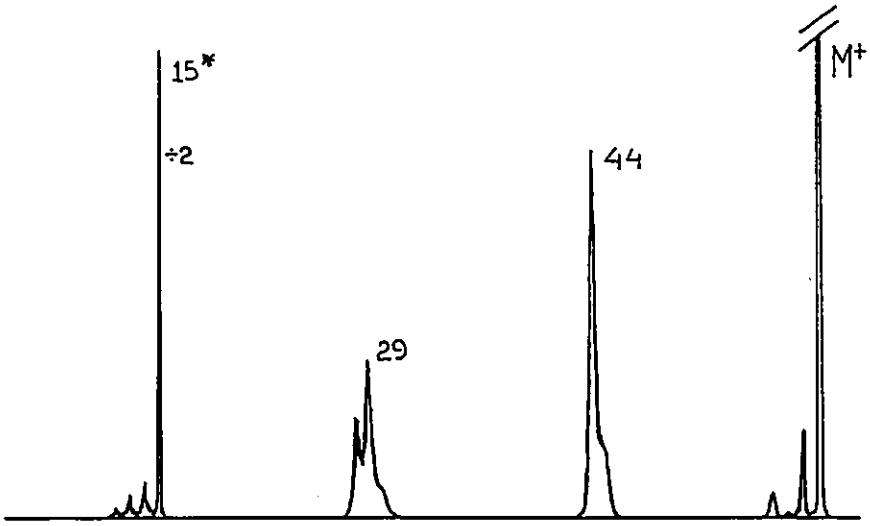

Figure 5.8 The CID mass spectrum of the mass selected m/z=59 ion, 8, obtained from a number of precursors, listed in Table 5-2.

The predicted heats of formation of these $[C_2H_3O_2]^+$ isomers, 8, and 9, from their relative energies in Table 5-1, are 504 and 618 kJ mol^{-1} respectively. These values are the lowest and highest predicted $\Delta H_f°$ values, for all the stable $[C_2H_3O_2]^+$ isomers considered. Appearance energy measurements have been made for the m/z=59 peak derived from a number of methyl esters, and are tabulated in Table 5-2. The resulting heats of formation for the $[C_2H_3O_2]^+$ ion are significantly lower than those which were reported earlier (99). However, not one value, but a range of values from 523 to 569 kJ mol^{-1}, is still observed, a range which is significantly above that heat of formation theoretically derived for 8.

As outlined in chapter 3.2, unusually high appearance energies (and thus $\Delta H_f°$ values larger than expected) may result from a competitive shift as well as a barrier for the reverse reaction. For all the precursor molecules except methyl chloroformate, there are competing fragmentations of substantially lower energy requirement, ranging from 0.5 to 1.2 eV below the AE for m/z=59. It is therefore possible that the majority of the $\Delta H_f°$ values in Table 5-2 suffer a competitive shift. Dimethyl carbonate has two such competing fragmentations some 0.5eV lower in energy, dissociation to m/z=61 (AE=10.94eV) and m/z=62 (AE=11.06eV), and yet the measured $\Delta H_f°$[m/z=59] is equal to that from methyl chloroformate.

TABLE 5-2 Measured Appearance Energies and Resultant $\Delta H_f°$ values for the $[C_2H_3O_2]^+$ Ions generated

M → N + $[C_2H_3O_2]^+$	$\Delta H_f°[M]$[1] (kJ mol^{-1})	AE[m/z=59] (eV ±0.05)	$\Delta H_f°[N]$[2] (kJ mol^{-1})	$\Delta H_f°[C_2H_3O_2]^+$ (kJ mol^{-1} ±5)
$(CH_3O)_2CO \rightarrow CH_3O\cdot(CH_2OH\cdot) + [C_2H_3O_2]^+$	-569	11.50	18(-26)	523(567)
$BrCH_2COOCH_3 \rightarrow \cdot CH_2Br + [C_2H_3O_2]^+$	-372±8[3]	11.16	174	531 ± 8
$ClCH_2COOCH_3 \rightarrow \cdot CH_2Cl + [C_2H_3O_2]^+$	-414±10[4] (-435)[5]	11.10	118	536 ± 10 (519)
$ClCOOCH_3 \rightarrow \cdot Cl + [C_2H_3O_2]^+$	-435[6]	11.24	122[7]	527
$CH_3COOCH_3 \rightarrow CH_3\cdot + [C_2H_3O_2]^+$	-410	11.32	146	536
cy $C_3H_5COOCH_3 \rightarrow$ cy $C_3H_5\cdot + [C_2H_3O_2]^+$	-303	10.56	167	548
$CH_3CH_2COOCH_3 \rightarrow CH_3CH_2\cdot + [C_2H_3O_2]^+$	-434	11.42	117	552
$HOCH_2COOCH_3 \rightarrow \cdot CH_2OH + [C_2H_3O_2]^+$	-556	11.38	-26	569
$CH_3COCOOCH_3 \rightarrow \cdot CH_3 + CO + [C_2H_3O_2]^+$	-506	11.50	(-110)[7]	569

[1]From (21) unless otherwise referenced. [2]From (117) unless otherwise referenced. [3]Stabilizing effect of Br ~ 38 kJ mol^{-1} from $\Delta H_f°$ of acetone and bromoacetone, and $\Delta H_f°[CH_3COOCH_3]$=-410 kJ mol^{-1}. [4]From $\Delta H_f°[ClCH_2COOH]-\Delta H_f°[CH_3COOH]$=-2.9±10 (20). [5]From $\Delta H_f°[CH_3COOCH_3]$ and assuming C-(Cl)(H)$_2$(CO)=C-(Cl)(H)$_2$(C)=-69 kJ mol^{-1} (21) whereas C-(H)$_3$(CO)=-42 kJ mol^{-1} (21). [6]Using $\Delta H_f°[CH_3COCl]$=-243 (20), $\Delta H_f°[CH_3COOCH_3]-\Delta H_f°[H_3COCH_3]$=410-218=-192 kJ mol^{-1}. Whence $\Delta H_f°[CH_3OCOCl]$=-435 kJ mol^{-1}. [7]From (26). [8]From (20).

The unequivocal identification, however, of the structure of the neutral $[C,H_3,O]\cdot$ accompanying the $[C_2H_3O_2]^+$ ion (see Table 5-2) is not possible. There is no metastable peak for this process which would allow identific-

ation of the neutral by collision induced dissociative ionization, as described in chapter 4.6. The neutral may therefore, be either $CH_3O\cdot$ or $\cdot CH_2OH$, a difference of 44 kJ mol^{-1} between them. Thus the $\Delta H_f°$ value for m/z 59 from dimethyl carbonate cannot be firmly established by experiment.

The formation of $[C_2H_3O_2]^+$ from methyl chloroformate, although not affected by a competitive shift, does contain some excess energy related to a reverse energy barrier. This is concluded from the intense, broad metastable peak ($T_{0.5}$=150meV) generated from the unimolecular loss of chlorine from the molecular ion. A reliable correction for this barrier to the heat of formation however, cannot be made (chapter 3.2).

Thus the calculated value of 504 kJ mol^{-1} for ion 8 is consistent with the upper limit value of ~527 kJ mol^{-1} established by experiment. The MI and CID spectra are characteristic of the predicted geometry. Assuming that these spectra are representative of the lower energy, unbridged structure, 8, it is unlikely that the CID mass spectrum from the bridged structure, 9, could contain any structurally significant fragment ions which could differentiate it from the former. Present techniques have, thus far, been unable to identify this hydrogen-bridged species which, although some 113 kJ mol^{-1} higher in energy than 8, is predicted to be stable.

5.2.IV Ions 10 and 11

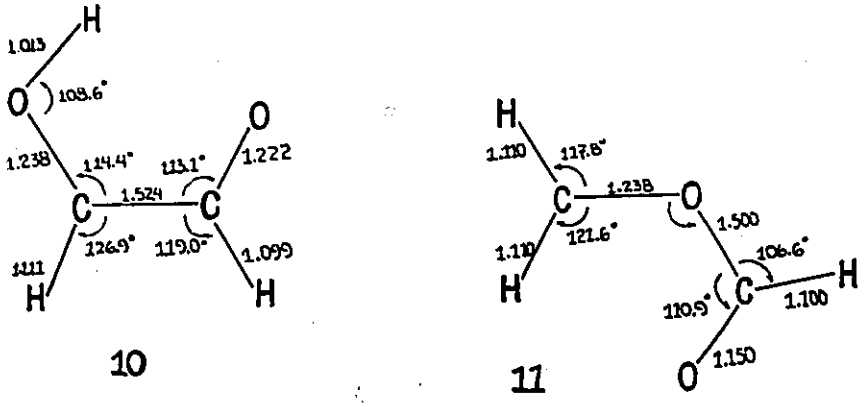

Figure 5.9 Geometry optimised structures of ions 10 and 11 via CASSCF4/STO-3G. with correlation corrections of the SCF/6-31G level, (94).*

Both isomeric ions of structures **10** and **11**, illustrated in *figure 5.9*, are proposed to have been generated experimentally by dissociative ionization, **10** by the gas-phase protonation of glyoxal,

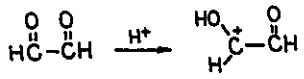

eq. (5.9)

and **11** by the loss of $CH_3\cdot$ from ionized ethyl formate,

$$CH_3\text{-}CH_2OC(=O)H^{+\cdot} \rightarrow CH_3\cdot + CH_2C(=O)H^{+\cdot} \qquad \textit{eq. (5.10)}$$

The MI mass spectrum of mass selected m/z=59 generated from protonated glyoxal shows a single, very weak peak at m/z=31 for CO loss, with an associated $T_{0.5}$ value of 140meV. The intensity of this rearrangement process indicates that interconversion of ions **10** and **4** via a 1,2-hydrogen shift is not a facile process, even at the higher internal energies associated with the metastable, mass selected species. The CID mass spectrum generated from protonated glyoxal is characteristic of the ionic structure **10**; note the absence of m/z=44, and the intensity of the m/z=29 and 58 peaks, reactions which compete favorably with the formation of m/z=31. The absence of m/z=17 and the much greater intensity of m/z=29 in *figure 5.10*, easily differentiate ions **4** from **10**, and do not support their interconversion.

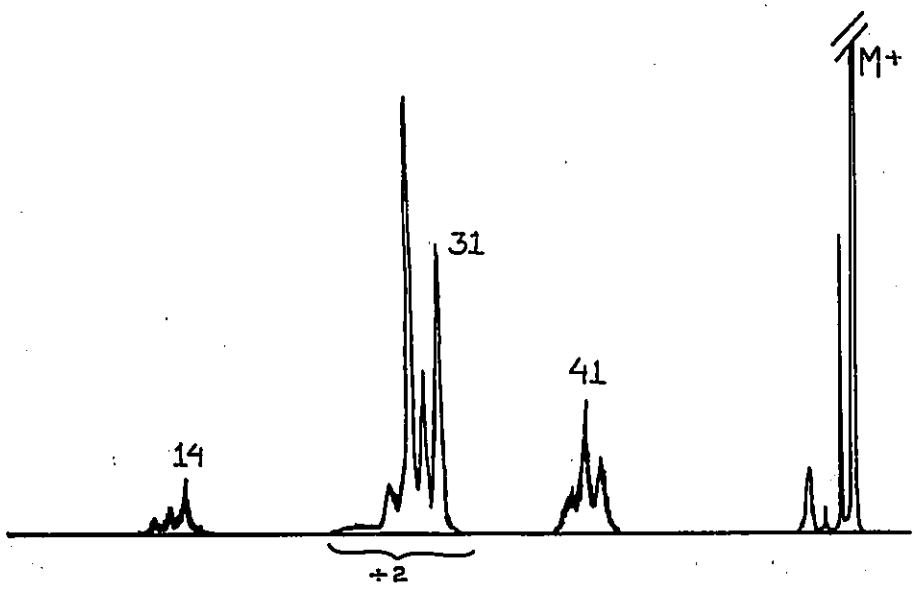

Figure 5.10 The CID mass spectrum of the m/z=59 ion, 10, generated in the ion source from glyoxal under conditions favoring protonation.

The theoretically derived heat of formation of ion **4** is 552 kJ mol^{-1}. This cannot be compared with an experimentally obtained value since the proton affinity of glyoxal has not been reported.

The m/z=59 peak in the EI mass spectrum of ethylformate is ca. 1% of the base peak (m/z=31). Labelling experiments clearly showed that loss of the CH_3· occurs without prior hydrogen atom exchange. The MI mass spectrum of this $[C_2H_3O_2]^+$ isomer contains a single Gaussian peak at m/z=31, from the loss of CO. The $T_{0.5}$ value is measured to be 18meV, and is inconsistent with ions **2**, **4**, or **10**. The CID mass spectrum of this ion, illustrated in *figure 5.11*, is similar to that of **4** *(figure 5.10)*, however the former produces a peak at m/z=44, indicative of a O-C-O structural unit, while the latter (its geometry lacks this unit), does not. Moreover, the relative intensity of the m/z=29 peak, indicative of CHO, is larger in **11** than in **4**, which cannot produce m/z=29 by direct cleavage.

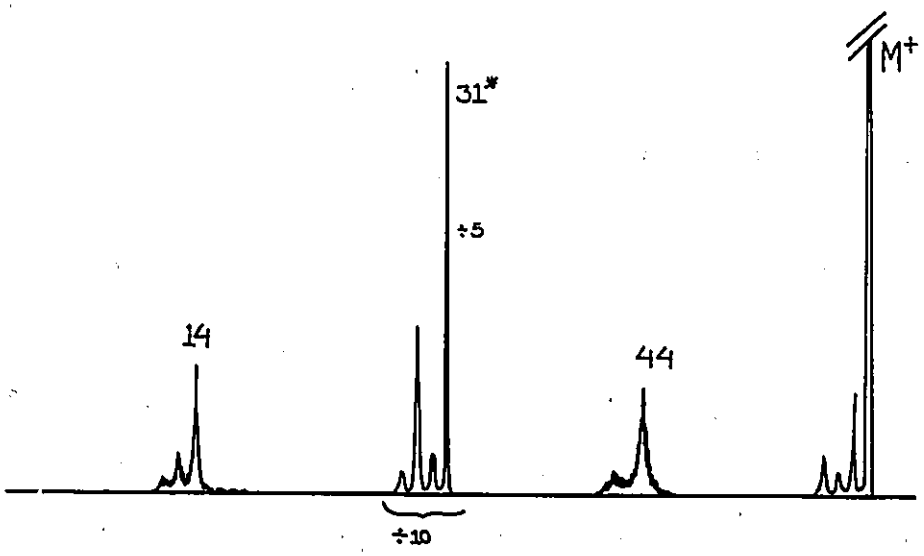

*Figure 5.11 The CID mass spectrum of mass selected m/z=59 ion, **11**, generated via electron impact from ethylformate.*

A limiting value of ≤11.8eV has been obtained for the appearance energy of $[C_2H_3O_2]^+$ from ethylformate, limited by the asymptotic approach of the weak peak's intensity to the energy axis. (A lower value of 11.5eV, reported nearly three decades ago (16) could not be reproduced.) This, together with $\Delta H_f°$[ethylformate]=-391 kJ mol^{-1} (21) and $\Delta H_f°[CH_3]$·=146

kJ mol^{-1} (117) gives $\Delta H_f°[11] \leq 602$ kJ mol^{-1}. This experimentally derived value is thus some 63 kJ mol^{-1} above the calculated value indicated in Table 5-1. Despite this disagreement (which may well be explained on the basis of a competitive shift or barrier for the reverse reaction as was observed for ion 8), the dissociative processes of this ion, at once unique and characteristic of the isomeric structure **11**, led to the conclusion that the ion **11** does represent the m/z=59 generated from ethylformate.

5.3 Summary

It is proposed that five stable isomers of the $[C_2H_3O_2]^+$ ion system have been characterized by experiment. The recorded dissociation characteristics of these species are quite distinct, and are consistent with the assigned structures. Ion **2** is proposed to be generated on loss of I· from iodoacetic acid. This hydroxy-substituted oxiranyl structure is proposed, because structure **1** is not found to correspond to a local minimum on the potential surface. Its heat of formation is believed to be well established at 590 kJ mol^{-1}. The metastable characteristics indicate a large barrier to CO loss, which must be via rearrangement. The CID mass spectrum is compatable with structure, **2**.

Based on the experimentally obtained heat of formation of the m/z=59 ion generated from iodoacetic acid, the theoretical heats of formation quoted for the remaining species have been derived from their predicted relative energies. These predicted values are necessarily the threshold values for the respective ions' formation. The higher values obtained by experiment are not *inconsistent* with theory, although good quantitative agreement between theory and experiment has not been achieved. The theoretically predicted stabilities, however, has been used *qualitatively*, in order to decide in favour of one structure over another, i.e. **2** over **1**.

Ion **8**, the methoxycarbonyl cation, has proven to be the thermodynamically most stable isomer. The experimentally obtained $\Delta H_f°$ value of $\leq$ 523

kJ mol ^{1} is in keeping with the predicted value of 504 kJ mol^{-1}. Both the MI and CID mass spectra are unique to, and characteristic of this ion. The dissociation process of least energy requirement, $CH_3^+ + CO_2$, is via direct cleavage, and indicative of a CH_3 structural unit. The CID mass spectrum, is also dominated by this m/z=15 peak, and lacks m/z=31, a peak present in the CID spectra of all the other isomers investigated.

The ion obtained by the protonation of glyoxal is argued to correspond to ion 10. The theoretical heat of formation, however, could not be compared with experiment. The metastable peak for m/z=31, is generated with a characteristic $T_{0.5}$ value of 140meV. The collision induced fragments are also consistent with the ionic structure, 10.

Tentative identification of the $[C_2H_3O_2]^+$ species generated from dihydroxyacetone and ethylformate as ions 4 and 11 respectively has also been made on the basis of their dissociation characteristics. While the fragment m/z=17, observed in the CID mass spectrum of 4 indicates the presence of a hydroxyl group, the peak at m/z=44 in the CID mass spectrum of 11 indicates the presence of a O-C-O group. The calculated and experimentally obtained heat of formation of 4 were in very poor agreement while only an upper limit was obtainable for the experimental heat of formation for 11.

Eleven potential isomers of the $[C_2H_3O_2]^+$ system, of conventional, i.e. CH_3-O-C=O$^{\gamma+}$, as well as unconventional structure, i.e. H_2C=O··H··O=C$^{\gamma+}$, have been considered theoretically. The relative enthalpies of seven of these isomers, which are predicted to exist as local minima on the $[C_2H_3O_2]^+$ potential energy surface, have been obtained by high level ab initio molecular orbital calculations and schematic drawings of their optimised geometries have been included. It is proposed that of those seven, five stable $[C_2H_3O_2]^+$ isomers have been identified, (although in some cases tentatively), by experiment.

Experimental Section

The CID mass spectra and metastable peak observations were recorded on the Vacuum Generators ZAB-2F described in section 2.2.I. A 100 μA electron beam of ionizing energy 70eV was used. The ion source temperature was 200°C and the accelerating voltage was set at 8 keV. Unless otherwise stated, all energy resolving slits (Y_1-Y_5 in figure 3.3) were fully open, to optimize sensitivity and to ensure easily reproducible conditions. The larger EI source slit was utilized in all experiments except for the generation of protonated glyoxal. To achieve high yields of the protonated species, the narrower CI slit was used and the source pressure was increased 100 fold by the addition of H_2O. A resulting intensity ratio of 10:1 was achieved for the protonated and unprotonated species, and thus little correction for ^{13}C contributions was required.

Metastable peak shapes were recorded under conditions of high energy resolution, obtained as described in 3.2.I. Main beam half-height widths of <4eV were generated while maintaining good signal-to-noise ratios.

CID mass spectra were obtained using O_2 as collision gas in the second cell, at an indicated pressure of $1.5x10^{-7}$ torr. This reading, as measured by the ion gauge situated over the down stream diffusion pump, corresponds to a beam reduction of 10%, and thus within the single collision regime. The asterix, *, marked on the CID mass spectra of the $[C_2H_3O_2]^+$ ions signifies a peak having metastable contributions.

Appearance energy measurements were recorded by Dr. F.P. Lossing with the electron energy selecting mass spectrometer described in section 2.2.III.

All compounds were obtained commercially and were of research grade purity. High purity was particularly important because m/z=59 corresponds tc $[C_3H_7O]^+$ as well as $[C_2H_3O_2]^+$. Such $[C_3H_7O]^+$ ions, present as a sample impurity, or as mass spectrometer background contamination, give significant m/z=31 and m/z=41 peaks in their MI and intense m/z=31 and m/z=43 in their CID mass spectra. The generation of both ions, $[C_2H_3O_2]^+$ and $[C_3H_7O]^+$, from precursors such as methyl isobutyrate and methyl valerate was also observed. Under high mass resolution, achieved with the resolving slits Y_1,Y_3, and Y_5, the separation of the former, at m/z=59.013303 and the latter, at m/z=59.049689 was possible.

Chapter 6

THE C_2H_5X SYSTEM
A COMPLETE MASS SPECTROMETRIC ANALYSIS

6.1 Introduction

In the past few years experimental and theoretical studies have firmly established the existence in the gas phase of simple organic ions having unusual structures, whose neutral counterparts are unknown or extremely reactive. The interest in the chemistry of these species seems to have been sparked by a number of reports appearing in 1981-82, one of the earliest examples of which involved the isomer of ionized methanol, the methyleneoxonium radical cation, $CH_2OH_2^{\neg +}\cdot$. This rather simple system will serve to introduce some fundamental aspects. Thereafter, a thorough analysis of its methyl analogue, the $C_2H_5X^{\neg +}\cdot/C_2H_5X$ system, where X represents F, Cl, Br, I, will be presented.

Ab initio molecular orbital theory calculations predicted not only that $CH_2OH_2^{\neg +}\cdot$ represented an additional stable isomer in the $[CH_4O]^+\cdot$ potential energy surface but that it lay some 45 kJ mol^{-1} lower in energy than the ion of conventional structure, $CH_3OH^{\neg +}\cdot$(118). Experimental verification for the existence of $CH_2OH_2^{\neg +}\cdot$ followed immediately. Electron impact was found to induce a rearrangement/fragmentation reaction in ethylene glycol resulting in the formation of neutral formaldehyde and an ion of m/z=32. Note that no *specific* structure is intended where species are enclosed in square brackets and represented in terms of the number and type of atoms only, i.e., $[C_2H_6O]^+\cdot$ versus $CH_3\text{-}O\text{-}CH_3^{\neg +}\cdot$ or $CH_3CH_2\text{-}OH^{\neg +}\cdot$.

$$HOCH_2CH_2OH \rightarrow [CH_4O]^+\cdot + CH_2O \qquad \textit{eq.(6.1)}$$

The CID spectrum of the $[CH_4O]^+\cdot$ fragment was clearly not that of $CH_3OH^{\neg +}\cdot$, but rather showed characteristic peaks which indicated that the ion indeed had the methyleneoxonium structure (90a,b).
$CH_2OH_2^{\neg +}\cdot$ is one of the simplest members of a new and still growing

"class" of structurally novel, stable radical cations being experimentally generated and characterized as well as, in the more simple systems, investigated theoretically. A wide variety of terms have been applied to these species, including 'stable ion-dipole complexes', 'ionized carbene/dipole complexes', 'localized radical cations', and 'non-classical' species. 'Distonic', the term now generally accepted, was defined by L. Radom et al. in 1984 (119) to encompass all radical cations in which the charge and radical sites are formally separated, as for example in $\cdot CH_2CH_2\overset{+}{O}H_2$. The term 'ylidion', (from ylide neutrals, species having formal, opposite charges on adjacent atoms) was suggested for the particular cases where these sites are at adjacent centers, such as $CH_2\dot{C}H\overset{+}{O}H_2$. Where larger species are encountered it has been proposed that the proximity of the radical and charged site be denoted by α, β, γ etc (120). However for C_2H_5X species, only α- and β-distonic ions are possible, and they will be referred to as ylidions and distonic ions respectively. Distonic ions might well be referred to as 'unconventional' but they have been found to be both common and stable! Knowledge of the properties of these species is therefore important for a better understanding of the behaviour of many simple radical cations.

The heats of formation of distonic ions are not, in general, lower than that of their conventional isomers, for example in the simplest of distonic species, $CH_2XH^{+}\cdot$, where X=OH, NH_2, and F the distonic ion is predicted to be more stable, while for X=SH, PH_2, and Cl the conventional ion has the lower heat of formation (120). There are however a number of commonalities which are observed when comparing distonic and conventional ions of the $\cdot CH_2\overset{+}{X}H/CH_3X^{+}\cdot$ system. There is a relatively high barrier for isomerization between the conventional and distonic ions, thus allowing these species to be analyzed separately (120). Stability of the dication for the distonic isomer is significant, the base peak in the charge stripping mass spectrum being $[CH_3X]^{2+}$, while for the conventional ion, it is absent or vanishingly weak (121). And finally, unlike their conventional isomers, the distonic ions have no corresponding stable neutral counterpart (120,122). Distonic radical cations therefore, unlike their conventional isomers, may not be formed by direct ionization, and thus their generation is via (i) *isomerization* and (ii) *rearrangement* processes prior to fragmentation of a suitable

precursor ion. Intramolecular hydrogen shift reactions in conventional cations, have been observed for many molecular ions including alcohols, as in *equation (6.2)*, and ethers, esters, and amines (8), to yield distonic species.

$$CH_3CH_2CH_2CH_2OH^{\cdot+} \rightarrow CH_2CH_2CH_2CH_2OH_2^{\cdot+} \qquad eq.(6.2)$$

By far the majority of distonic ions studied via mass spectrometry however, have been formed by rearrangement-cum-fragmentation processes, e.g.

$$ClCH_2COOH^{\cdot+} \rightarrow CH_2ClH^{\cdot+} + CO_2 \qquad eq.(6.3)$$

where methyl and halogen as well as hydrogen atom transfer reactions have been observed (123).

Identification of distonic species, mixed with the molecular ions of conventional structure, is not straightforward, the commonly used method of CID being particularly compromised where unresolved mixtures are involved. The now widespread availability of reverse geometry, double focussing mass spectrometers explains in part the recent surge of distonic ion studies. These instruments enable the mass selection and subsequent analysis of a specific fragment ion, such as the unusual fragment $CH_2ClH^{\cdot+}$ generated in *eq.(6.3)*. Such a procedure requires that the formation of the distonic ion of interest be from a suitable precursor via rearrangement/fragmentation, and this mode of formation is indeed predominant.

The $[CH_3X]^{+\cdot}$ ($X=NH_2$, OH, SH, PH_2, F, Cl, Br, I) isomeric species and their neutral counterparts have now been well investigated via experiment (45,79,90a,b,121,124,125) and high level ab initio calculations (118-120,122,123,126). In the investigation of larger, more complex systems however, such calculations are increasingly limited, placing the emphasis for structure assignment largely upon experimental work. This is indeed true of the system of interest, $[C_2H_5X]$ ($X=F,Cl,Br,I$), where theoretical consideration of distonic radical cations has been limited to three studies (130-132) which will be discussed later, and no theoretical investigations of their corresponding distonic neutrals have been made. The structural assignment of the unconventional isomers of ethylhalide radical cations and their corresponding neutrals has therefore been

solely based on experimentally obtained thermodynamic and dissociative properties.

Some groundwork has already been laid in the investigation of isomeric radical cations of the ethylhalides. In 1983, via the investigation of the electron impact induced CO_2 loss from methyl chloro- bromo- and iodoacetate, Schwarz et al. (127), characterized the first isomeric pair, $CH_3ClCH_2^{\cdot+}$ and $CH_3BrCH_2^{\cdot+}$. Since that time the distonic isomers of the ethylhalide ions have been the subject of a number of reports (57,128-130). A brief summary of these investigations will be included in the following sections 6.2.II-V. However, unless referenced otherwise, all spectral and thermochemical data presented have been compiled in this laboratory. As emphasised in chapter 4, the majority of the mass spectrometric analytical techniques rely heavily on comparisons, necessitating the use of data obtained under closely similar experimental conditions. To this end nearly all previously published spectral data of the $[C_2H_5X]^{\cdot+}$ isomeric system have been re-examined under the standard set of experimental conditions used in the present investigation. In a number of cases where significant dissimilarities were observed, a reassessment of the published data is proposed. The following is believed to contain the most comprehensive collection of experimental mass spectrometric data of $[C_2H_5X]^{\cdot+}$ halogen isomers presently available.

Far less is known of the structure and thermochemistry of the neutral counterparts of these unconventional ions. The generation of $CH_3\overset{+}{\underset{-}{X}}CH_2$, ylide isomers of ethylbromide and iodide, were first reported by Olah et al. in 1975 (133a). The 'methylhalonium methylides' were considered to have been formed as reactive reaction intermediates in the hydrogen/deuterium exchange of the corresponding dimethylhalonium ions in deuterated sulfuric acid, but they could not be isolated. Since that time little information on these or other C_2H_5X distonic neutrals has been obtainable due to their characteristic high reactivity. The recent advent of the technique known as Neutralization-Reionization Mass Spectrometry, NRMS, has however, enabled structural information for such reactive neutrals to be gained via their reionization mass spectra. The reactivity of the distonic neutrals coupled with the relative stability of their radical cationic counterparts make the system ideally suited for

examination by NRMS (45,119). Section 6.3 will deal with the neutralization-reionization mass spectrometric investigation of the neutral counterpart of those distonic radical cations characterized in section 6.2.

6.2 The Isomeric Radical Cations

Four isomeric radical cations of the $[C_2H_5X]^{+\cdot}$ system may be proposed; the conventional isomer, $CH_3CH_2X^{\urcorner+\cdot}$, two ylid or α-distonic isomers, $CH_3XCH_2^{\urcorner+\cdot}$ and $CH_3CHXH^{\urcorner+\cdot}$, and the β-distonic species $CH_2CH_2XH^{\urcorner+\cdot}$. The first is produced by direct ionization of the neutral species, however rearrangement/fragmentation reactions must necessarily be employed in the generation of the distonic isomers. Establishing the heat of formation of the ions will be made wherever possible via experimentally determined appearance energies. The dissociation characteristics of the ion, via the EI, MI, CID, and CS mass spectrometric techniques (described in chapter 4), will also be established or reassessed under standardized experimental conditions, as outlined in the appendix. All MI, CID, and CS mass spectra have been corrected, where applicable, for the ^{13}C contributions from $[M-1]^+$. As well the metastable ion peak intensities have been subtracted from the corresponding CID mass spectra, and that of the corresponding metastable neutrals, from the NRMS, as described in chapter 4.7.

6.2.I $CH_3CH_2X^{\urcorner+\cdot}$ The Conventional Ion

It is necessary to firmly establish the heats of formation as well as the dissociative processes of the conventional isomers, $CH_3CH_2X^{\urcorner+\cdot}$ (X=F,Cl,Br,I) thereby establishing reference energies with which comparisons may later be made. These radical cations, formed directly by electron impact ionization of their corresponding neutrals, are the obvious choice for a set of reference compounds; all four neutrals, CH_3CH_2F, CH_3CH_2Cl, CH_3CH_2Br, and CH_3CH_2I are stable, readily available in a pure state, and all directly generate significant quantities of their molecular ion on electron impact.

$CH_3CH_2F^{\cdot+}$

The electron impact mass spectrum of ethylfluoride (seen in *figure 6.1*), in good agreement with that published in the data base collection of the National Bureau of Standards, shows $C_2H_4F^{\cdot+}$, m/z 47, to be the base peak, while the molecular ion, m/z=48, is only some 12% of m/z 47. A vertical ionization energy of 12.43eV for ethyl fluoride was reported in 1973 by Yamazaki et al. (134), from the PE spectrum. Using this value and $\Delta H_f°[CH_3CH_2F]$= -263 kJ mol^{-1} (135), the heat of formation of the ethylfluoride radical cation is calculated to be 936 kJ mol^{-1}. The onset of the PE spectrum however is significantly lower than 12.43eV, the first local maximum being just below 11.80eV (136). A value of 11.78eV has been obtained for the adiabatic ionization energy of ethylfluoride, and is believed to be the first such measurement reported. This yields a significantly lower $\Delta H_f°$ of 873 kJ mol^{-1} for the molecular ion.

TABLE C-1 Heat of Formation of $[C_2H_5F]^{\cdot+}$

IE	$\Delta H_f°[CH_3CH_2F]$	$\Delta H_f°[C_2H_5F]^{\cdot+}$
IE(v)=12.43eV	-263 kJ mol^{-1}	936 kJ mol^{-1}
IE(ad)=11.78eV	"	873 kJ mol^{-1}

The unusually large deviation of 0.65eV between vertical and adiabatic IE, indicates that a considerable geometry difference must exist between the neutral and ionized species, and that ionization via electron impact, a mainly vertical process, will produce highly excited ions. This may well account for the rather low intensity of the molecular ion, with respect to the hydrogen loss species, $[C_2H_4F]^+$. A value of 12.04±0.3eV for the AE of m/z=47 from ethylfluoride was recorded in 1975 (135), in the present study a value of 12.14±0.05eV has been obtained. Loss of H· therefore, from a threshold ion, requires only an additional 0.36eV or 34 kJ mol^{-1}, and for those molecular ions formed vertically, it will occur spontaneously.

Two peaks are observed in the MI mass spectrum of the ethylfluoride molecular ion, m/z=46 and m/z=47. The metastable process for hydrogen

radical loss generates a thin Gaussian peak with a $T_{0.5}$~8meV. The energy barrier for the reaction is calculated to be 912 kJ mol^{-1}, from the measured AE for m/z=47 of 12.14eV, an AE involving little or no contribution from reverse activation energy as indicated by the very narrow profile of the metastable peak.

TABLE 6-2 $CH_3CH_2F^{+\cdot}$ Metastable Characteristics

		m/z	Peak Shape	$T_{0.5}$
$CH_3CH_2F^{+\cdot}$	$\overset{*}{\rightarrow}$ $[C_2H_4F]^+$	47	Gaussian	8 meV
	$\overset{*}{\rightarrow}$ $[C_2H_3F]^{+\cdot}$	46	Dish-topped	310 meV

The metastable formation of $[C_2H_3F]^{+\cdot}$ results in a broad, dished peak having a $T_{0.5}$=310meV, a large kinetic energy release indicative of a significant reverse activation energy. The heat of formation of $[C_2H_3F]^{+\cdot}$, was calculated from, -138.9 kJ mol^{-1}, the heat of formation of its neutral (137), and 10.37eV, the corresponding IE (26), giving a value of 862 kJ mol^{-1}. That loss of hydrogen radical competes favorably with formation of $[C_2H_3F]^{+\cdot}$, on the metastable time frame, despite a calculated energy difference of 50 kJ mol^{-1} between the two, is explained by the sizable reverse activation energy associated with the formation of $[C_2H_3F]^{+\cdot}$.

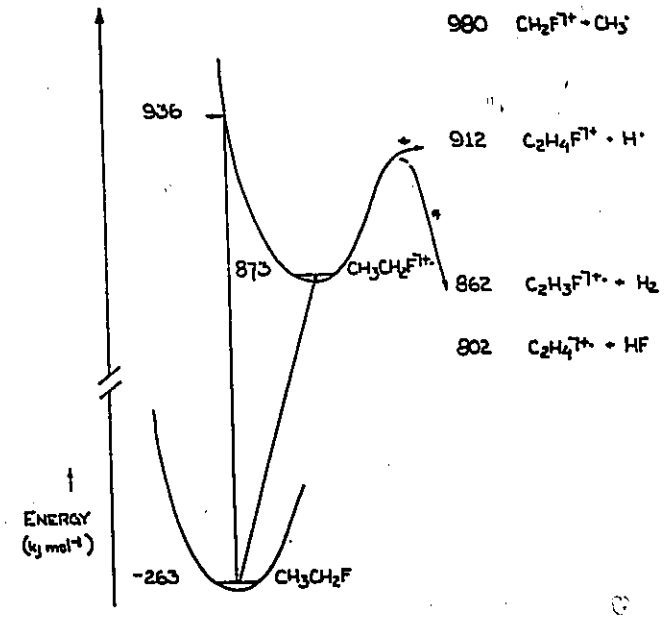

Figure 6.1 Schematic energy diagram for ethyl fluoride, its molecular ion, and lower energy dissociation processes.

An additional peak, the loss of a methyl radical to generate the methylenefluoride cation, m/z=33, was also proposed (129) to have unimolecular contributions. However, with $\Delta H_f°[CH_3]$=142 kJ mol^{-1} (26) and $\Delta H_f°[CH_2F]^+$=838 kJ mol^{-1} (26), the threshold energy for this process lies at 980 kJ mol^{-1}, considerably above that for direct hydrogen atom loss at 912 kJ mol^{-1}. In the MI mass spectrum, m/z=33 was less than 1/500 the intensity of m/z=46 and m/z=47. Coupled with its large cross-section for collisional formation (CH_2F^+ dominates the CID), this peak is proposed to have no unimolecular metastable generated component. Experimental investigations support this conclusion. Comparison of the 'unimolecular':'collision induced' ratio -strictly speaking, those processes occurring outside and inside the collision cell respectively- as separared by a voltage on the collision cell, was made over a range of collision gas pressures. The ratio, virtually unchanged over a range of pressures from conditions of CID to those associated with MI mass spectra showed that no significant unimolecular contributions are present.

The collision induced dissociation mass spectrum of ethylfluoride is in good agreement with its EI mass spectrum as seen in *figure (6.2)*, the structure characteristic fragments, dominated by m/z=15, 27, 33 and 47, corresponding to $CH_3^+\cdot$, $C_2H_3^+$, CH_2^+ and $CH_3CHF^+\cdot$, being observed in both spectra. Note the lack of m/z=29. Vertical ionization of CH_3CH_2F will generate species above the threshold for H· loss, giving m/z=47 which, consistent with the presence of m/z=15 and m/z=27 and lack of m/z=28, is believed to be $CH_3CHF^{\neg+}\cdot$. It is concluded that no rearrangement of the mass selected ethylfluoride ion occurs prior to and directly after its collisional excitation, and this in turn indicates that the CID mass spectrum may be taken as specifically characteristic of $CH_3CH_2F^{\neg+}\cdot$. The CID mass spectrum is, however, not in agreement with a previously published spectrum (129), the experimental parameters for which were not reported. Despite the use of the target gases He and O_2 over a wide range of pressures from ~10% to 80% beam reduction, the published, computer averaged, scans could not be reproduced. The major discrepancies involve the C_2-C_2H_5 fragments; no peak intensity for m/z=26, a single value, uncorrected for ^{13}C contributions from $[C_2H_4F]^+\cdot$, for m/z=27/28, and a significant intensity for m/z=29 were reported. The CID mass spectrum does contain ^{13}C contributions, most notably the large

m/z=27 observed in the MI and CID of mass selected m z 47 which accounts for more than 70% of the m z=28 seen in the CID mass spectrum of the ethylfluoride molecular ion.

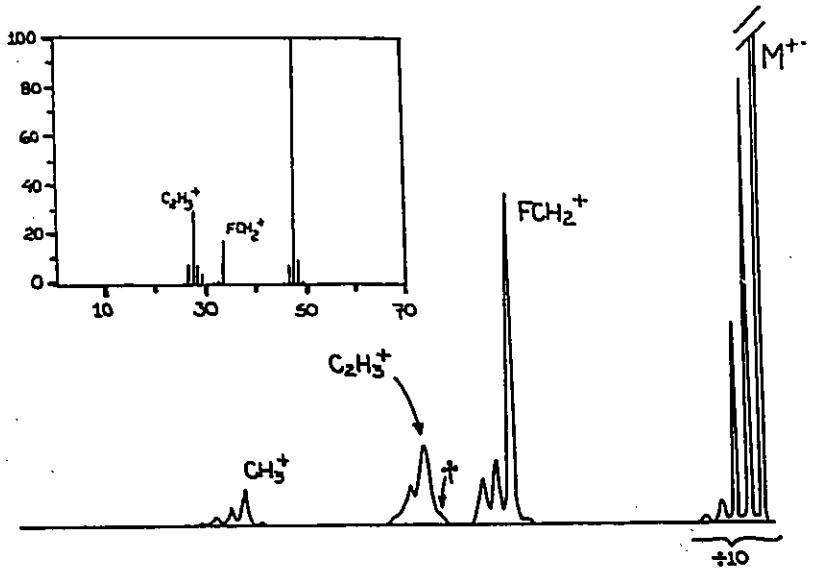

Figure 6.2 The EI and CID mass spectrum of ethyl fluoride. † indicates peak corrected for ^{13}C contributions.

A doubly charged molecular ion of ethylfluoride will have an apparent m/z=24 (also corresponding to the singly charged C_2^+). The much weaker charge stripping mass spectrum could not be obtained free of interference, and thus no CS spectrum is reported for ethylfluoride.

$CH_3CH_2Cl^{+\cdot}$

The EI spectrum recorded for ethylchloride is consistent with the NBS data base, $CH_3CH_2{}^{35}Cl^{+\cdot}$, m/z=64, is the base peak, indicative of a molecular ion of considerable stability.

The vertical ionization energy of ethylchloride is reported to be 11.01eV (27). The measured adiabatic ionization energy, 11.04±0.05eV, is close to this value, unlike the fluoro derivative. With $\Delta H_f°[CH_3CH_2Cl]$ reported to be -112 kJ mol^{-1} (138), a heat of formation of 950 kJ mol^{-1} for $[CH_3CH_2Cl]^{+\cdot}$ can be confidently assigned.

The molecular ion of ethylchloride undergoes loss of HCl within the metastable time frame. A vanishingly weak process for the loss of Cl· is

also observed. The dominance of m/z=28 in the MI mass spectrum of the ethylchloride molecular ion is expected from the larger energy requirement for direct C Cl bond cleavage to yield m/z=29. The measured appearance energy for m/z=29 is 11.83±0.06 eV (26), corresponding to a product energy of 1031±6 kJ mol^{-1}. From $\Delta H_f°[C_2H_5]^+$=917 kJ mol^{-1} + $\Delta H_f°Cl\cdot$ 122 kJ mol^{-1}, the energy for this process is calculated to be 1039 kJ mol^{-1} (26), and indicates that Cl· loss is indeed a threshold process. Similarly, the loss of HCl has a calculated threshold energy of 983 kJ mol^{-1} (from $\Delta H_f°[CH_2CH_2]^+\cdot$=1075 kJ mol^{-1} and $\Delta H_f°[HCl]$= -92 kJ mol^{-1} (26)), which corresponds well with the value of 981 kJ mol^{-1} from the reported AE of 11.33±0.05eV (26). The loss of CH_3, generating CH_2Cl^+, was also reported to occur on the metastable time frame (119), but is inconsistent with the present experimental data, as well as being thermodynamically unlikely. With $\Delta H_f°CH_3$=142 kJ mol^{-1} and the heat of formation of CH_2Cl^+ = 950 kJ mol^{-1} (139), the minimum energy requirement for this decomposition lies some 53 kJ mol^{-1} higher yet than for the (vanishingly) weak metastable loss of Cl·.

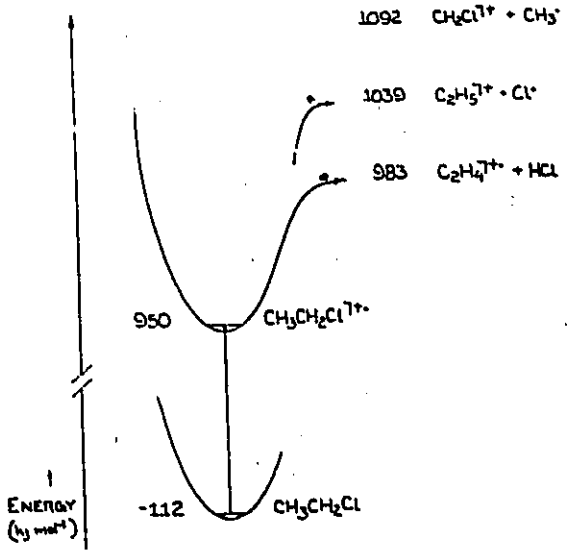

Figure 6.3 Schematic energy diagram for ethyl chloride, its molecular ion, and lower dissociation processes.

TABLE 6-3 $CH_3CH_2Cl^{\ddagger+}$· Metastable Characteristics

	m/z	Peak Shape	$T_{0.5}$
$CH_3CH_2Cl^{\ddagger+}\cdot \xrightarrow{*} [C_2H_4]^+\cdot$	28	~Gaussian	24 meV
$CD_3CH_2Cl^{\ddagger+}\cdot \xrightarrow{*} [C_2D_2H_2]^+\cdot$	30	Composite	69 meV

The metastable peak for loss of HCl has a $T_{0.5}$~21meV, and which is possibly composite in nature, is illustrated in *figure (6.4)*. The MI mass spectrum of the labelled species, $CD_3CH_2Cl^{\cdot+}$, generated a similarly intense, but much more clearly composite metastable peak for m/z 30 as well as two peaks of less than 1/100 the intensity at m/z 31 and 32. This almost exclusive loss of DCl indicates that up to the internal energy associated with the first dissociation threshold, no intramolecular hydrogen scrambling occurs. The $T_{0.5}$=69meV for DCl loss from the labelled species, contains a large proportion of a broad component.

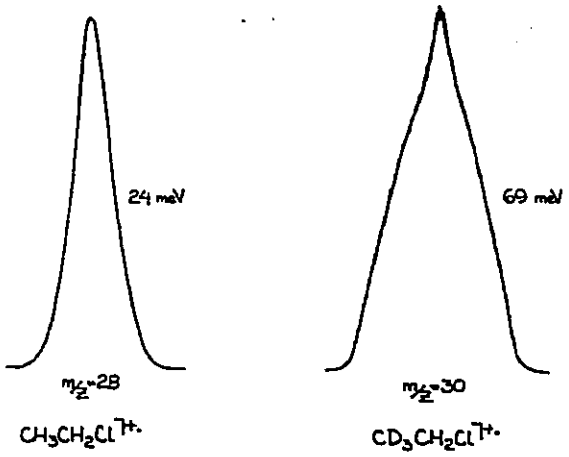

Figure 6.4 Metastable peak shapes for the loss of HCl and DCl from $CH_3CH_2Cl^{\cdot+}$ and $CD_3CH_2Cl^{\cdot+}$ respectively.

The composite nature for HCl/DCl loss from $CH_3CH_2Cl^{\cdot+}/CD_3CH_2Cl^{\cdot+}$ can only be speculated upon at present, the formation of two unique daughter ions seems unlikely on a thermodynamic basis. The heat of formation of $CH_3CH^{\cdot+}$ is estimated (140), stabilization of $-CH_3$ on charge bearing site graph with CH_2^+=334 kcal mol^{-1}) to be 1155 kJ mol^{-1}, some 80 kJ mol^{-1} above that of its isomer $CH_2CH_2^{\cdot+}$ and more energy demanding than the direct loss of Cl·. Also, the formation of highly excited $CH_2CH_2^{\cdot+}$ might be expected to generate a broader metastable peak, in keeping with the much larger reverse activation energy.

The CID mass spectrum of ethylchloride, corrected for contributions from the unimolecular process for HCl loss, is dominated by the simple loss of Cl· as illustrated in *figure (6.5)*. The formation of Cl^+ and $HCl^{\cdot+}$ compete unfavorably with the formation of $[C_2H_5]^+$ and $[C_2H_4]^{\cdot+}$, but the relative intensities, Cl^+>$HCl^{\cdot+}$, are as expected for the ethylchloride structure.

The CID spectrum is consistent with that produced by electron impact ionization, and thus will be taken as specific for the structure $CH_3CH_2Cl^{+\cdot}$.

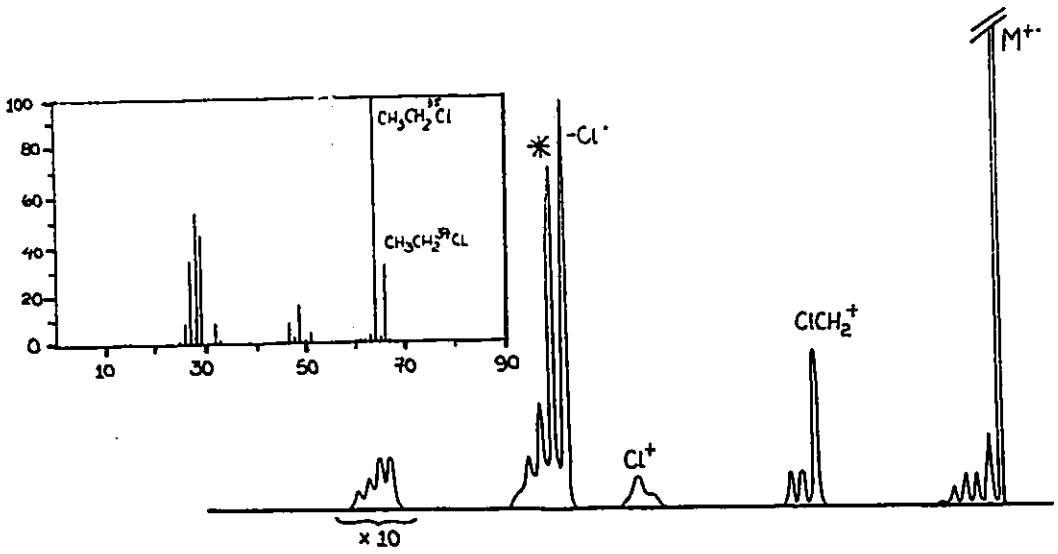

*Figure 6.5 The EI and CID mass spectra of ethyl chloride, * indicates the peaks corrected for metastastable contributions.*

The charge stripping mass spectrum is visible under increased gain, the CS peaks being ~1/100 the intensity of the singly charged fragments. The most intense doubly charged peak corresponds to $[C_2H_3Cl]^{2+}$; ethylchloride does not generate a stable molecular dication (Table 6-5), a characteristic of its lower homologue $CH_3Cl^{+\cdot}$ (121,122).

$CH_3CH_2Br^{+\cdot}$

The electron impact mass spectrum of ethylbromide as published in the NBS data base is also well reproduced, the $CH_3CH_2{}^{79}Br$ isotope producing m/z=108, its molecular ion, as the base peak in the spectrum.

The energy required for the vertical ionization of ethylbromide is reported to be 10.28eV (27), a value believed to correspond closely with the adiabatic process. Together with the published value of -62 kJ mol^{-1} (138) for $\Delta H_f°[CH_3CH_2Br]$, the heat of formation of the ethylbromide radical cation is calculated to be 930 kJ mol^{-1}. An energy range of nearly 100 kJ mol^{-1} exists between a molecular ion generated at threshold

and the cheapest pathway to dissociation, *eq.(6.4)*.

$$CH_3CH_2Br^{\cdot+} \rightarrow [C_2H_5]^+ + Br\cdot \qquad eq.(6.4)$$

calculated from the sum of 917 kJ mol^{-1} and 112 kJ mol^{-1}, $\Delta H_f°[CH_3CH_2]^+$ and $\Delta H_f°[Br]\cdot$ respectively (26).

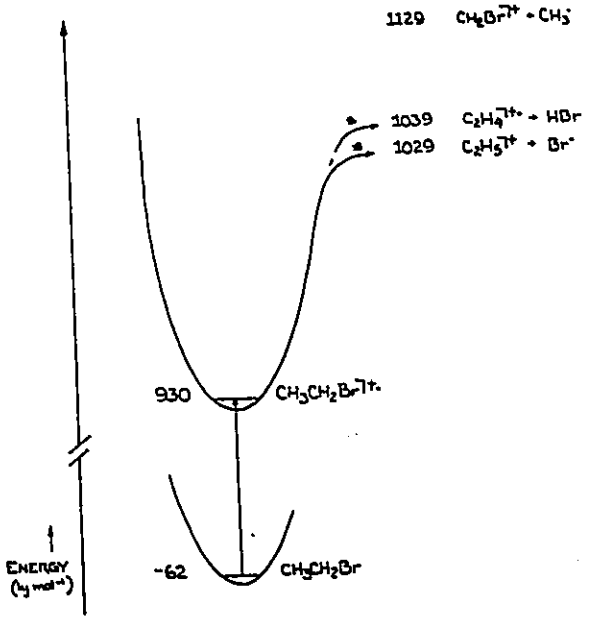

Figure 6.6 Schematic energy diagram for ethyl bromide, its molecular ion and lower energy processes.

The unimolecular fragmentation for the formation of $CH_3CH_2^{\cdot+}$ via *eq.(6.4)* is observed in the first field free region of the MS-902S and, albeit very weak, is therefore concluded to be a metastable process. At longer lifetimes, as in the second field free region of the VG ZAB-2F, the situation is less clear. A large gain factor, 10^5 increase from full scale deflection of the main beam, was required to generate fragment signals (the chloro analogue required a gain factor of ~2×10^2 to obtain an observable MI). At such high gain however, the origin of the fragment signals may be twofold, a weak metastable process, or alternatively, a collision induced dissociation generated from the residual gas pressure present in the second field free region of the instrument. Due to the numerous peaks observed in addition to m/z=29 (the process of lowest energy requirement) the intensity ratios of which mirror those in the CID, these peaks are considered to be 'residual CID' and not metastable.

The loss of $CH_3\cdot$ was also proposed to have unimolecular contributions (127). From $\Delta H_f°[CH_2Br]^+$, determined to be 987 kJ mol^{-1} (141), and $\Delta H_f°[CH_3]\cdot$=142 kJ mol^{-1} (27), the threshold energy for this process

corresponds to 1129 kJ mol^{-1}, 100 kJ mol^{-1} above the threshold for the *equation (6.4)*, which is itself limitingly weak. As in the chloro analogue, it is proposed that the loss of $CH_3\cdot$, reported present under 'MI' conditions is indeed generated by collision.

The ethyl cation, via direct loss of Br·, is the base peak in the collision induced dissociation mass spectrum of ethylbromide. The peaks corresponding to Br^+ and CH_2Br^+ are also characteristic fragments of the CH_3CH_2Br structure. Not inconsistent with the spectrum generated by electron impact, the CID mass spectrum of the ethylbromide molecular ion, as illustrated in *figure (6.7)*, is considered representative of the ionic structure $CH_3CH_2Br^{\urcorner +}\cdot$.

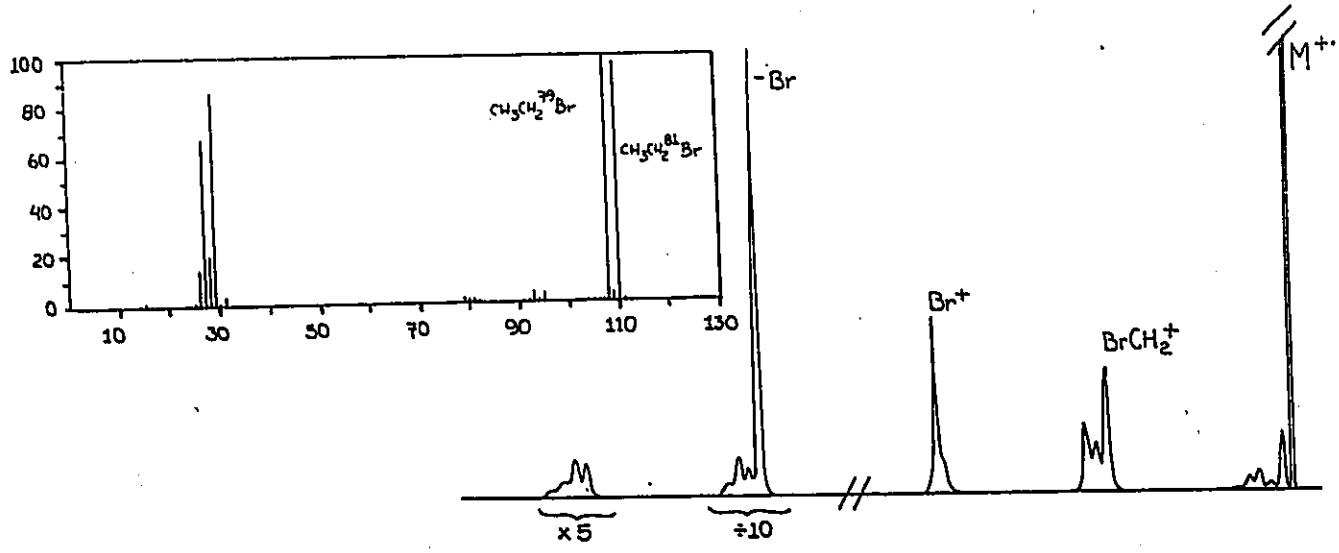

Figure 6.7 The EI and CID mass spectra of ethyl bromide.

The CS mass spectrum of ethylbromide and ethylchloride are of similar intensity, and pattern, as indicated in Table (6-5). The CS peaks are ~1/100 the intensity of the singly charged peaks, the most intense corresponds to $[C_2H_3Br]^{2+}$, and no peak corresponding to the doubly charged molecular ion, M^{2+}, is observed. The predicted instability of $CH_3Br^{\urcorner 2+}$ is witnessed as well in its methyl analogue, $CH_3CH_2Br^{\urcorner 2+}$.

$CH_3CH_2I^{\urcorner +}\cdot$

Electron impact of ethyliodide, the final member of the series, underlines a basic similarity for chloro-, bromo-, and iodoethane under

conditions of electron impact ionization. The intensity of the molecular ion represents the base peak in the spectrum, indicating a relative stability to vertical ionization. Halogen radical loss is favored as well, and the loss of $CH_3\cdot$ produces the characteristic methylene iodide cation, CH_2I^+.

Vertical and adiabatic ionization energy measurements for ethyl iodide, as in the chloro analogue, generate a common value, 9.34±0.03eV (138). From the published heat of formation of the neutral, -7.5 kJ mol^{-1} (138), $\Delta H_f°$ of the ethyliodide radical cation, $CH_3CH_2I^{\cdot+}$, is calculated to be 894 kJ mol^{-1}.

The thermodynamically cheapest fragmentation process, at 1024 kJ mol^{-1}, is the generation of $CH_3CH_2^+$ via loss of I·, the $\Delta H_f°$ values for these fragments are 917 kJ mol^{-1} and 107 kJ mol^{-1} respectively (26). This is not, however, an intensely metastable process. The MI mass spectrum, as in ethylbromide, resembles no more than a very weak CID mass spectrum resulting from the residual gas pressure within the instrument. The application of a voltage to the collision cell, causing the separation of processes inside and outside the collision cell, yielded similar 'MI':'CID' ratios for all the fragment peaks. Thus the ethyliodide molecular ion, its threshold heat of formation some 130 kJ mol^{-1} below that for its cheapest barrier to dissociation, is concluded to be stable over the time scale associated with the second field free region of the VG ZAB-2F.

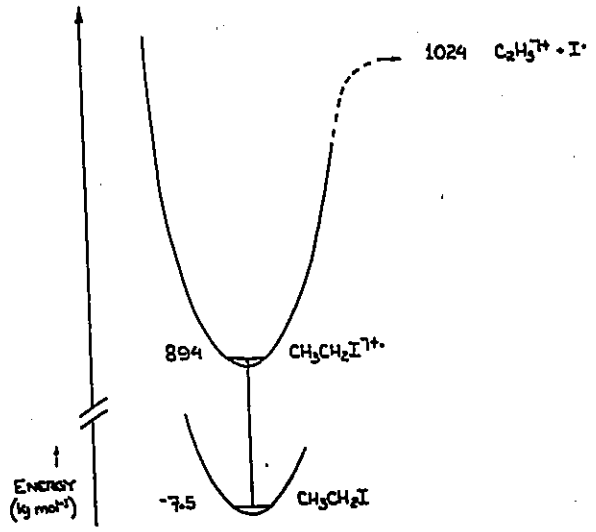

Figure 6.8 Schematic energy diagram for ethyl iodide, its molecular ion, and lowest energy dissociation process.

The CID mass spectrum, as illustrated in *figure (6.9)*, reflects the structure of the molecular ion. The characteristic fragment ions, CH_3^+, $C_2H_5^+$, I^+ and CH_2I^+, present as well in the EI mass spectrum, indicate that rearrangement of the ion prior to collision induced dissociation does not occur.

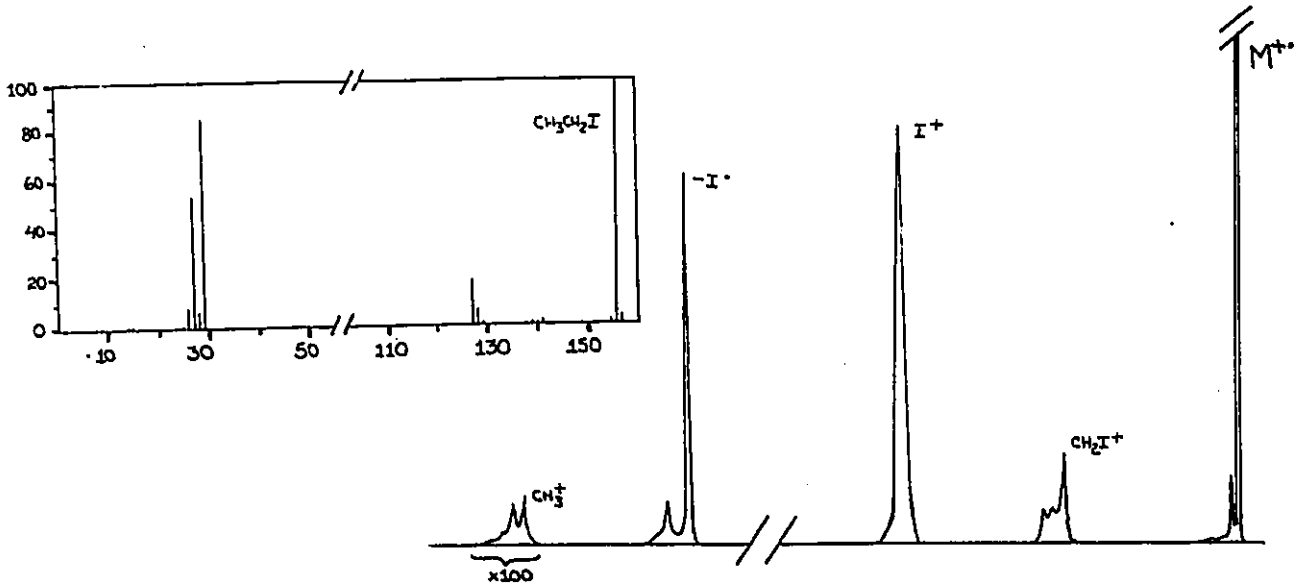

Figure 6.9 The EI and CID mass spectra of ethyl iodide.

The charge stripping mass spectrum of ethyl iodide, quite weak in intensity, is reproduced in Table (6-5). As in its chloro- and bromo-analogues, a molecular dication is not observed in the charge stripping mass spectrum and it is concluded that the $CH_3CH_2I^{\urcorner +\cdot}$ radical cation has no stable dicationic counterpart. The similarity in intensity of the $C_2H_4I^{\urcorner 2+}$ and $C_2H_3I^{\urcorner 2+}$ species is however specific to ethyl iodide.

Summary of the Conventional Ions' Properties

The $\Delta H_f°$'s of the ethyl halide radical cations, as summarized in Table 6-4, have been calculated from the ionization energies of their neutrals. In fluoroethane alone is a significant difference observed between the adiabatic and vertical IE values. With a widening energy range separating the threshold for ionization and the dissociation process of lowest energy requirement, an increasing stability with respect to metastable dissociations from the fluoro to the iodo analogue is observed.

TABLE 6-4 Heat of Formation of $CH_3CH_2X^{\urcorner +}\cdot$

X	IE/AE	$\Delta H_f°[M]$	$\Delta H_f°[C_3CH_2X]^+\cdot$
F	12.43eV (v)	-263 kJ mol^{-1}	936 kJ mol^{-1}
	11.78eV (ad)	"	873 kJ mol^{-1}
Cl	11.01eV (v)	-112 kJ mol^{-1}	950 kJ mol^{-1}
	11.04eV (ad)	"	953 kJ mol^{-1}
Br	10.28eV (v)	-62 kJ mol^{-1}	930 kJ mol^{-1}
I	9.34eV (v)	-7.5 kJ mol^{-1}	894 kJ mol^{-1}
	" (ad)	"	"

The stability of the doubly charged molecular ion, $[C_2H_5X]^{2+}$, is insufficient to enable the detection of the dication. In all cases collision induced dissociation of the stable, mass selected $[C_2H_5X]^+\cdot$ yielded a spectrum very similar to the EI mass spectrum from ionization of the neutrals in the ion source. The spectra above are therefore considered to be uniquely characteristic for the mass selected species $[C_2H_5X]^+\cdot$ of the structure $CH_3CH_2X^{\urcorner +}\cdot$.

TABLE 6-5 Charge Stripping Mass Spectra of $CH_3CH_2X^{\urcorner +}\cdot$

X	M^{2+}	$[M-1]^{2+}$	$[M-2]^{2+}$	$[M-3]^{2+}$	$[M-4]^{2+}$	A
Cl	-	4	100	36	-	1/100
Br	-	27	100	40	5	1/100
I	-	100	90	50	20	~1/1000

A = Approximate intensity of CS peaks with respect to CID peaks

6.2.II $CH_3XCH_2^{\urcorner +}\cdot$ An Ylid Isomer

The radical cations $CH_3XCH_2^{\urcorner +}\cdot$, (X=Cl,Br), ylid isomers of $CH_3CH_2X^{\urcorner +}\cdot$ were proposed as the species formed from the methyl haloacetates on the elimination of carbon dioxide by electron impact in the ion source (127).

$$XCH_2COOCH_3 \rightarrow CO_2 + CH_3XCH_2^{\urcorner +}\cdot \qquad \textit{eq.(6.5)}$$

Note that in a similar reaction the iodo species was not observed. These species, first reported in 1983, were considered to be the first cases of haloalkane cationic radicals containing a divalent halogen atom bonded to two carbons. Analysis by CID mass spectra of the $[C_2H_5Cl(Br)]^{+\cdot}$ ions and $[C_2H_2D_3Cl(Br)]^{+\cdot}$ generated from $(Br)ClCH_2COOCH_3$ and $(Br)ClCH_2COOCD_3$ respectively, supported the proposed ylid structure (127). Further experimental analyses, involving their ionic heats of formation, their metastable processes, as well as the stability of the corresponding dication and neutral however, were not made. A year later an attempted generation of the fluoro analogue, $CH_3FCH_2^{+\cdot}$, from FCH_2COOCH_3 was published (129). The conclusion that only the conventional isomer was formed, was based upon comparison of CID mass spectra, and no other experimental information was reported.

In electron impact ionization of the methyl haloacetates, in the case of fluorine, chlorine, and bromine, a peak corresponding to $[C_2H_5X]^{+\cdot}$ is generated in significant intensity, due to the loss of CO_2. No significant intensity for the equivalent process in the iodo compound has been observed in agreement with the first findings by Schwarz et al. (127), and thus the following discussion will involve the former three halogen species only.

$CH_3ClCH_2^{+\cdot}$ and $CH_3BrCH_2^{+\cdot}$

Adiabatic appearance energy measurements for the chloro and bromo species produced via the following equations have been made.

$$ClCH_2COOCH_3 \rightarrow CH_3ClCH_2^{+\cdot} + CO_2 \qquad \textit{eq.(6.6a)}$$
$$BrCH_2COOCH_3 \rightarrow CH_3BrCH_2^{+\cdot} + CO^2 \qquad \textit{eq.(6.6b)}$$

However due to the severe tailing near threshold electron energies, accurate AE's and thus precise heats of formation of the ions were not obtained. For *eq.(6.6a)* and *eq.(6.6b)* appearance energies of 10.7±0.2eV, and 10.8±0.2eV were observed, respectively. With the neutral methylchloroacetate and methylbromoacetate heats of formation, calculated by additivity to be -414 kJ mol^{-1} and -377 kJ mol^{-1}, and $\Delta H_f°[CO_2]$= -393.5 kJ mol^{-1} (26), the measured AE values lead to a $\Delta H_f°[CH_3ClCH_2]^{+\cdot}$ of 1012±20 kJ mol^{-1}, and 1058±20 kJ mol^{-1} for $\Delta H_f°[CH_3BrCH_2]^{+\cdot}$.

These values are considerably higher, by 62±20 and 128±20 kJ mol^{-1}, than those corresponding to their conventional ions, obtained from their measured IE.

TABLE 6-6 Heat of Formation of $CH_3XCH_2^{\urcorner +}\cdot$

X	AE	$\Delta H_f°[XCH_2COOCH_3]$	$\Delta H_f°[CO_2]$	$\Delta H_f°[CH_3XCH_2]^{\urcorner +}\cdot$
Cl	10.7eV	-414 kJ mol^{-1}	-393 kJ mol^{-1}	1012 kJ mol^{-1}
Br	10.8eV	-377 kJ mol^{-1}	"	1058 kJ mol^{-1}

This is similar to the $CH_3X^+\cdot/\cdot CH_2XH^+$ system, where, for X=Cl, $\Delta H_f°$ for the ylidion is calculated to be 46 kJ mol^{-1} above that of its conventional isomer (120). Ab initio molecular orbital calculations (127,131), restricted to $[C_2H_5Cl]^+\cdot$, were in qualitative agreement with experiment, placing $\Delta H_f°[CH_3ClCH_2]^+\cdot$ 27 kJ mol^{-1} above $\Delta H_f°[CH_3CH_2Cl]^+\cdot$ at the UMP/6-31G*//STO-3G level. In terms of this molecular theory (127,131), $CH_3ClCH_2^{\urcorner +}\cdot$ is considered to be best described as a complex between $CH_2Cl\cdot$ and CH_3^+, where the electrophile is bonded by the chlorine's lone pair electrons.

$T_{0.5}$ values of 26.9meV and 30.8meV were reported for the metastable peaks corresponding to processes *(6.6a)* and *(6.6b)*, and it was proposed that the ylid radical cations were generated in the metastable time frame (127) as well as by collision. Such moderate $T_{0.5}$ values argue against the possibility that the AE, and thus $\Delta H_f°$ results, were excessively high due to the energy for the reverse reaction. Significant metastable generation of the ylids, $CH_3ClCH_2^{\urcorner +}\cdot$ and $CH_3BrCH_2^{\urcorner +}\cdot$, would have enabled the measurement of AE's free of possible kinetic shifts. The kinetic energy release values which were reported are however consistent with collision induced processes. A careful analysis of these peaks showed that metastable generation of neither ylidic species occurs in the second field free region of the VG ZAB-2F.

The metastable ion mass spectrum of the $[C_2H_5Cl]^+\cdot$ radical cation generated from methyl chloroacetate, is unique, producing m/z=29 and m/z=28 in an intensity ratio of ~10:1 (contrary to an earlier report

(127), no metastable generation of CH_2X^+ is observed). The $T_{0.5}$ values for the metastable peaks of this ylidion and its labelled analogue are given in Table (6-7), while the relative intensities and peak shapes are reproduced in *Figure 6.10* below.

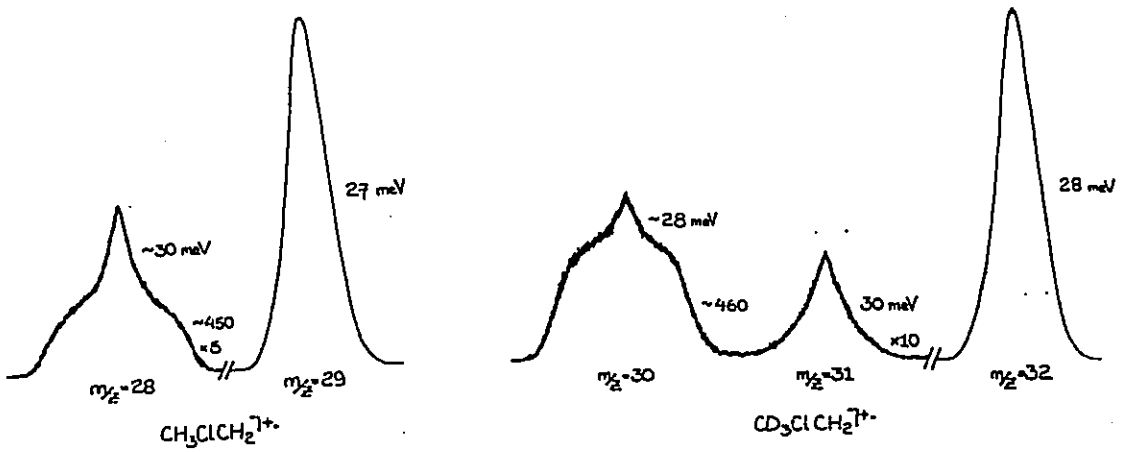

Figure 6.10 The metastable peak shapes observed for the unlabelled and labelled ylidions, $CH_3ClCH_2]^{+}\cdot$ and $CD_3ClCH_2]^{+}\cdot$.

TABLE 6-7 $CH_3ClCH_2]^{+}\cdot$ Metastable Characteristics

			m/z	Peak Shape	$T_{0.5}$
$CH_3ClCH_2]^{+}\cdot$	$\overset{*}{\rightarrow}$	$[C_2H_4]^+\cdot$	28	Composite -Narrow	~30 meV
				-Broad	~450 meV
	$\overset{*}{\rightarrow}$	$[C_2H_5]^+$	29	Gaussian	27 meV
$CD_3ClCH_2]^{+}\cdot$	$\overset{*}{\rightarrow}$	$[C_2D_2H_2]^+\cdot$	30	Composite -Narrow	~28 meV
				-Broad	~460 meV
	$\overset{*}{\rightarrow}$	$[C_2D_3H]^+\cdot$	31	Gaussian	30 meV
	$\overset{*}{\rightarrow}$	$[C_2D_3H_2]^+$	32	Gaussian	28 meV

The peak at m/z=29, a vanishingly weak peak in the MI mass spectrum of ethylchloride, must correspond to $CH_3CH_2^+$ via loss of Cl·. The metastable loss of HCl generates a composite peak, and the separate $T_{0.5}$ values of the broad, dished component and the narrow Gaussian component have been estimated. Similarly, the $T_{0.5}$ values for the broad and narrow components of the composite peak, generated by loss of DCl from $CD_3ClCH_2]^{+}\cdot$, were also obtained.

The composite nature of m/z=28 is proposed to result from the formation of two isomeric daughter ions, $CH_2CH_2^{+}\cdot$ and $CH_3CH^{+}\cdot$. Their heats of formation, as discussed in section 6.2.I, are estimated to differ by ~80 kJ mol^{-1}.

$$CH_3ClCH_2^{+}\cdot \overset{*}{\rightarrow} CH_3CH^{+}\cdot + HCl \qquad \text{(i) } \Delta H_f^\circ(\text{Prod.}) \approx 1063 \text{ kJ mol}^{-1}$$
$$\overset{*}{\rightarrow} CH_2CH_2^{+}\cdot + HCl \qquad \text{(ii) } \Delta H_f^\circ(\text{Prod.}) = 983 \text{ kJ mol}^{-1}$$
$$\Delta(\Delta H_f^\circ) \sim 80 \text{ kJ mol}^{-1}$$

Process (i) will, therefore, correspond to the narrow component in the composite metastable peak, the fragments having been generated near threshold. The generation of an energy rich ethylene radical cation via a barrier of similar height is proposed to produce the very broad component of the composite C_2H_4 peak (similarly the generation of energy rich $CD_2CH_2^{+}\cdot$ from $CD_3ClCH_2^{+}\cdot$). It is interesting to note that loss of HCl from the labelled species, observed as a *narrow* Gaussian peak, should result in the specific formation of $CD_3CH^{+}\cdot$, with seemingly no rearrangement. This process, not isolated in the unlabelled species, accounts for the larger relative intensity of the narrow component in m/z=28. The dissimilarity of the peaks for DCl and HCl loss from $CD_3ClCH_2^{+}\cdot$ suggests that little or no hydrogen/deuterium scrambling occurs prior to dissociation. Figure 6.21 is an illustrative comparison of the metastable processes of the $[C_2H_5Cl]^{+}\cdot$ isomers, based on the above proposal. It will be discussed further in the following section, and is presented in the summary of the distonic ions, 6.2.V.

TABLE 6-8 $CH_3BrCH_2^{+}\cdot$ Metastable Characteristics

		m/z	Peak Shape	$T_{0.5}$
$CH_3BrCH_2^{+}\cdot \overset{*}{\rightarrow}$	$[C_2H_4]^{+}\cdot$	28	Gaussian	~40 meV
$\overset{*}{\rightarrow}$	$[C_2H_5]^{+}$	29	Gaussian	43 meV

The bromine derivative, $CH_3BrCH_2^{+}\cdot$, yields a very weak metastable peak at m/z=28 and one at m/z=29 in an intensity ratio of ~1:40. The increased intensity of the metastably generated ethyl radical cation from $CH_3BrCH_2^{+}\cdot$ may be the result of a reduced energy difference between the heat of formation of the radical cation and its subsequent barrier to

dissociation. However $\Delta H_f^\circ[CH_3BrCH_2]^+\cdot$ at 1058 kJ mol^{-1}, places the ion above the calculated thresholds for loss of both Br•, at 1029, and HBr, at 1039 kJ mol^{-1}. The relatively weak generation of m/z=28 therefore, indicates a significant barrier for this fragmentation pathway.

The collision induced dissociation mass spectra of both the chloro and bromo analogues of the ylid radical cation $CH_3XCH_2^{+}\cdot$ are illustrated in *figures (6.11)* and *(6.12)*. Good qualitative agreement is observed with those obtained earlier (127) despite differences in the experimental conditions.

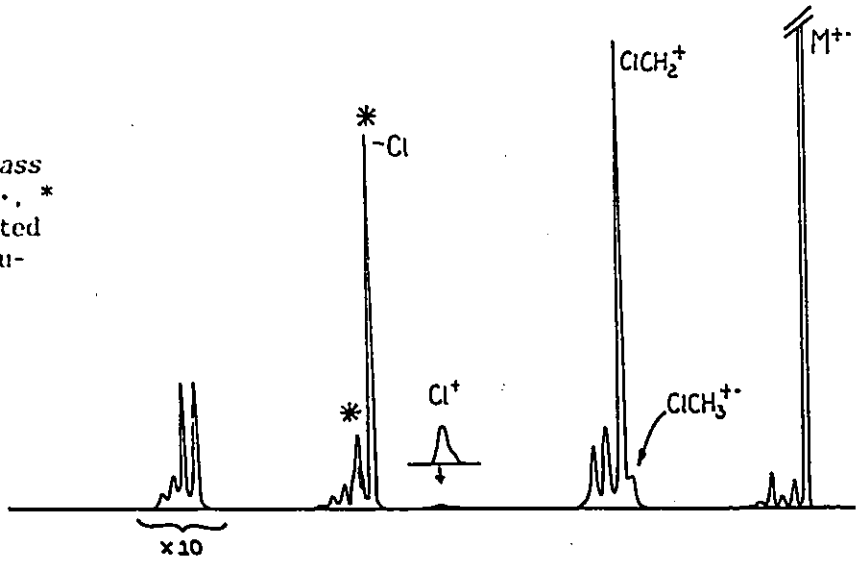

Figure 6.11 The CID mass spectrum of $CH_3ClCH_2^{+}\cdot$, * indicates peaks corrected for metastable contributions.

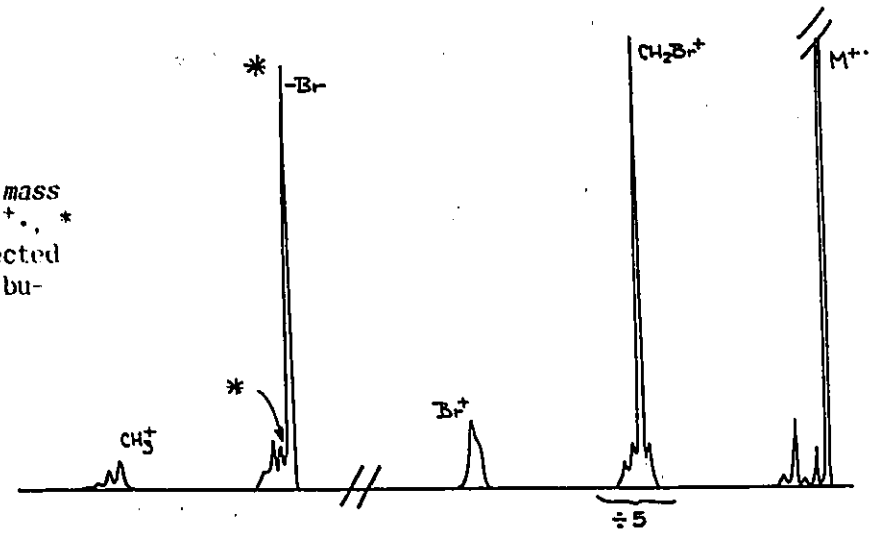

Figure 6.12 The CID mass spectrum of $CH_3BrCH_2^{+}\cdot$, * indicates peaks corrected for metastable contributions.

A reduced relative intensity of the C_2 cluster, indicative of a C-C bond, as well as an increased intensity of the CH_2X^+ fragment is immediately evident on comparison with the CID of the conventional species *(figures 6.3* and *6.6)*. However it is the less intense but structurally signif-

icant presence of the $CH_3X^{+}\cdot$ fragment which characterizes the $CH_3XCH_2^{+}\cdot$ isomers. The dissociative fragmentation of the labelled species $CD_3ClCH_2^{+}\cdot$, producing $CD_3Cl^{+}\cdot$, underlines the characteristic structure of the ylid; the absence of any significant $ClCD_2H^{+}$ indicates little or no hydrogen/deuterium scrambling prior to or directly after collisional excitation.

The charge stripping mass spectra for $CH_3ClCH_2^{+}\cdot$ and $CH_3BrCH_2^{+}\cdot$, represented in Table (6-16), are very weak, ~1/1000 of the intensity of the singly charged species. With the base peak corresponding to M^{2+}, it would appear that the $CH_3XCH_2^{+}\cdot$ ylidic ions, unlike their conventional counterparts, generate corresponding dications, albeit weakly. This is consistent with the behaviour of the $CH_3X^{+}\cdot/CH_2XH^{+}\cdot$ pair.

Attempted Generation of $CH_3FCH_2^{+}\cdot$

Methylfluoroacetate is unique among the methylhaloacetates studied in having metastable loss of CO_2 for the unimolecular generation of $[C_2H_5F]^{+}\cdot$. The appearance energy for $[C_2H_5F]^{+}\cdot$ at m/z=48 could therefore be measured from both the source and metastably generated species. From the source generated species, using energy selected electrons, an AE of 10.90±0.05eV has been obtained. This result is considered to be free of any significant reverse activation energy due to the fairly small $T_{0.5}$ value of 22meV associated with the metastable loss of CO_2. The AE for the metastably generated species, via threshold energy comparisons, results in 11.06±0.1eV, a value which possesses little kinetic shift error and which agrees well with the first measurement.

TABLE 6-9 Heat of Formation of $[C_2H_5F]^{+}\cdot$ from FCH_2COOCH_3

AE	$\Delta H_f°[FCH_2COOCH_3]$	$\Delta H_f°[CO_2]$	$\Delta H_f°[C_2H_5F]^{+}\cdot$
10.90eV[1]	-587 kJ mol^{-1}	-393 kJ mol^{-1}	858 kJ mol^{-1}
11.06eV[2]	"	"	873 kJ mol^{-1}

[1] From source generated species onset
[2] From metastably generated species in 1st field free region

With $\Delta H_f°$ of the methylfluoroacetate neutral calculated by additivity to be -587 kJ mol^{-1}, the heat of formation of the ion produced via CO_2 loss

is calculated to be 858 kJ mol $^{-1}$, using the AE value of 10.90eV, and 873 kJ mol $^{-1}$, from the value 11.06eV. While the former is within experimental error, the latter value is identical to the $\Delta H_f°[CH_3CH_2F]^{+\cdot}$ calculated from the measured adiabatic IE of ethylfluoride.

The $[C_2H_5F]^{+\cdot}$ ion obtained from methylfluoroacetate metastably generates m/z 47 and m/z 46 of similar intensity (and no m/z=33, CH_2F^+, of any significance). The peak corresponding to $[C_2H_3F]^{+\cdot}$ is broad and dished, with a measured $T_{0.5}$ value of 360meV. That corresponding to $[C_2H_4F]^+$ is narrow, a Gaussian shaped peak having a $T_{0.5}$≈10meV. These values are very similar to the values of 310 and 8meV, obtained from ionized ethylfluoride. Under reduced resolution, the metastable peak, m/z=47, appears significantly broader with a $T_{0.5}$~55meV. High resolution indicates a broad interference at the base, favoured at higher magnet settings, which may be subtracted from the true, narrower metastable peak.

The collision induced dissociation of the $[C_2H_5F]^{+\cdot}$ radical cation, (generated in a 1:1 ratio with $[C_2H_4F]^+$ in the EI of the ester), requires little ^{13}C correction, and generates a mass spectrum indistinguishable from the ^{13}C corrected CID mass spectrum of $CH_3CH_2F^{\neg+\cdot}$ illustrated in *figure (6.2)*. This spectrum, as discussed previously, is not in agreement with the tabulated results published earlier (129), but the indistinguishability of the $[C_2H_5F]^{+\cdot}$ CID mass spectra from the two precursors, CH_3CH_2F and FCH_2COOCH_3 is consistent. The CID mass spectrum of the metastably generated $[C_2H_5F]^{+\cdot}$ showed no inconsistencies.

Ethylfluoroacetate, via loss of CO_2, is thus not observed to generate $CH_3FCH_2^{\neg+\cdot}$ over the wide range of internal energies sampled. CID mass spectra of the source as well as metastably generated $[C_2H_5F]^{+\cdot}$ are indistinguishable with that from $CH_3CH_2F^{\neg+\cdot}$. The experimentally derived $\Delta H_f°$s and metastable characteristics are also equal.

Based on the trend observed in the hydrogen homologues, and the very significant generation of both $CH_3ClCH_2^{\neg+\cdot}$ and $CH_3BrCH_2^{\neg+\cdot}$, the inability to observe the fluoro analogue is, however, surprising. From Table 6-10, $\Delta H_f°$[ylidion] might well be extrapolated to be near that of its conventional isomer.

TABLE 6-10 Relative Stabilities of $CH_3CH_2X^{\neg +}\cdot$ and $CH_3XCH_2^{\neg +}\cdot$

X	$\Delta H_f°$[Conventional Ion] - $\Delta H_f°$[Ylidion] kJ mol^{-1}	
	$[CH_3X]^{+}\cdot - [CH_2XH]^{+}\cdot$ [1]	$[CH_3CH_2X]^{+}\cdot - [CH_3XCH_2]^{+}\cdot$ [2]
F	-19	-
Cl	+46	+62
Br	-	+128

[1]From theoretical calculations (5)
[2]From experimental results reported herein

The generation of the $CH_3XCH_2^{\neg +}\cdot$ ylidion from methyl haloacetate requires the migration of the methyl group, via a five membered ring, to the halogen atom. For both X=Cl,Br this is observed. The different migratory behavior of the CH_3 group in methyl fluoroacetate may be the result of a different site of protonation in the ester (compare a and b), as a result of the greater electron affinity of fluorine.

a. 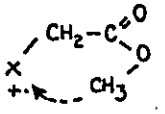

b. 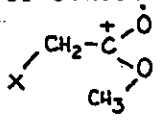

6.2.III $CH_3CHXH^{+}\cdot$ A Second Ylidion

The ylidions, $CH_3CHXH^{\neg +}\cdot$, X=Cl,Br, were first reported by Holmes, Terlouw, and Schwarz et al. (57) as stable complexes between $CH_3CH^{+}\cdot$ and HX, generated by loss of CO_2 from the precursors, $CH_3CHXCOOH$.

$$CH_3CHXCOOH \rightarrow CH_3CHXH^{\neg +}\cdot + CO_2 \qquad eq.(6.7)$$

The CID mass spectra were found to differ significantly from those of $CH_3CH_2X^{\neg +}\cdot$ and $CH_3XCH_2^{\neg +}\cdot$, and intense CS peaks were observed. Analyses via the CID mass spectra of $CH_3CHClH^{\neg +}\cdot$, $^{13}CH_3CHClH^{\neg +}\cdot$, generated from $^{13}CH_3CHClCOOH$, and $CD_3CHClH^{\neg +}\cdot$, generated from $CD_3CHClCOOH$, indicated that the methyl group in the precursor and product ion remained intact, and thus $CH_3CHClH^{\neg +}\cdot$ rather than $CH_2CH_2ClH^{\neg +}\cdot$ was proposed. A $\Delta H_f°[CH_3CHClH]^{+}\cdot$=951 kJ mol^{-1} was obtained from the measured AE of 10.72eV and the $\Delta H_f°[CH_3CHClCOOH]$=-477 kJ mol^{-1} (21). The metastable ion spectra for X=Cl was also unique. The labelled species $CH_3CHClD^{\neg +}\cdot$ and $CH_3CDClH^{\neg +}\cdot$ were reported to lose HCl only, while $CD_3CHClH^{\neg +}\cdot$ generated HCl and DCl in a 1:2.1 ratio. AE measurements for both $C_2H_4^{\neg +}\cdot$ and $C_2H_5^{\neg +}$, 11.4eV and ≤11.5eV respectively, indicated a common dissociation

threshold, and thus the conclusion was drawn that the ylidic radical cation rearranged to an energy rich $CH_3CH_2Cl^{+\cdot}$ species prior to metastable dissociation. The CID and CS mass spectra of the unlabelled Bromo analogue were also reported.

The bulk of mass spectral data for the $[C_2H_5Cl]^{+\cdot}$ and $[C_2H_5Br]^{+\cdot}$ radical cations generated via *equation (6.7)* have been reproduced, under standard experimental conditions, and unless otherwise stated are in good experimental agreement with the earlier results. The metastable processes for the chloro analogue have also been reanalyzed. The heat of formation and MI characteristics of the bromo analogue are also reported. Generation of the fluoro analogue $CH_3CHFH^{+\cdot}$, was not pursued, the ion corresponding to loss of CO_2 was reported *absent* in the EI mass spectrum of 2-fluoropropionic acid (129). Neither is the iodo analogue produced, $CH_3CHICOOH$ generates $C_2H_4I^+$, not $C_2H_5I^{+\cdot}$, in its EI mass spectrum, and the molecular ion loses mainly I·, unimolecularly and by collision.

$CH_3CHClH^{+\cdot}$ and $CH_3CHBrH^{+\cdot}$

Electron impact ionization of both 2-chloro and 2-bromopropionic acid generate $[C_2H_5X]^{+\cdot}$ radical cations in significant intensity, ~80% and 70% respectively of their base peaks, m/z=28. In the case of 2-chloropropanoic acid the process also occurs metastably, with a very narrow $T_{0.5}$~3.5meV, suggestive of a threshold reaction.

The AE for $[C_2H_5Cl]^{+\cdot}$ generated from 2-chloropropanoic acid, as mentioned above, results in a heat of formation of $CH_3CHClH^{+\cdot}$ within experimental error, equal to that of $CH_3CH_2Cl^{+\cdot}$, thus the ylid ion structure, $CH_3CHClH^{+\cdot}$ is 61±20 kJ mol^{-1} more stable than its isomer $CH_3ClCH_2^{+\cdot}$.

TABLE 6-11 Heat of Formation of $CH_3CHXH^{+\cdot}$

X	AE	$\Delta H_f°[XCH_2CH_2COOH]$	$\Delta H_f°[CO_2]$	$\Delta H_f°[CH_3CHXH]^{+\cdot}$
Cl	10.72eV	-477 kJ mol^{-1}	-393 kJ mol^{-1}	951 kJ mol^{-1}
Br	10.70eV	-431 kJ mol^{-1}	"	995 kJ mol^{-1}

The adiabatic appearance energy for the bromo analogue has been measured, 10.70±0.05eV. With a $\Delta H_f°[CH_3CHBrCOOH]$ of -431 kJ mol^{-1}, the heat of formation for the ylid ion, $CH_3CHBrH^{\urcorner +}\cdot$ is calculated to be 995 kJ mol^{-1}, also 63±20 kJ mol^{-1} more stable than its ylid isomer $CH_3BrCH_2^{\urcorner +}\cdot$.

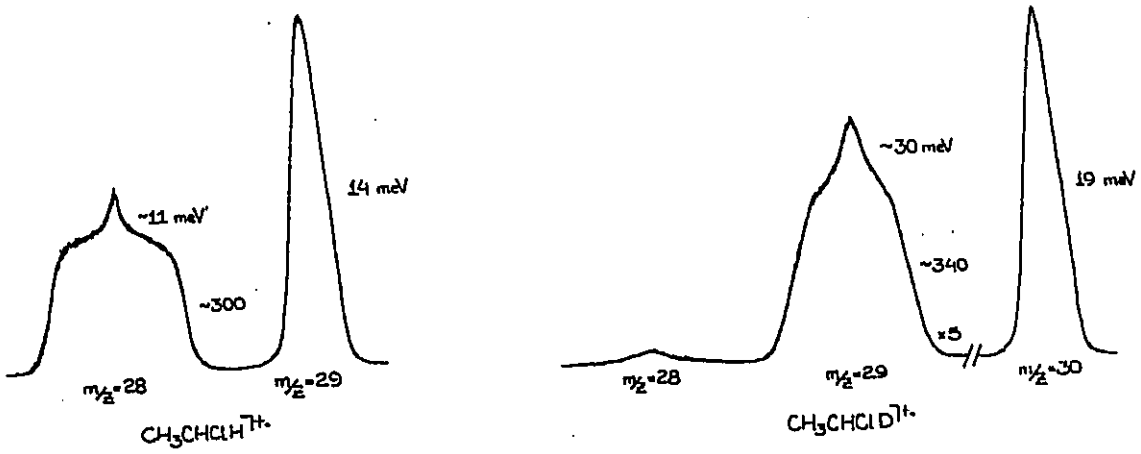

Figure 6.13 Metastable peak shapes observed for the unlabelled and labelled ylid ions, $CH_3CHClH^{\urcorner +}\cdot$ and $CH_3CHClD^{\urcorner +}\cdot$ respectively.

TABLE 6-12 $CH_3CHCl^{\urcorner +}\cdot$ Metastable Characteristics

			m/z	Peak Shape	$T_{0.5}$
$CH_3CHClH^{\urcorner +}\cdot$	$\xrightarrow{*}$	$[C_2H_4]^+\cdot$	28	Composite -Narrow	~11 meV
				-Broad	~300 meV
	$\xrightarrow{*}$	$[C_2H_5]^+$	29	Gaussian	14 meV
$CH_3CHClD^{\urcorner +}\cdot$	$\xrightarrow{*}$	$[C_2H_4]^+\cdot$	28	-	v.weak
	$\xrightarrow{*}$	$[C_2DH_3]^+\cdot$	29	Composite -Narrow	~30 meV
				-Broad	~340 meV
	$\xrightarrow{*}$	$[C_2DH_4]^+$	30	Gaussian	19 meV

$CH_3CHClH^{\urcorner +}\cdot$ undergoes metastable loss of Cl· and HCl, as outlined in Table 6-12, and illustrated in *figure (6.13)*. These values follow a similar pattern as the half-height widths of the metastable peaks associated with $CH_3ClCH_2^{\urcorner +}\cdot$. Thus the composite nature of the $[C_2H_4]^+\cdot$ metastable peak from the ylid ion $CH_3CHClH^{\urcorner +}\cdot$ is, as for $CH_3ClCH_2^{\urcorner +}\cdot$, proposed to result from the generation of both $CH_2CH_2^{\urcorner +}\cdot$ and $CH_3CH^{\urcorner +}\cdot$.

Therefore, as illustrated in *figure (6.20)* in 6.2.V, the broad component results from the formation of the ethylene radical cation well above its thermodynamic threshold, while the narrow component corresponds to the near threshold formation of $CH_3CH^{\neg +}\cdot$.

It is possible that the $[C_2H_4]^{+}\cdot$ isomeric ions are formed via a common transition state. Semi-empirical molecular orbital calculations using Dewar's MNDO procedure (141), suggested two reasonable transitions states illustrated below, TS_1 and TS_2 (57), of which the energetically less favored species, TS_2, is of interest here.

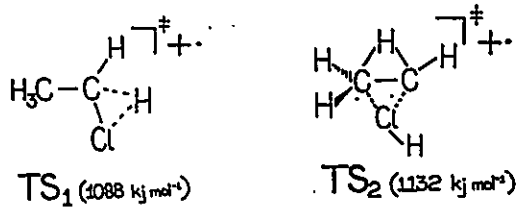

Figure 6.14 Possible transition states for the generation of $[C_2H_4]^{+}\cdot$ from $[C_2H_5Cl]^{+}\cdot$, and their calculated heats of formation, (15).

Via this latter intermediate, both $[C_2H_4]^{+}\cdot$ isomers may be produced, $CH_3CH^{\neg +}\cdot$ + HCl near the estimated thermodynamic threshold of ~1063 kJ mol^{-1}, and $CH_2CH_2^{\neg +}\cdot$ with a large excess energy. The loss of Cl·, observed in both ylid isomers, is not expected to proceed via TS_2. The kinetic energy release associated with this loss would be far greater than the value implied by the measured $T_{0.5}$ values of 14 and 27mev for $CH_3ClCH_2^{\neg +}\cdot$ and $CH_3CHClH^{\neg +}\cdot$ respectively. Moreover the intensity ratio for Cl·:HCl loss in the two ylid species is significantly different. That loss of Cl· and HCl compete thermodynamically on the metastable time frame, and that the measured appearance energies for these processes are similar (57), would however suggest that the transition states for these processes are not too widely different in energy.

The MI mass spectrum of the labelled species, $CH_3CHClD^{\neg +}\cdot$, from $CH_3CHClCOOD$, is in good agreement with the earlier investigation (57). The measured $T_{0.5}$ values are given in Table 6-12. Very little loss of DCl via direct fragmentation, was observed in the MI mass spectrum.

The metastable processes of the bromo analogue, $CH_3CHBrH^{\urcorner +}\cdot$, involve the loss of Br· and HBr, in an intensity ratio of ~40:1, as expected from the higher energy level associated with the formation of $CH_2CH_2^{\urcorner +}\cdot$ and HBr.

TABLE 6-13 $CH_3CHBrH^{\urcorner +}\cdot$ Metastable Characteristics

		m/z	Peak Shape	$T_{0.5}$
$CH_3CHBrH^{\urcorner +}\cdot$	$[C_2H_4]^+\cdot$	28	Gaussian	12 mev
	$[C_2H_5]^+\cdot$	29	Gaussian	24 meV

Despite the similar MI intensity ratios for $CH_3CHBrH^{\urcorner +}\cdot$ and $CH_3BrCH_2^{\urcorner +}\cdot$, the $T_{0.5}$ values are distinctly different, and thus interconversion of these species, even at the higher internal energies associated with metastable ions, does not occur.

The collision induced dissociation mass spectra of the $CH_3CHXH^{\urcorner +}\cdot$ species, for both chlorine and bromine are illustrated in *figures (6.15)* and *(6.16)*. These species generate several unique features including, domination of the C_2 cluster by m/z=28, greater relative intensity of $HX^+\cdot$ with respect to X^+, near absence of the CH_2X^+ fragment, and very intense charge stripping peaks.

The base peaks in the CS mass spectra for the chloro and bromo analogues, in Table (6-16), correspond to the undissociated doubly charged species, $[C_2H_5X]^{2+}$, in both cases. Whereas the absolute intensities of the CS spectra for the two ylid isomers are widely different, the relative intensities of the peaks themselves are quite similar. The very weak CS peaks observed in the CID of $CH_3XCH_2^{\urcorner +}\cdot$ may well result from the presence of trace $CH_3CHXH^{\urcorner +}\cdot$ species, not unrealistic in the light of the similar unimolecular characteristics and proposed common transition state for metastable formation of m/z=28, the dissociation of lowest energy requirement.

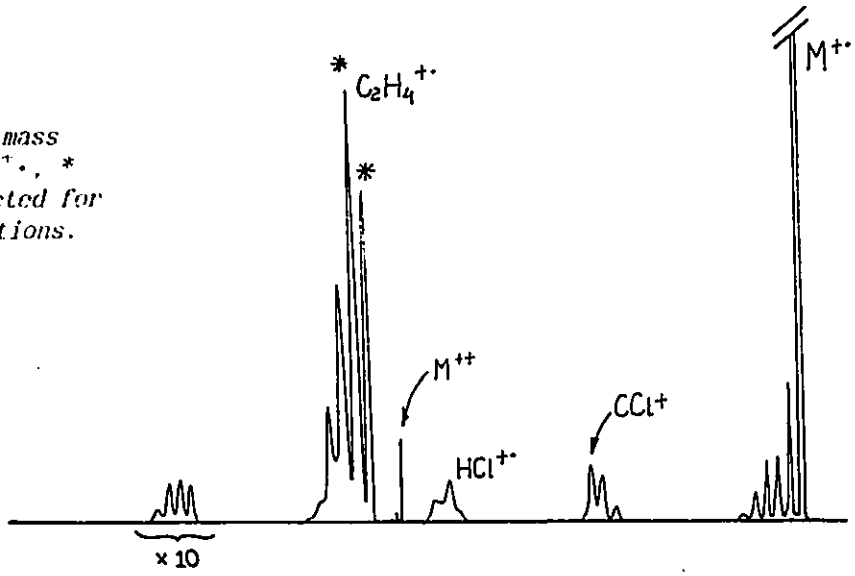

*Figure 6.15 The CID mass spectrum of $CH_3CHClH^{+\cdot}$, * indicates peak corrected for metastable contributions.*

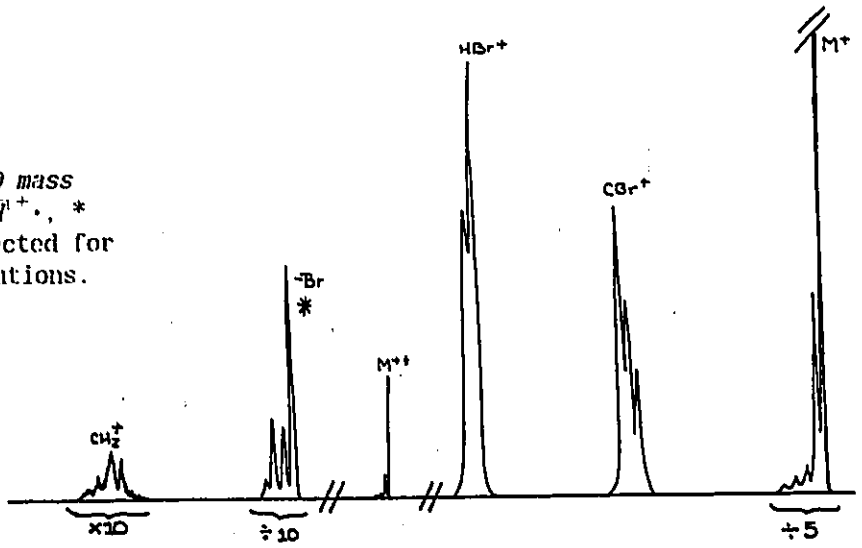

*Figure 6.16 The CID mass Spectrum of $CH_3ClBrH^{+\cdot}$, * indicates peak corrected for metastable contributions.*

6.2.IV $CH_2CH_2XH^+$· A Distonic Isomer

No positive results for the generation of distonic isomers, $CH_2CH_2XH^{+\cdot}$, have been reported. The possible generation of $CH_2\dot{C}H_2ClH^{+\cdot}$ by loss of CO_2 from ionized 2-chloropropanoic acid was ruled out via deuterium and ^{13}C labelling studies (57). Also, further potential precursors were investigated via the following processes below (57);

i. $ClCH_2CH_2COOH \rightarrow [C_2H_5Cl]^{+\cdot} + CO_2$
ii. $ClCH_2CH_2CH_2OH \rightarrow [C_2H_5Cl]^{+\cdot} + CH_2O$
iii. $ClCH_2CH_2OCHO \rightarrow [C_2H_5Cl]^{+\cdot} + CO_2$

but of the above precursors none were reported to generate a $[C_2H_5Cl]^{+\cdot}$ ion on electron impact excitation. Closer analysis has found otherwise.

Small, but reproducibly significant signals, ~1% of the base peak (m/z=58, and m/z=31 respectively) corresponding to the $[C_3H_5X]^{+\cdot}$ species, for X=^{35}Cl(^{37}Cl) and ^{79}Br(^{81}Br), were observed in the EI mass spectra of $ClCH_2CH_2CH_2OH$ and $BrCH_2CH_2CH_2OH$. A very weak signal for the fluoro analogue is present in the EI mass spectrum of $FCH_2CH_2CH_2OH$. Based on the unique MI, CID, and CS mass spectra of these ions, a fourth stable isomer of the $[C_2H_5X]^{+\cdot}$ system is believed to have been generated, the distonic radical cation $CH_2CH_2XH^{+\cdot}$.

$\Delta H_f°[CH_2CH_2XH]^{+\cdot}$

Due to their relatively low intensity, appearance energies and thus experimentally derived heats of formation, were unobtainable for these $[C_2H_5X]^{+\cdot}$ distonic ions derived from 3-fluoro, 3-chloro and 3-bromo-propanol. Two very recent theoretical analyses of these "protonated β-halogenoethyl radicals" of fluorine and chlorine have however, been reported (130,132).

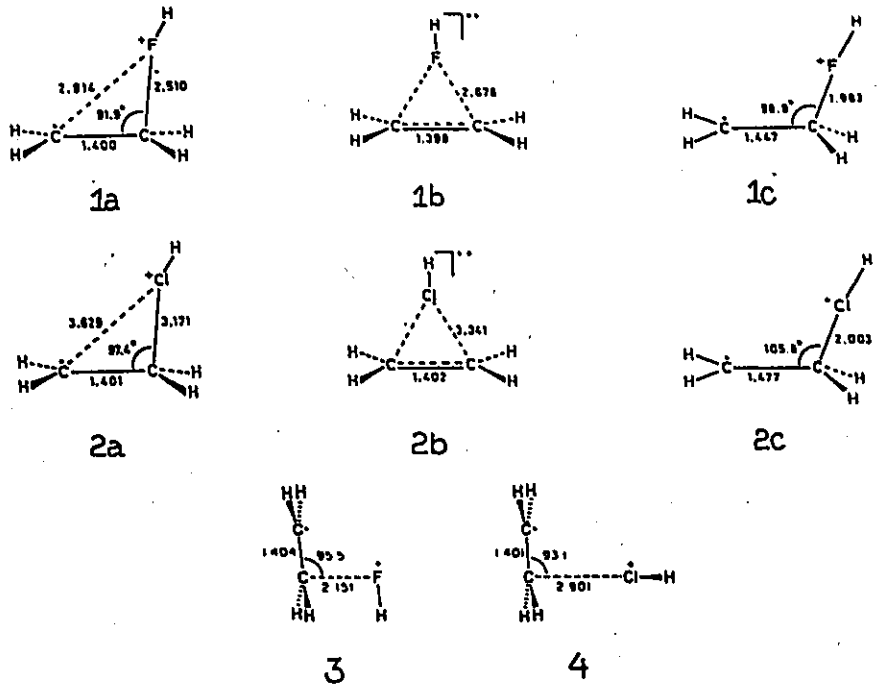

Figure 6.17 Geometry optimized strctures of the fluoro and chloro distonic radical cations, and their bridged counterparts (130,132).

Geometry optimisations with the 6-31G* basis set followed by single point MP2/6-31G* energy calculations predict that the bridged structures of the fluoro and chloro ions, 1a,b and 2a,b, are clearly bound, relative to the ethylene radical cation and the appropriate hydrogen halide neutral. The distonic species, 1c and 2c, however are predicted to be 94 and 44 kJ mol^{-1} less stable than their assymetrically bridged isomers, as well as 40 and 15 kJ mol^{-1} above the threshold energy for $C_2H_4^{+}\cdot$ + HX formation (130).

Based on these calculations (130), the stable, $[C_2H_5X]^{+}\cdot$ radical cations generated from 3-fluoropropanol and 3-chloropropanol may well be of the nonclassical form depicted in a or b. The bridged forms of $[C_2H_5F]^{+}\cdot$ are predicted to be 125 kJ mol^{-1} more stable than the conventional ethylfluoride ion, while for chlorine, 2a and b show a stability which is slightly less than that of the ethylchloride ion. Another recent theoretical investigation, involving 3-21G* optimized structures and MP2/6-31G* calculated total energies, of a wide collection of distonic and conventional radical cations, report the $CH_2CH_2FH^{+}\cdot$, 3, and $CH_2CH_2ClH^{+}\cdot$, 4, distonic ions to be 74 and 15 kJ mol^{-1} more stable than their conventional counterparts (132).

TABLE 6-14 Heat of Formation of $CH_2CH_2XH^{+}\cdot$

	Relative Energies	$\Delta H_f°[CH_2CH_2XH]^{+}\cdot$
$[C_2H_4]^{+}\cdot$ + HF	0	
1a	-54 kJ mol^{-1} [1]	748 kJ mol^{-1}
1b	-54 kJ mol^{-1} [1]	748 kJ mol^{-1}
1c	40 kJ mol^{-1} [1]	842 kJ mol^{-1}
$[C_2H_4]^{+}\cdot$ + HCl	0	
2a	-29 kJ mol^{-1} [1]	954 kJ mol^{-1}
2b	-22 kJ mol^{-1} [1]	961 kJ mol^{-1}
2c	15 kJ mol^{-1} [1]	998 kJ mol^{-1}
$CH_3CH_2F^{+}\cdot$	0	
3	-74 kJ mol^{-1} [2]	799 kJ mol^{-1}
$CH_3CH_2Cl^{+}\cdot$	0	
4	-15 kJ mol^{-1} [2]	935 kJ mol^{-1}

[1]Ref 130 MP2/6-31G*//6-31G*
[2]Ref 132 MP2/6-31G*//3-21G*

$CH_2CH_2FH^{\neg +}\cdot$

Due to the low intensity of the mass selected beam in the case of the fluorine analogue, analysis of the metastable processes could not be done under conditions of high energy resolution. Significantly intense peaks at both m/z=47 and m/z=46, as observed in the MI of ethylfluoride, are generated, but a third peak is also seen. A broad peak, the $T_{0.5}$ value set at approximately 600meV, corresponds to loss of HF. Correction for ^{13}C contribution, from the metastable loss of HF from m/z=47, is necessary but accounts for no more than 30% of the observed peak intensity. Due to the large cross-section for its generation via collision, as indicated by the CID illustrated in *figure (6.18)*, some may also be due to residual collision gas pressures, however the breadth of this peak is quite uncharacteristically wide for a collision induced process. Therefore, the loss of HF is concluded to occur in the metastable time frame. This is far from unexpected, energetically: generation of ethylene radical cation ($\Delta H_f°$=1075 kJ mol^{-1} (138)) and hydrogenfluoride ($\Delta H_f°$=-273.3 kJ mol^{-1} (138)) is at 802 kJ mol^{-1}, and as depicted in *figure (6.1)*, is the lowest calculated threshold for dissociation of the C_2H_5F system. On the other hand, no metastable generation of $C_2H_4^+\cdot$ is observed for the molecular ion of ethylfluoride, and even by collision induced dissociation this process is a very minor one. It is therefore quite likely that the loss of HF is not favored kinetically, i.e. its k(E) versus E curve rises less steeply than that for loss of H· (a similar argument has been used for the metastable loss of CH_3 versus CH_4 from simple ketone molecular ions, (143)). That the process is metastable, albeit weakly, for the distonic species may well be explained on the grounds that unlike ethylfluoride, loss of HF may proceed via direct bond cleavage. As illustrated in *figure 3.2*, relatively steeper slopes for the k(E) versus E curves are observed for dissociations via direct cleavage than those involving rearrangement.

The CID mass spectrum of the distonic ion, $CH_2CH_2FH^{\neg +}\cdot$, contains features uniquely, and predictably characteristic of the proposed distonic structure. The significant peaks corresponding to CH_2^+ and $HF^+\cdot$, and the intense m/z=28, are at once very uncharacteristic of ethylfluoride and easily attributed to the distonic form.

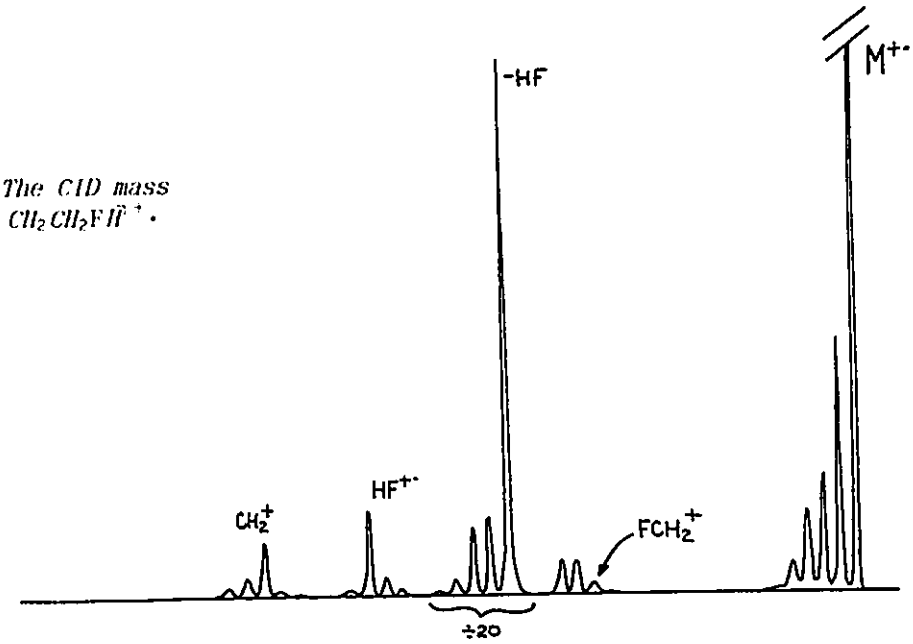

Figure 6.18 The CID mass spectrum of $CH_2CH_2FH^{\neg +}\cdot$

$CH_2CH_2ClH^{\neg +}\cdot$ and $CH_2CH_2BrH^{\neg +}\cdot$

The $[C_2H_5Cl]^+\cdot$ species generated from 3-chloropropanol produce no intense metastable peaks; under conditions of maximum gain no more than a 'residual ClD' is produced. The generation of ethylene radical cation may be weakly unimolecular but the low intensity of the main beam does not allow for a realistic search for this process in the first field free region of either the VG ZAB-2F or MS-902S. This species is therefore, quite separate from its ylidic isomers in the absence of *any* significant metastable loss of Cl·. The bromo analogue on the other hand does undergo the metastable loss of halogen, to give a very narrow, Gaussian shaped peak with a corresponding $T_{0.5}$~7meV, but no metastable loss of HBr is observed.

The chloro and bromo analogues also generate CID mass spectra containing features predictably characteristic of the proposed distonic structure, $CH_2CH_2XH^{\neg +}\cdot$, as illustrated in *figures (6.19)* and *(6.20)*. The lack of intensity at m/z=15 indicates the absence of the structural unit CH_3. The dominance of m/z=28 and near lack of m/z=29 is indicative of C_2H_4 in the chlorine compound, while the minor intensity of m/z=29 in the bromine compound, after correcting for the metastable process, points to an inability to generate the $[C_2H_5]^+$ species by direct cleavage. As well, the $HX^+\cdot$ fragment is of significantly greater intensity than that of X^+.

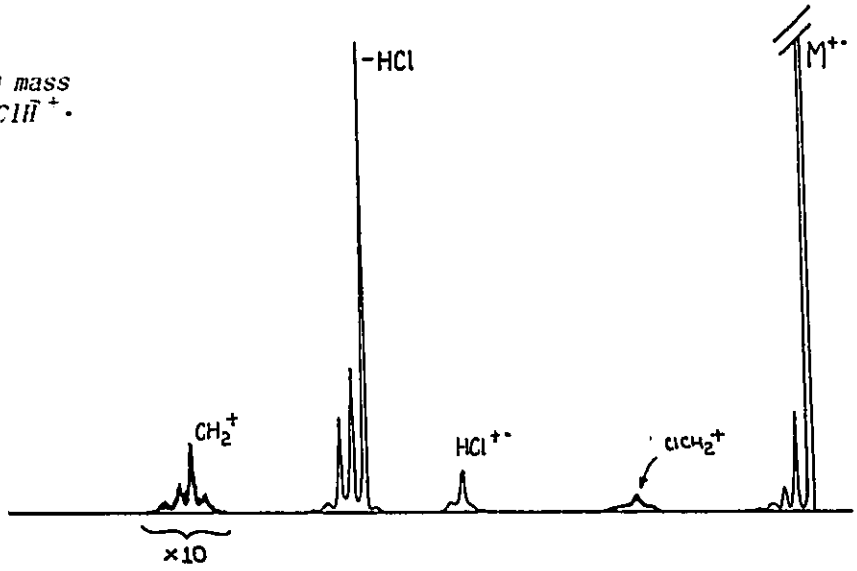

Figure 6.19 The CID mass spectrum of $CH_2CH_2Cl\bar{H}^{+\cdot}$.

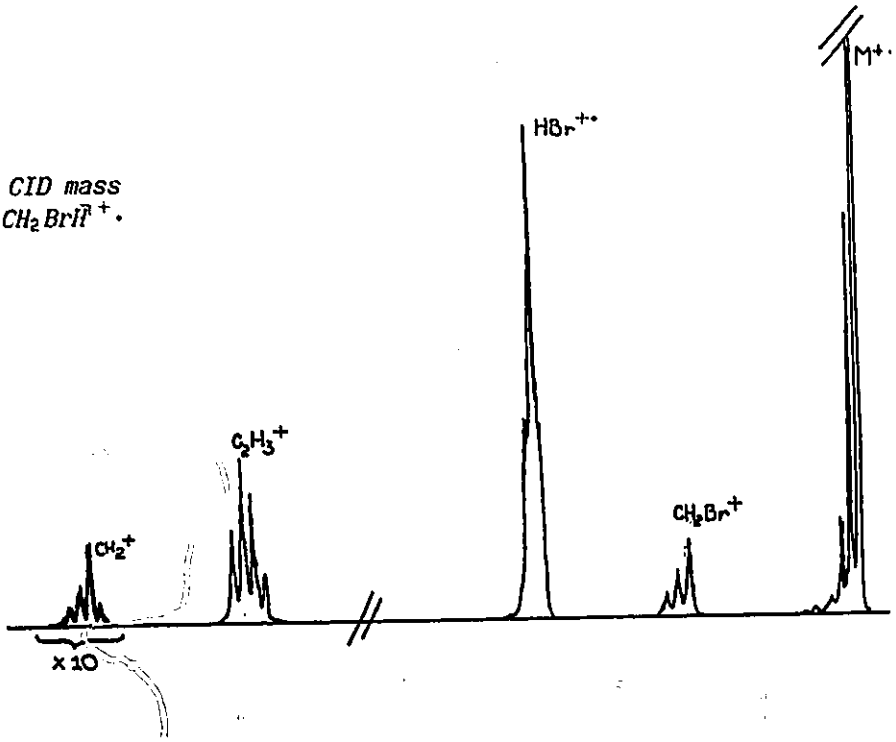

Figure 6.20 The CID mass spectrum of $CH_2CH_2Br\bar{H}^{+\cdot}$.

The charge stripping mass spectra of the chloro and bromo species, refer to Table (6-16), are of intermediate intensity, and the base peaks correspond in both cases to the undissociated, M^{+2}; it is unlikely that these signals result from trace impurities of another isomer (consider the intensity and characteristic pattern of the CS spectra).

Based on the dissociation characteristics of these $[C_2H_5X]^{+\cdot}$ (X=F,Cl,Br) however, assignment of either the distonic, $\cdot CH_2CH_2XH$, or nonclassical, bridged structure is equally valid. For the sake of simplicity alone, these species have been represented by the distonic structure, and labelled as such in the figures and tables.

6.2.V Summary of the Ylid and Distonic Species, $[C_2H_5X]^{+\cdot}$

Rearrangement-cum-fragmentation processes generate the $CH_3XCH_2^{+\cdot}$ and $CH_3CHXH^{+\cdot}$ ylid species for X=Cl,Br, and the distonic species, $CH_2CH_2XH^{+\cdot}$ are proposed to be generated for X=F,Cl,Br. No iodo distonic species have been observed, preferred loss of the relatively weakly bonded I$\cdot$ from the molecular ions of the selected iodo precursors preclude their formation. The ΔH_f° values of these unconventional species, as obtained by experiment in the case of the ylid species, and the theoretical values calculated for the distonic ions (for X=F,Cl), are summarized in Table 6-15.

TABLE 6-15 Heat of Formation of the $[C_2H_5X]^{+\cdot}$ Isomers (kJ mol^{-1})

X	$CH_3CH_2X^{+\cdot}$	$CH_3XCH_2^{+\cdot}$	$CH_3CHXH^{+\cdot}$	$CH_2CH_2XH^{+\cdot}$
F	873			748-842[1]
Cl	950	1012	951	935-998[1]
Br	930	1058	995	

[1]Refer to Table 6-14

The ylidions are in general higher in energy than their conventional counterparts, but are quite stable with respect to isomerization. The distonic isomers are predicted to be the most stable of the unconventional species.

The metastable processes observed for the isomers of the ethylchloride and ethylbromide radical ion are illustrated schematically in *figures (6.21)* and *(6.22)*. The $[C_2H_5X]^{+\cdot}$ isomers which have been characterized, generate unique and distinguishable MI as well as CID mass spectra. Thus all are stable with respect to unimolecular rearrangement, with the

proposed exception of the two ylid $[C_2H_5Cl]^{+\cdot}$ species, as discussed in section IV. Unlike their conventional counterparts, the ylid and distonic radical cations, for X=Cl,Br, generate $[C_2H_5X]^{2+}$ dications which dominate their respective CS spectra as observed in Table 6-16.

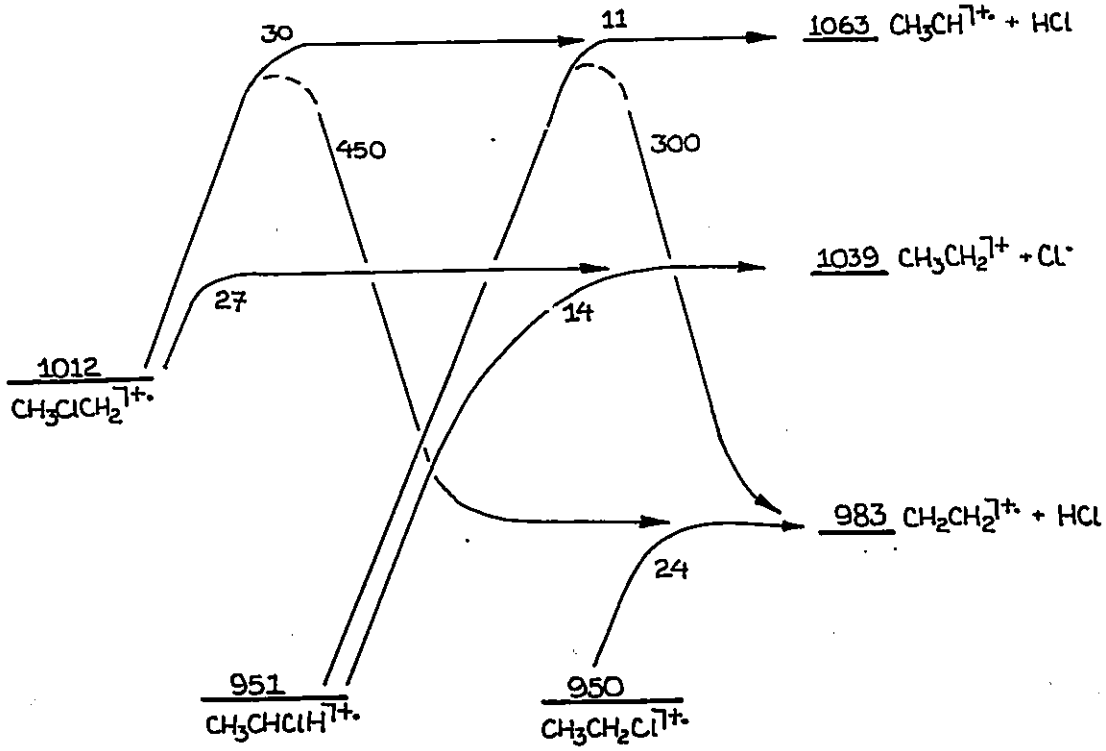

Figure 6.21 The proposed metastable processes and measured $T_{0.5}$ values for the $[C_2H_5Cl]^{+\cdot}$ isomers, note $CH_2CH_2ClH^{+\cdot}$ has no observable MI mass spectrum.

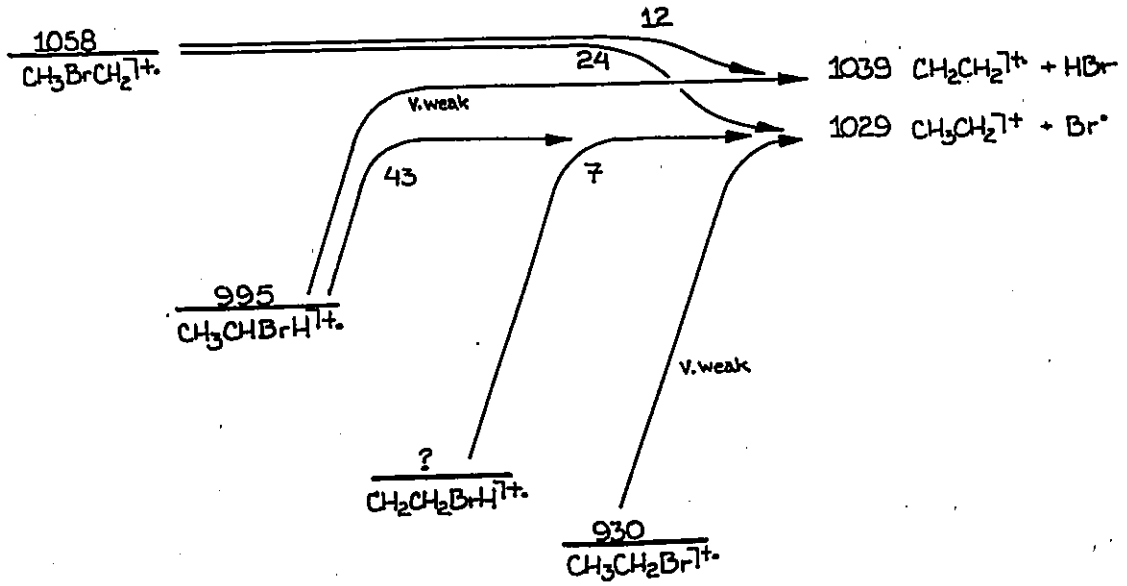

Figure 6.22 The metastable processes and $T_{0.5}$ values observed for the $[C_2H_5Br]^{+\cdot}$ isomers.

The very low intensity of the $CH_3XCH_2^{\neg +}\cdot$ CS spectra and close similarity to the surprisingly intense CS mass spectra of $CH_3CHXH^{\neg +}\cdot$ has led to the conclusion that doubly charged $CH_3XCH_2^{\neg 2+}$ are not produced, and that stable dications are observed only where the divalent halogen atom is asymmetrically bonded, i.e. to hydrogen and carbon, in keeping with the well known stability of the $CH_2XH^{\neg 2+}$ species.

TABLE 6-16 Charge Stripping Mass Spectra of the Distonic Ions

Ylidion	M^{2+}	$[M-1]^{2+}$	$[M-2]^{2+}$	$[M-3]^{2+}$	A
$CH_3ClCH_2^{\neg +}\cdot$	100	17	2	4	1/1000
$CH_3BrCH_2^{\neg +}\cdot$	~100	-	-	-	1/1000
$CH_3CHClH^{\neg +}\cdot$	100	14	1	3	1/1
$CH_3CHBrH^{\neg +}\cdot$	100	13	3	2	1/1
$CH_2CH_2ClH^{\neg +}\cdot$	100	36	44	2	1/50
$CH_2CH_2BrH^{\neg +}\cdot$	100	19	18	2	1/50

A = Approximate intensity of CS peaks with respect to CID peaks

6.3 The Neutral Ylide and Distonic Species

The range of gas phase investigations now possible via mass spectrometry has been enlarged to include analysis of an ion's neutral counterpart, via the recently introduced technique of neutralization-reionization mass spectrometry, as detailed in chapter 4. The neutral counterparts of the stable ylid and distonic ions described above, unlike their conventional isomeric neutrals, are believed to be unstable, and thus particularly suited for such an examination by NRMS. Examination of the neutral ethylhalides via NRMS has also been included, to present a complete picture and allow comparative analyses by establishing reference spectra. Theoretical calculations to establish the heats of formation of the unconventional neutrals will no doubt be performed in the near future, but at present neither experimental nor theoretical data associated with these species have been reported.

6.3.I CH_3CH_2X The Conventional Neutral

Ethylhalide radical cations are produced by electron impact, directly, unrearranged, from their stable, neutral counterparts. Excitation of these neutrals via electron impact is similar, as discussed in chapter 4.7, to the excitation of fast neutrals via collisional excitation with target gas. Such fast neutrals are formed by collision induced charge exchange of mass selected ions, and their subsequent collision induced dissociative reionization constitutes an NR mass spectrum. Thus, for neutral species which are stable to formation by collisional charge exchange, the NR mass spectra of the cations are expected to be similar to the corresponding EI mass spectra. Moreover, the close resemblence of the EI and CID mass spectra of the ethylhalides allows comparison of the CID and NR mass spectra. Where extensive isomerization does not occur, the CID and NR mass spectra are expected to be similar. This is indeed observed for all the ethylhalides, as a comparison of their respective CID and NRMS illustrate. The NR mass spectra, *figures (6.23-6.26)*, are presented alongside the respective CID mass spectra, introduced earlier.

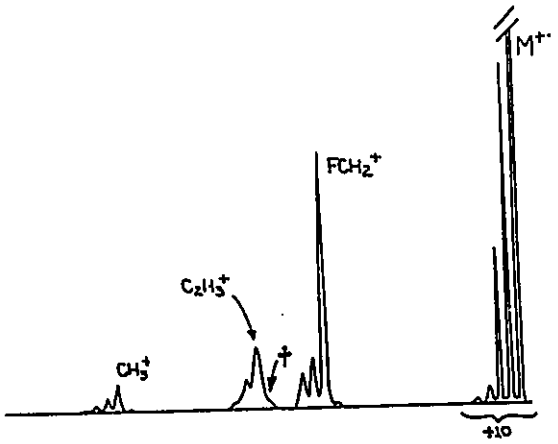

The CID mass spectrum of $CH_3CH_2F^{+\cdot}$.

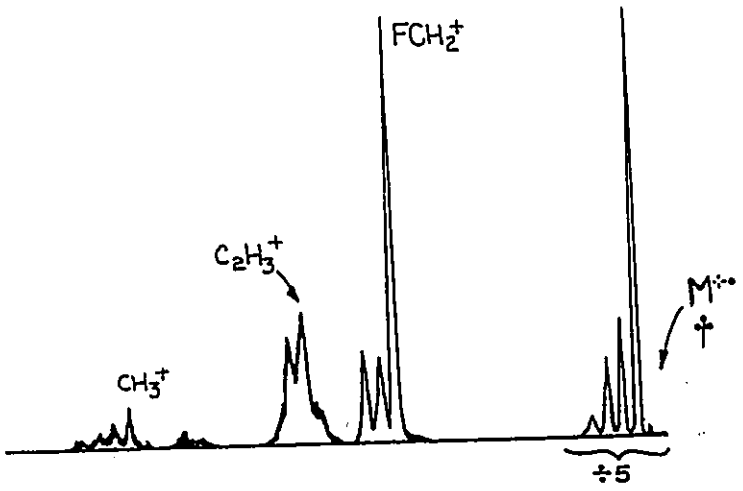

Figure 6.23 NR mass spectrum of $CH_3CH_2F^{+\cdot}$.

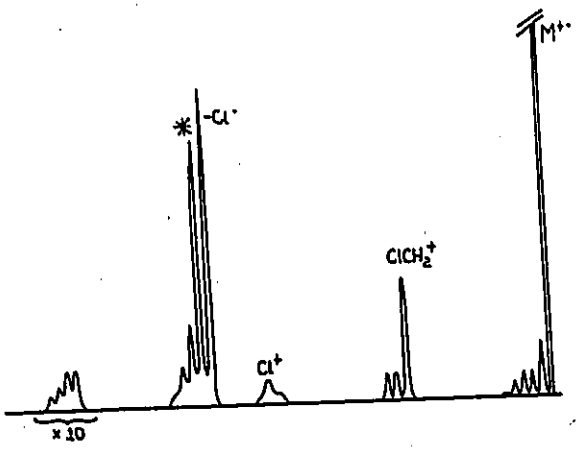

The CID mass spectrum of $CH_3CH_2Cl^{+\cdot}$.

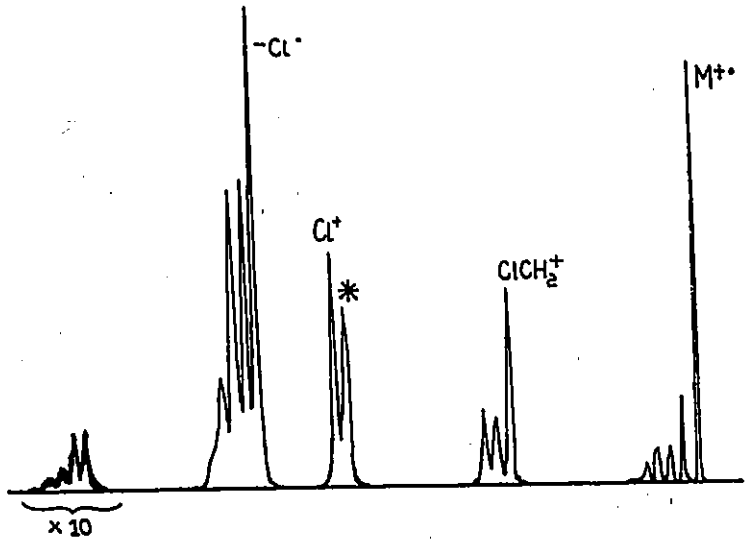

*Figure 6.24 NR mass spectrum of $CH_3CH_2Cl^{+\cdot}$., *, peak corrected for metastable contributions*

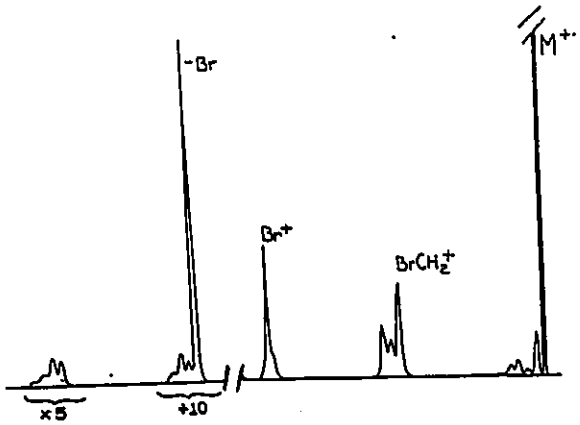

The CID mass spectrum of $CH_3CH_2Br^{\cdot+}$.

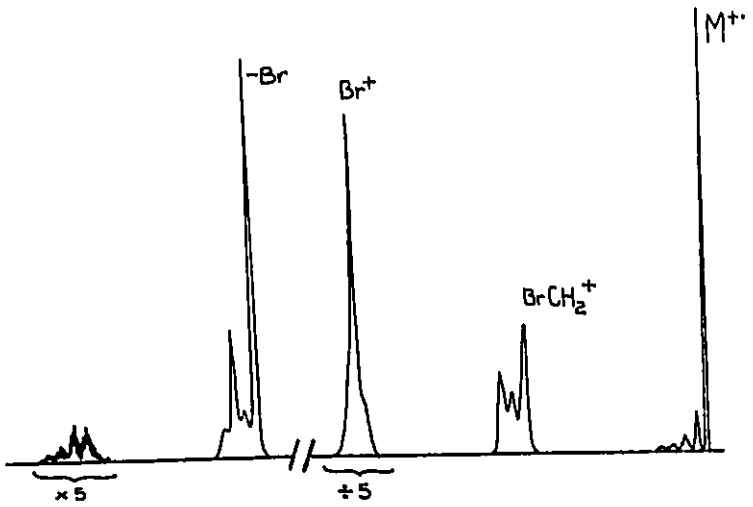

Figure 6.25 NR mass spectrum of $CH_3CH_2Br^{\cdot+}$.

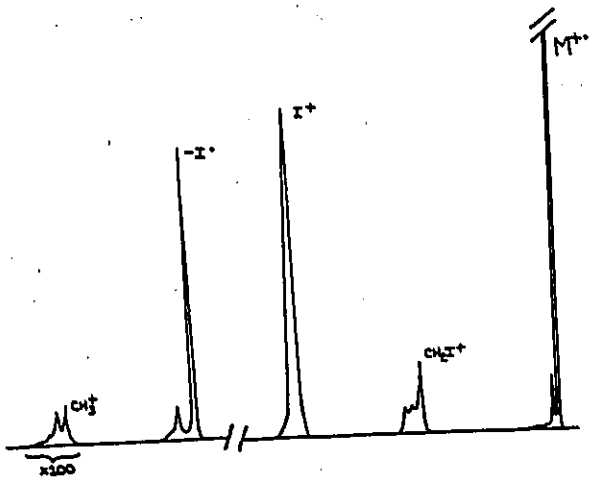

The CID mass spectrum of $CH_3CH_2I^{\cdot+}$.

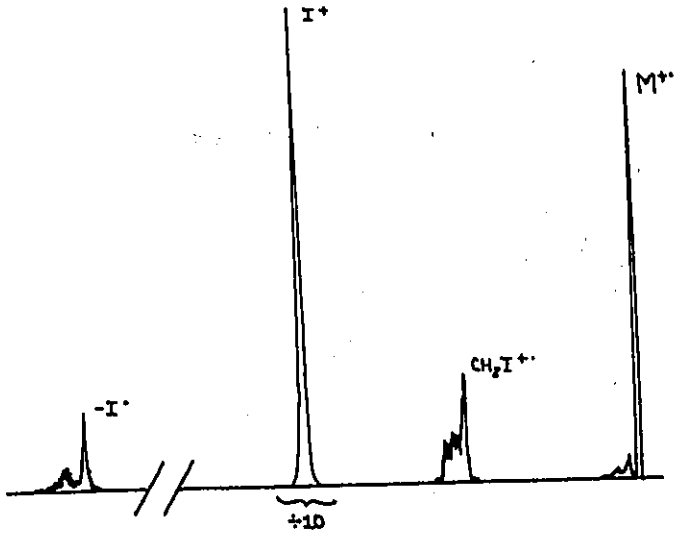

Figure 6.26 NR mass spectrum of $CH_3CH_2I^{\cdot+}$.

In the case of ethylfluoride, barring the lack of a recovered $M^{+}\cdot$ species, which will be discussed below, the CID and NR mass spectra are nearly identical. In the NRMS of the ethylchloride, bromide and iodide, there are some minor discrepancies. Although the spectra clearly point to a common geometry for ion and neutral, there are slight but increasing differences in relative intensities of fragment peaks from the CID to NR mass spectra. Increased intensity of the halogen ion, X^{+}, and reduced intensity of the peaks corresponding to m/z=26-29 is observed in the NRMS, the differences becoming more significant from the chloro, to bromo, to the iodo analogue. Partial dissociation of the neutral prior to reionization, i.e.

$$CH_3CH_2X \overset{*}{\rightarrow} [C_2H_5]\cdot + X\cdot \qquad \textit{eq.(6.8a)}$$
$$\overset{*}{\rightarrow} [C_2H_4] + HX \qquad \textit{eq.(6.8b)}$$

would result in increased fragment intensities of X^{+}, $HX^{+}\cdot$, $[C_2H_4]^{+}\cdot$ and $[C_2H_5]^{+}$ upon reionization. That process *(6.8a)* is increasingly favored for the larger halides may well be accounted for by the corresponding reduction in energy requirement for the homolytic R-X bond cleavage of the neutral. Moreover this halogen loss becomes increasingly competitive with the process for HX loss as X=Cl→Br→I, and for ethyliodide, only reionized $I\cdot$ is observed.

TABLE 6-17 Homolytic Bond Cleavage versus Loss of HX

	X	D(R-X)[1]	E_a(HX)[2]
increasing relative intensity of X in NRMS ↓	Cl	330	243
	Br	272	222
	I	218	213

[1] Homolytic bond cleavage for the ethyl halides, kJ mol^{-1} (144)
[2] Activation energy for HX loss from ethyl halides, kJ mol^{-1} (144)

However, as strikingly observed in the NRMS of ethyl iodide, the dissociation process in *eq.(6.8a)* does not result in a similarly intense peak at m/z=29. The reduced intensity associated with the lower masses is accounted for by the lower translational energies (9). In the case of ethyl iodide, $[C_2H_5]\cdot$ has a translational energy of only [(29/156)·8eV ≈ 1.5eV] while that of the $I\cdot$ [(127/156)·8eV ≈ 6.5eV].

The relatively intense peak corresponding to the regenerated molecular radical cation, is a striking feature present in all but ethylfluoride. These survivors are indicative of the stability of the neutral, C_2H_5X, with respect to vertical neutralization of its corresponding radical cation. They also indicate that the cation, $[C_2H_5X]^{+}\cdot$, is sufficiently stable to vertical reionization, i.e. that not all those produced, dissociate on collision with the reionizing target gas. The neutral species generated by vertical neutralization of the ethylchloride, bromide, and iodide molecular ions, are concluded to be of the ethylhalide form and stable with respect to dissociation or rearrangement.

The absence of molecular ions in the NR mass spectrum of ethylfluoride, after correcting for a significant ^{13}C contribution from m/z=47, is not unexpected. Collisional charge exchange must generate a significant flux of neutrals, as indicated by the intensity of the NR mass spectrum. As well, these neutrals must be stable and of the ethylfluoride structure, a conclusion drawn from the close similarity of the CID and NR mass spectra. However vertical ionization of neutral ethylfluoride, as seen in the EI mass spectrum of CH_3CH_2F, and indicated by the large discrepancy in vertical and adiabatic IE values, produces excited molecular ions, a great majority of which have sufficient energy to undergo fragmentation. Thus it is the instability of the ethylfluoride molecular ion following vertical formation, not that of its neutral counterpart, which results in an absence of m/z=48 survivors in the NRMS. Conversely, the absence of $[C_2H_5F]^{+}\cdot$ survivors in the NRMS of ethylfluoride shows that collisional reionization is a *strongly* vertical process (compare the relative intensities of m/z=47 and m/z=48 in the EI and NR mass spectra).

6.3.II $CH_3\overset{+}{X}\overset{-}{C}H_2$ A Neutral Ylide

Reported originally to have been formed as intermediates in solution chemistry, isolation of the distonic neutral species $CH_3\overset{+}{X}\overset{-}{C}H_2$ (X=Br,I) was unsuccessful (133). Ab initio molecular orbital theory calculations of the neutral distonic hydrogen analogues $\overset{-}{C}H_2\overset{+}{X}H$, X=F,Cl,OH,SH,$NH_2$,$PH_2$, as well, indicate an instability with respect to rearrangement and/or dissociation (120). Thus, neutralization of the stable distonic radical cations, $CH_3\overset{+}{X}\overset{-}{C}H_2$ (X=Cl,Br), via collisional charge exchange is expected

to generate unstable neutral counterparts.

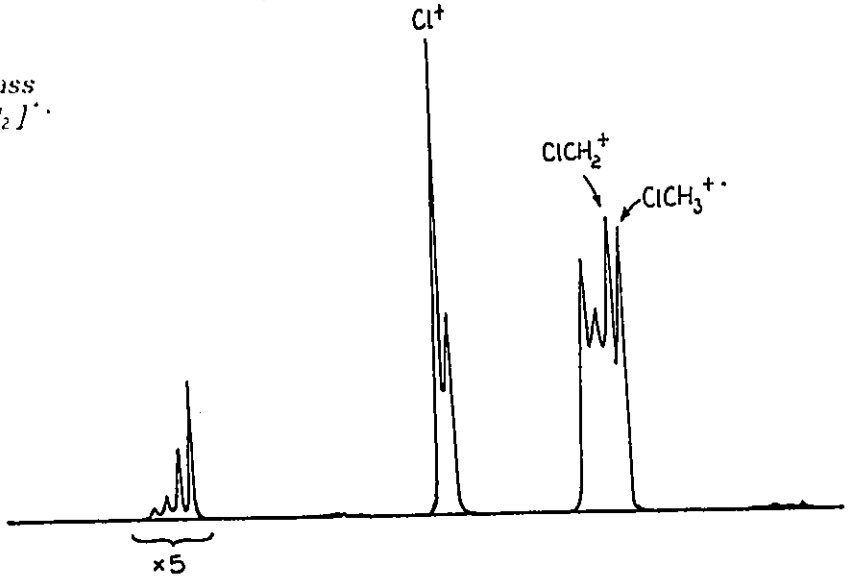

Figure 6.27 The NR mass spectrum of $[CH_3ClCH_2]^{+\cdot}$.

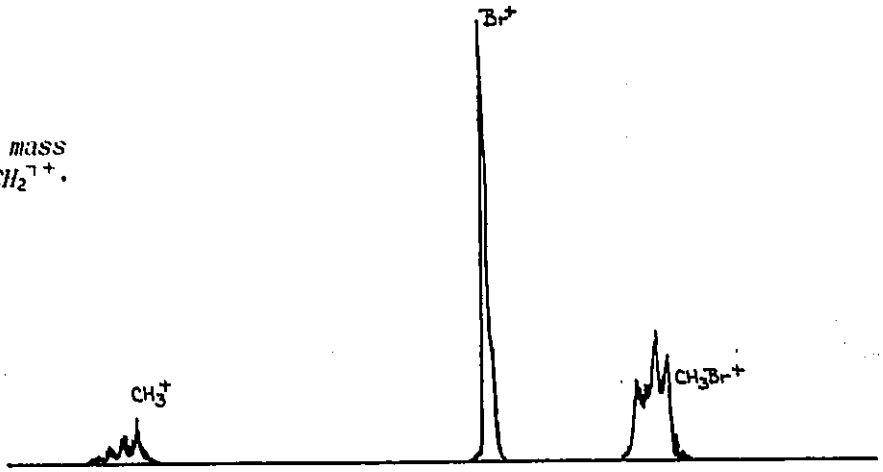

Figure 6.28 The NR mass spectrum of $CH_3BrCH_2^{+\cdot}$.

The NR mass spectra of $CH_3ClCH_2^{+\cdot}$ and $CH_3BrCH_2^{+\cdot}$, illustrated in *figures (6.27)* and *(6.28)*, support this proposal explicitly, the spectra are composed entirely of fragment ions, no $[C_2H_5X]^{+\cdot}$ survivors or even their hydrogen loss species are observed. This absence of survivors, unlike the ethylfluoride case, results from the instability of the neutral. The distonic ion is believed to be sufficiently stable to be "regenerated" vertically, the EI mass spectrum of the precursors, XCH_2COOCH_3, sport relatively intense signals corresponding to the $CH_3XCH_2^{+\cdot}$ radical ions, produced under non-threshold energy conditions. Also, the NR mass spectra indicate that the $CH_3\overset{+}{X}\overset{-}{C}H_2$ neutral, unstable with respect to dissociation, does not however, undergo rearrangement

prior to fragmentation. The fragment ions are characteristic of the $CH_3\overset{+}{X}\overset{-}{C}H_2$ ylid structure, note specifically the *absence of any* C_2 fragments (indicative of a C-C bond), and the very similar intensity of the $CH_2X^{\neg +}$ and $CH_3X^{\neg +}\cdot$ fragments. The significantly increased intensity of the $CH_3X^{\neg +}\cdot$ fragment from the CID to the NR spectrum of $CH_3ClCH_2^{\neg +}\cdot$ and $CH_3BrCH_2^{\neg +}\cdot$ may be explained on the basis of thermochemistry. The loss of $CH_3\cdot$ is very energetically favoured over the loss of CH_2 in the ionic species. This wide discrepancy however, favouring CH_3 loss, is lost in the neutral species, as outlined in Table (6-18).

TABLE 6-18 CH_2 Versus $CH_3\cdot$ Loss

Precursor	Products	$\Sigma\Delta H_f°$ of Products Neutral/Neutal	Ion/Neutal
CH_3ClCH_2	$CH_2Cl + CH_3$	257 kJ mol^{-1}	1092 kJ mol^{-1}
	$CH_3Cl + CH_2$	311 kJ mol^{-1}	1406 kJ mol^{-1}
	$\Delta\ \Sigma\Delta H_f°$	54	314
CH_3BrCH_2	$CH_2Br + CH_3$	312 kJ mol^{-1}	1129 kJ mol^{-1}
	$CH_3Br + CH_2$	357 kJ mol^{-1}	1389 kJ mol^{-1}
	$\Delta\ \Sigma\Delta H_f°$	45	260

$\Delta H_f°[CH_2Cl\cdot]$= 115±5 kJ mol^{-1}, and $\Delta H_f°[CH_2Br\cdot]$=170±5 kJ mol^{-1} (145)

Neutralization-reionization may provide a good alternative means of structure assignment, as strikingly illustrated in the case of these distonic radical cations. Thus, when direct analysis of the ion itself proves inconclusive, NRMS, not CID, may be the analytical technique of choice. Positive assignment of the distonic structure, due to the similarities of the CID spectra for $CH_3CH_2Cl^{\neg +}\cdot$ and $CH_3ClCH_2^{\neg +}\cdot$, necessitated labelling studies (127). The NR mass spectra of these isomers however are conclusive in themselves.

6.3.III $CH_3\overset{-}{C}H\overset{+}{X}H$ A Second Neutral Ylide

The neutral species $CH_3\overset{-}{C}H\overset{+}{X}H$, X=Cl,Br, have not been investigated theoretically in terms of their relative stability towards rearrangement or dissociation, however in light of the NRMS results reported here, it may

be of considerable interest to do so. The hydrogen analogue of the chloro species, $\bar{C}H_2\overset{+}{C}lH$, which has been well investigated via theory as well as NRMS, has itself been the subject of some controversy. Most recent ab initio calculations (120) have placed the heat of formation of this neutral 429 kJ mol^{-1} above CH_2Cl, with a bond energy of just 1 kJ mol^{-1} with respect to $CH_2(^1A_1)$ + HCl. Based on the experimental observation of survivors in the NRMS, a stable species had been proposed (80). Most recent experimental investigations however, contend that the neutral ylide is indeed unstable. The observed survivors in the NRMS of CH_2ClH, after correcting for ^{13}C contributions have been shown to result from a small but significant flux of $CH_3Cl^{+\cdot}$ from the ion source (146).

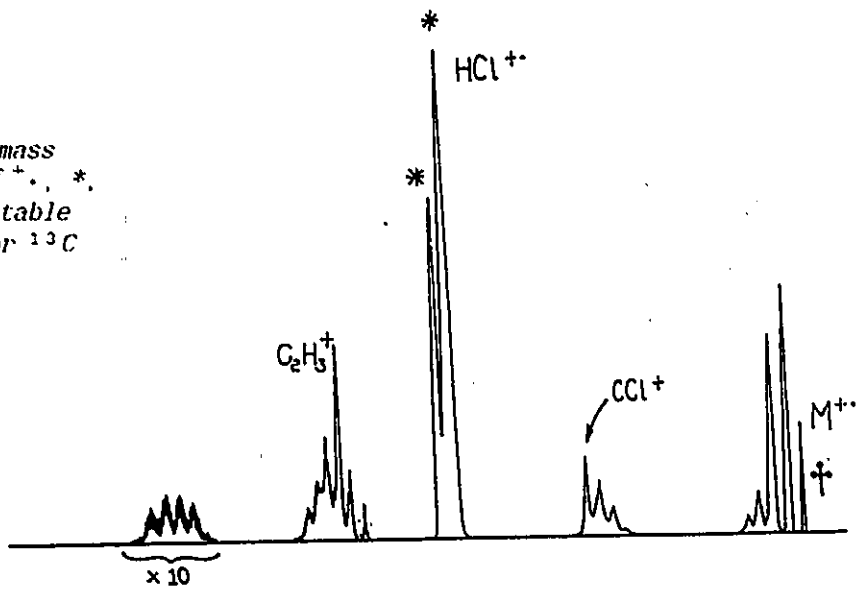

*Figure 6.29 The NR mass spectrum of $CH_2ClHCl\bar{H}^{+\cdot}$. *, correction for metastable contributions, †, for ^{13}C contributions.*

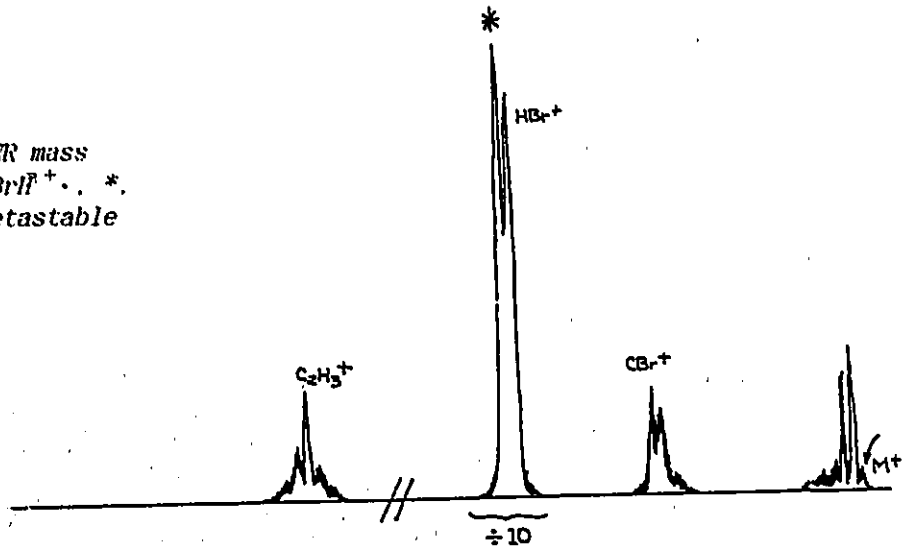

*Figure 6.30 The NR mass spectrum of $CH_3CHBr\bar{H}^{+\cdot}$. *, corrections for metastable contributions.*

Unlike the $CH_3\overset{+}{X}\overset{-}{C}H_2$ ylide, complete decomposition of the $CH_3\overset{-}{C}H\overset{+}{X}H$ neutrals is not observed in their neutralization-reionization mass spectra; note for instance the intensity of the hydrogen loss species. Significant similarities are observed on comparison of the CID and NR mass spectra in *figures (6.29)* and *(6.30)*. Coupled with a lack of increased intensity for peaks characteristic of other isomeric species, i.e. $C_2H_5^{\urcorner+}\cdot$, $CH_2X^{\urcorner+}$, it is concluded that significant rearrangement of the neutral, once formed, does not occur prior to dissociation. Therefore the neutral ylide, $CH_3\overset{-}{C}H\overset{+}{X}H$, for X=Cl,Br, must not be completely decomposed on the mass spectrometric time scale with respect to its formation via non-resonant collision induced charge exchange.

This belief may be underlined by the observation of weak but significant intensities of $[C_2H_5X]^+\cdot$ survivors in the ^{13}C corrected NRMS. As was argued for $\overset{-}{C}H_2\overset{+}{C}lH$, these survivors may not be of the $CH_3\overset{-}{C}H\overset{+}{X}H$ structure. In the case of $\overset{-}{C}H_2\overset{+}{C}lH$, the very characteristic charge stripping peaks associated with $CH_3Cl^+\cdot$ rather than $CH_2ClH^+\cdot$ were observed under conditions of high gain in the NR mass spectrum, pointing to a survivor of conventional structure (48). No such CS spectra are observed in the NRMS of either $CH_3CHClH^{\urcorner+}\cdot$ or $CH_3CHBrH^{\urcorner+}\cdot$ under conditions of maximum gain, due to either the low intensity of the recovered $[C_2H_5X]^+\cdot$ species and/or the very weak CS spectrum associated with $CH_3CH_2X^{\urcorner+}\cdot$. However, unlike its hydrogen analogue, the observed "survivors" cannot be attributed to a small but significant flux of the conventional isomer. The very low intensity observed for the $[C_2H_5]^+$ and XCH_2^+ fragments argue against any contribution from $CH_3CH_2Cl^{\urcorner+}\cdot$ and $CH_3CH_2Br^{\urcorner+}\cdot$ in the NRMS of $CH_3CHClH^{\urcorner+}\cdot$ and $CH_3CHBrH^{\urcorner+}\cdot$ respectively.

6.3.IV $\overset{-}{C}H_2CH_2\overset{+}{X}H$ A Distonic Neutral

As discussed in section 6.2.IV, the stable $CH_2CH_2XH^{\urcorner+}\cdot$ distonic isomers of ethylfluoride, chloride and bromide are believed to have been produced, albeit in small intensity, as shown by their respective, characteristic CID mass spectra. Only the chloro and the bromo derivatives, generate sufficient flux for observation of their NR mass spectra under present conditions, the latter requiring use of the multiscan signal averaging program, ZABCAT (50). The NR mass spectra of the

distonic ions $CH_2CH_2ClH^{+\cdot}$ and $CH_2CH_2BrH^{+\cdot}$ in *figures (6.31)* and *(6.32)*, illustrate what appears to be an unexpected stability of their distonic neutral counterpart.

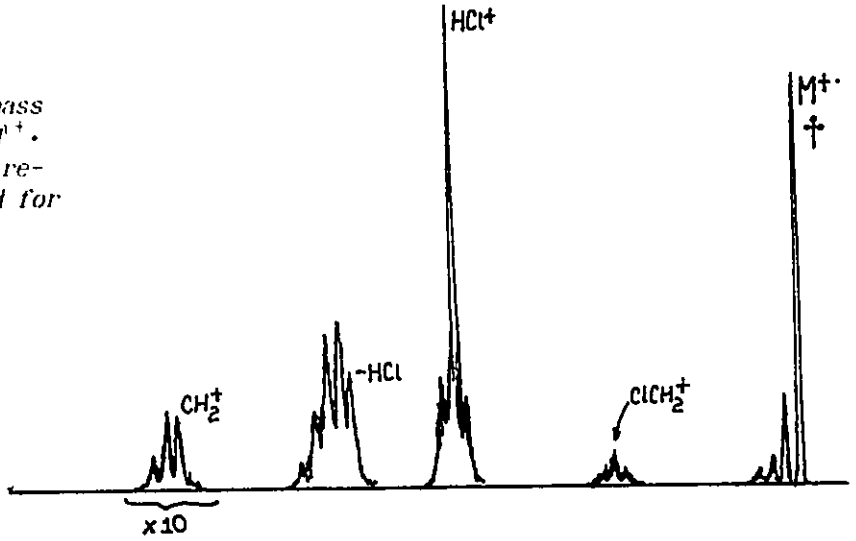

Figure 6.31 The NR mass spectrum of $CH_2CH_2ClH^{+\cdot}$. Signal averaging was required. †, corrected for ^{13}C contributions.

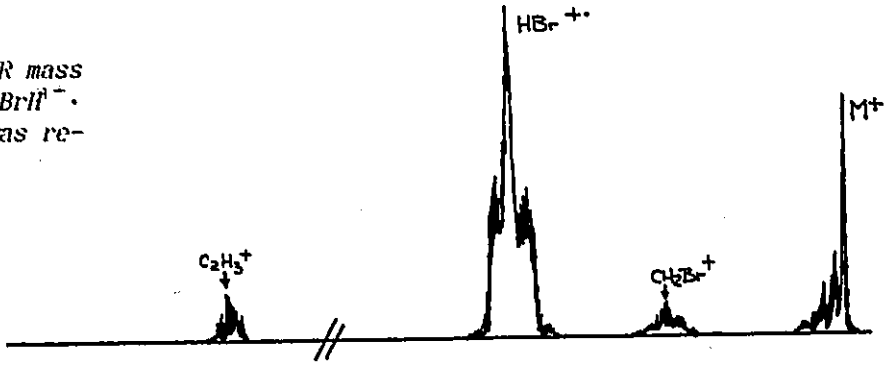

Figure 6.32 The NR mass spectrum of $CH_2CH_2BrH^{+\cdot}$. Signal averaging was required.

There is a good similarity between the CID and NRMS of these distonic species, greater than for either of the ylid isomers, although some dissociation of the neutral must occur as may be concluded from the larger relative intensity of $HX^{+\cdot}$. The less intense, slightly asymmetrical peaks which are observed to flank that of $HX^{+\cdot}$ in *figures (6.31)* and *(6.32)*, are also present in the CID mass spectra. They do not correspond to exact mass units, and thus must result from a *composite* $HX^{+\cdot}$ peak. Observed previously for the I^+ peak in the CID of $CH_3I^{+\cdot}$ (147), the explanation for this pattern was considered to be that formation of the ion occurs from two isolated electronic states.

The intensity of recovered $[C_2H_5X]^{+\cdot}$ species is, however, the most surprising, rivalling the recovery observed in the NRMS of the well known, stable neutrals, ethylchloride and bromide. This intensity is not due to ^{13}C contributions, nor can it be explained in terms of a 'distonic to conventional ion' rearrangement. Again, the very low intensity of the $[C_2H_5]^+$ and CH_2X^+ fragments observed in the NRMS of the distonic ions rule out any contribution to $M^{+\cdot}$ from the respective ethylhalides. The distonic neutral, CH_2CH_2XH, for the cases observed X=Cl,Br, appears to be of considerable stability to unimolecular rearrangement or dissociation. Based on the structure of the distonic radical cation, for which several variations have been proposed in the case of fluorine and chlorine, section 6.2.IV, the actual structure of the neutral counterpart is speculative.

6.3.V Summary of the neutral Ylide and Distonic Species

Neutral counterparts of distonic ions are believed to be unstable. This has been underlined by the reaction of the stable ylidion, $CH_3XCH_2^{\neg+\cdot}$, to neutralization. However, the neutral counterparts of the ylid and distonic ions, $CH_3CHXH^{\neg+\cdot}$ and $CH_2CH_2XH^{\neg+\cdot}$ respectively, behaved contrary to expectations.

The ethylhalide molecular ions generate NRMS which are very similar to their EI and CID mass spectra, and with the exception of X=F, contain an intense, recovered molecular ion. All indicate stability of the neutral counterpart towards decomposition and isomerization. The lack of "survivors" in the NRMS of ethylfluoride has been attributed, not to the instability of the neutral, but rather to fragmentation on subsequent collisional reionization.

The neutrals of the $CH_3XCH_2^{\neg+\cdot}$ ylidions (for X=Cl,Br) are concluded to be unstable, as expected. The NR mass spectra are composed entirely of fragment ions, all neutrals generated by charge exchange in cell 1 fragment before they can be reionized in cell 2. The NRMS of these ylidions however, remain very structure specific, and are, in fact, more so than their corresponding CID mass spectra.

The unconventional ions, $CH_3CHXH^{\cdot +}$ and $CH_2CH_2XH^{\cdot +}$ (for X=Cl,Br), contrary to expectations, generate NR mass spectra which are not composed entirely of fragment ions but which are similar to their CID mass spectra. Attributed to the stability of the neutrals, this conclusion is underlined by the intensity of the recovered $[C_2H_5X]^{+\cdot}$ ions. These "survivors" are accounted for by neither ^{13}C contributions nor an interfering flux of the conventional isomer. And thus, without evidence to the contrary, the distonic neutrals $CH_3\overset{-}{C}H\overset{+}{X}H$ and $\overset{-}{C}H_2CH_2\overset{+}{X}H$ are proposed to be stable.

Experimental Section

The metastable and collision induced dissociative processes were recorded on the Vacuum Generators ZAB-2F described in section 2.2.I. A 100 μA electron beam of 70eV ionising energy was used. The ion source temperature was 200°C and the accelerating voltage was set at 8keV. Except for metastable peak shapes and the respective $T_{0.5}$ values, all experimental work was done with the resolving slits fully open, under conditions of minimal energy resolution. The EI source slit only was used.

The origin of the observed metastable peaks were tested by; an analysis of the intensity reduction of the peak and the main beam as the magnet is offtuned, and an analysis of the separation of processes occuring inside and outside the collision cell under CID conditions. Once established as metastable, the peak shapes were recorded under conditions of high energy resolution, and the $T_{0.5}$ values obtained.

The CID mass spectra were obtained using O_2 as the collision gas in the second cell, at an indicated pressure of $1.5x10^{-7}$ torr, corresponding to ~90% transmission. Where applicable, the CID mass spectra were corrected for contributions from metastable processes. By floating the second cell at a voltage (between +500 and -500eV), the metastable contribution is semi-quantitatively isolated. Those peaks marked by * in the illustrated CID mass spectra have been corrected for their metastable contributions. Corrections for $[^{13}CCH_4F]^+$ were also required in the CID of $[C_2H_5F]^+$ from ethylfluoride.

O_2 has been labelled a "soft" target gas and its use has led to an optimal generation of doubly charged species. The charge stripping mass spectra are recorded under conditions applicable to CID, but where necessary, under increased gain.

Neutralization-reionization mass spectra have been recorded under the following standard conditions. Oxygen is admitted, maintaining a constant pressure reading of $1.5x10^{-7}$ torr, to the second cell. A voltage of 1700eV is applied to the deflector electrode. Xenon is introduced into the first collision cell to a pressure reading on the first ionization gauge of $3.5x10^{-6}$ torr. This pressure reading for Xe is consistent with ~90% transmission of the beam through cell 1. By floating cell 1 at a voltage (between +500 and -500eV), separation of the neutral fragments generated metastably, prior to the cell, may be made. Those peaks in the NRMS, marked by * have been corrected for metastable contributions. The separation obtained for cell 1 is less accurate and account had to be taken of the signicant percentage (~25%) of collision processes occuring outside the cell. Those peaks marked by † required correction for significant ^{13}C contributions.

The GEC-AEI MS-902S allowed the appearance energy of the $[C_2H_5F]^{+\cdot}$ fragment from methyl fluoroacetate to be measured, via comparison with the reference metastable loss of methyl from diethyl ether. The metastable characteristics of the $[C_2H_5Br]^{+\cdot}$ fragment ion from methyl bromoacetate were also investigated in the first field free region.

All ionization and appearance energy measurements of source generated species, not referenced otherwise, were recorded by Dr. F.P. Lossing, via the electron energy selecting mass spectrometer described in section 2.2.III.

The majority of the chemicals used were obtained commercially of research grade purity, and used without further purification. $FCH_2CH_2CH_2OH$ was prepared by Dr. J.M. Buscheck via 3-Chloro-1-propanol, anhydrous KF and ethylene glycol, (F.W. Hoffmann, *J. Org. Chem.*, *15*, *425*, *1950*), and purified by GC. $ClCH_2COOCD_3$ was prepared via the microscale esterification of $ClCH_2COOH$ with CD_3OD. $CH_3CHClCOOD$ was obtained within the ion source via hydrogen/deuterium exchange with D_2O, and the $[C_2H_4D^{37}Cl]$ species at m/z=67, a mass to charge ratio not observed in the unlabelled species, was mass selected. Hydrogen/Deuterium exchange was similarly pursued for generation of $FCH_2CH_2CH_2OD$, however, unavoidable interferences from the unlabelled precursor allowed for comparative analyses only. Signal averaging was required only for the very weak spectra, the NRMS of the $[C_2H_5X]^{+\cdot}$ species generated from $ClCH_2CH_2CH_2OH$ and $BrCH_2CH_2CH_2OH$, and in the ^{13}C correction of the CS and NR mass spectra of the latter.

References

1. R.W. Kiser, 'Introduction to Mass Spectrometry and its Applications', Prentice-Hall Inc., (1965).

2. E. Goldstein, *Berl. Ber.*, *39*, *691*, *(1886)*.

3. W. Wien, *Wied. Ann.*, *65*, *440*, *(1898)*., and *Ann. Physik*, *8*, *244*, *(1902)*.

4. A.J. Dempster, *Phys. Rev.*, *11*, *316*, *(1918)*.

5. R. Conrad, *Phys. Z.*, *31*, *888*, *(1930)*.

6. J. Franck, *Trans. Faraday Soc.*, *21*, *536*, *(1926)*.

7. E.U. Condon, *Phys. Rev.*, *32*, *858*, *(1928)*.

8. S. Meyerson, *Org. Mass Spectrom.*, *21*, *197*, *(1986)*.

9. J.L. Holmes, A.A. Mommers, J.K. Terlouw and C.E.C.A. Hop, *Int. J. Mass Spectrom. Ion Proc.*, *68*, *249*, *(1986)*.

10. R.P. Morgan, J.H. Beynon, R.H. Bateman and B.N. Green, *Int. J. Mass Spectrom. Ion Phys.*, *28*, *172*, *(1978)*., and R.P. Morgan, A.G. Brenton and J.H. Beynon, *Int. J. Mass Spectrom. Ion Phys.*, *29*, *195*, *(1979)*.

11. J.L. Holmes, P.C. Burgers and J.K. Terlouw, *Can. J. Chem.*, *59*, *1805*, *(1981)*.

12. K. Maeda, G.P. Semeluk and F.P. Lossing, *Int. J. Mass Spectrom. Ion Phys.*, *1*, *395*, *(1968)*., and F.P. Lossing and J.C. Traeger, *Int. J. Mass Spectrom. Ion Phys.*, *19*, *9*, *(1976)*.

13. A.A. Mommers, *Ph. D Thesis*, University of Utrecht, Utrecht, The Netherlands, (1985).

14. E.W. Schlag and R.A. Sandsmark, *J. Chem. Phys.*, *37*, *168*, *(1962)*.

15. M.V. Vestal in "Fundamental Processes in Radiation Chemistry", (P.Ausloos, ed.,) Interscience, New York, (1968), Chapter 2.

16. H.M. Rosenstock, M.B. Wallenstein, A.L. Wahrhafig and H. Eyring, *Proc. Nat. Acad. Sci.*, *38*, *667*, *(1952)*.

17. H.M. Rosenstock and M. Krauss, in "Mass Spectrometry of Organic Ions", (F.W. McLafferty, ed.,) Academic Press, New York, (1963).

18. C. Lifshitz in "Advances in Mass Spectrometry", Vol 7, Heyden, London, (1977).

19. R.W.A. Johnstone, in "Mass Spectrometry for Organic Chemists", University Press, Cambridge, (1972).

20. Sussex-NPL Computer Analyzed Thermochemical Data: Organic and Organometallic Compounds, University of Sussex (1977). J.B. Pedley and J. Rylance.

21. S.W. Benson, "Thermochemical Kinetics", 2nd. ed., Wiley-Inter science, New York, (1976).

22. J.L. Holmes and F.P. Lossing, *J. Am. Chem. Soc.*, *102*, *1591*, *(1980)*.

23. J.L. Holmes and F.P. Lossing, *J. Am. Chem. Soc.*, *104*, *2648*, *(1982)*

24. J.C. Traeger and R.G. McLoughlin, *Int. J. Mass Spectrom. Ion Phys.*, *27*, *319*, *(1978)*.

25. P.C. Burgers and J.L. Holmes, *Org. Mass Spectrom.*, *17*, *123*, *(1982)*.

26. H.M. Rosenstock, K. Draxl, B.W. Steiner and J.T. Herron, *J. Phys. Chem. Ref. Data 6, Suppl. 1, pp. 16-18, (1977)*.

27. R.D. Levin and S.G. Lias, "Ionization and Appearance Energy Measurements", Nat. Stand. Ref. Data Ser., Natl. Bur. Stand. (U.S.), 71, (1982).

28. K.C. Kim, J.H. Beynon and R.G. Cooks, *J. Chem. Phys.*, *61*, *1305*, *(1974)*.

29. J.A. Hipple and E.U. Condon, *Phys. Rev.*, *68*, *54*, *(1945)*.

30. R.G. Cooks, J.H. Beynon, R.M. Caprioli and G.R. Lester, "Metastable Ions", Elsevier Scientific Publishing Co., Amsterdam, (1973).

31. C. Ottinger, *Phys. Lett.*, *17*, *269*, *(1965)*.

32. H.D. Smyth, *Phys. Rev.*, *25*, *452*, *(1925)*.

33. K.R. Jennings, *Int. J. Mass Spectrom. Ion Phys.*, *1*, *227*, *(1968)*.

34. W.F. Haddon and F.W. McLafferty, *J. Am. Chem. Soc.*, *90*, *4745*, *(1968)*.

35. P.J. Todd and F.W. McLafferty, *Int. J. Mass Spectrom. Ion Phys.*, *38*, *371*, *(1981)*.

36. P.O. Danis, R. Feng and F.W. McLafferty, *Anal. Chem.*, *58*, *355*, *(1986)*.

37. J.L. Holmes, *Org. Mass Spectrom.*, *20*, *169*, *(1985)*.

38. R.G. Cooks, J.H. Beynon and T. Ast, *J. Am. Chem. Soc.*, *94*, *1004*, *(1972)*.

39. P.C. Burgers, J.L. Holmes, A.A. Mommers, J.E. Szulejko and J.K. Terlouw, *Org. Mass Spectrom.*, *19*, *442*, *(1984)*.

40. P.C. Burgers, J.L. Holmes, A.A. Mommers and J.K. Terlouw, *Chem. Phys. Lett.*, *102*, *1*, *(1983)*.

41. J.L. Holmes and A.A. Mommers, *Org. Mass Spectrom.*, *19*, *460*, *(1984)*.

42. R. Clair, J.L. Holmes, A.A. Mommers and P.C. Burgers, *Org. Mass Spectrom.*, *20*, *207*, *(1985)*.

43. F.M. Devienne, *Entropie*, *24*, *35*, *(1968)*

44. M. Durup, G. Parlant, J. Appell, J. Durup and A. Ozenne, *J. Chem. Phys.* *25*, *245*, *(1977)*.

45. P.O. Danis, C. Wesdemiotis and F.W. McLafferty, *J. Am. Chem. Soc.*, *105*, *7454*, *(1983)*.

46a. F.W. McLafferty, P.J. Todd, M.C. McGilvery and M.A. Baldwin, *J. Am. Chem. Soc.*, *102*, *3360*, *(1980)*., b. C.A. Lieder and J.I. Brauman, *J. Am. Chem. Soc.*, *96*, *4028*, *(1974)*., c. W. Williams and R.F. Porter, *J. Chem. Phys.*, *73*, *5598*, *(1980)*., d. G.I. Gellene and R.F. Porter, *Acc. Chem. Res.*, *16*, *200*, *(1983)*.

47. P.O. Danis, R. Feng and F.W. McLafferty, *Anal. Chem.*, *58*, *348*, *(1986)*.

48. J.K. Terlouw, W.M. Kieskamp, J.L. Holmes, A.A. Mommers and P.C. Burgers, *Int. J. Mass Spectrom. Ion Proc.*, *64*, *245*, *(1985)*.

49. A substantially larger electrode voltage than that quoted for CIDI is required for NRMS, collision prior to the deflector will cause ion beam broadening.

50. A.A. Mommers and J.C. Traeger, *Org. Mass Spectrom.*, *22*, *(in press)*, *(1987)*.

51. P.C. Burgers and J.L. Holmes, *Int. J. Mass Spectrom. Ion Proc.*, *58*, *15*, *(1984)*.

52. P.C. Burgers, A.A. Mommers and J.L. Holmes, *J. Am. Chem. Soc.*, *105*, *5976*, *(1983)*.

53. J.L. Holmes, M. Fingas and F.P. Lossing, *Can. J. Chem.*, *59*, *80*, *(1981)*.

54. J.L. Holmes and F.P. Lossing, in "Current Topics in Mass Spectrometry and Chemical Kinetics", Heyden and Sons, London, (1982).

55. J.L. Holmes and F.P. Lossing, *Can. J. Chem.*, *60*, *2365*, *(1982)*.

56. F.P. Lossing and J.L. Holmes, *J. Am. Chem. Soc.*, *106*, *6917*, *(1984)*.

57. J.L. Holmes, P.C. Burgers, J.K. Terlouw, H. Schwarz, B. Ciommer and H. Halin, *Org. Mass Spectrom.*, *18*, *208*, *(1983)*.

58. T. Baer and T.E. Carney, *J. Chem. Phys.*, *76*, *1304*, *(1982)*.

59. C.L. Lifshitz, P. Gotchiguian and R. Roller, *Chem. Phys. Lett.*, *95*, *106*, *(1983)*.

60a. P.K. Pearson, H.F. Schaefer and U. Wahlgren, *J. Chem. Phys.*, *62*, *350*, *(1975)*., b. C.F. Pau and W.J. Hehre, *J. Phys. Chem.*, *86*, *321*, *(1982)*.

61. T.S. Shannon and F.W. McLafferty, *J. Am. Chem. Soc.*, *88*, *5021*, *(1966)*.

62. H.M. Rosenstock, V.H. Dibeler and F.N. Harllee, *J. Chem. Phys.*, *40*, *591*, *(1964)*.

63. J.L. Holmes, A.A. Mommers, J.E. Szulejko and J.K. Terlouw, *J. Chem. Soc.*, *Chem. Commun.*, *165*, *(1984)*.

64. E.G. Jones, L.E. Baumann, J.H. Beynon, and R.G. Cooks, *Org. Mass Spectrom.*, *7*, *185*, *(1973)*.

65. J.L. Holmes and J.K. Terlouw, *Org. Mass Spectrom.*, *15*, *383*, *(1980)*.

66. G. Hvistendahl and D.H. Williams, *J. Am. Chem. Soc.*, *97*, *3097*, *(1975)*.

67. P. Wolkoff, J.L. Holmes and F.P. Lossing, *Org. Mass Spectrom.*, *20*, *14*, *(1985)*.

68. J.L. Holmes, P.C. Burgers and J.K. Terlouw, *Org. Mass Spectrom.*, *15*, *140*, *(1980)*.

69. F.W. McLafferty, P.F. Bente III, R. Kornfeld, S.C. Tsai and I. Howe, *J. Amer. Chem. Soc.*, *95*, *2120*, *(1973)*.

70. F.W. McLafferty, R. Kornfeld, W.F. Haddon, K. Levsen, I. Sakai, P.F. Bente III, S.C. Tsai and H.D.R. Schuddemage, *J. Amer. Chem. Soc.*, *95*, *3886*, *(1973)*.

71. P.C. Burgers, J.L. Holmes and J.K. Terlouw, *Org. Mass Spectrom.*, *20*, *202*, *(1985)*.

72. J.K. Terlouw, W. Heerma and G. Dijkstra, *Org. Mass Spectrom.*, *16*, *326*, *(1981)*.

73. M.C. Blanchette, J.L. Holmes and F.P. Lossing, *J. Am. Chem. Soc.*, *109*, *1392*, *(1987)*.

74. F.W. McLafferty, A. Hirota, M.P. Barbalas and R.F. Pegues, *Int. J. Mass Spectrom. Ion Phys.*, *35*, *299*, *(1980)*.

75. P.C. Burgers, J.L. Holmes and J.E. Szulejko, *Int. J. Mass Spectrom. Ion Proc.*, *57*, *159*, *(1984)*.

76. F.W. McLafferty and J. Winkler, *J. Am. Chem. Soc.*, *96*, *5182*, *(1974)*.

77. J.L. Holmes, J.K. Terlouw, P.C. Burgers and R.T.B. Rye, *Org. Mass Spectrom.*, *15*, *149*, *(1980)*.

78. K. Levsen, "Fundamental Aspects of Organic Mass Spectrometry" Ed. H. Budzikiewicz in "Progress in Mass Spectrometry" Vol. IV, Verlag Chemie, New York, (1978).

79. J.K. Terlouw, W. Heerma, G. Dijkstra, J.L. Holmes and P.C. Burgers, *Int. J. Mass Spectrom. Ion Phys.*, *47*, *147*, *(1983)*.

80. C. Wesdemiotis, R. Feng, P.O. Danis, E.R. Williams and F.W. McLafferty, *J. Amer.Chem. Soc.*, *108*, *5847*, *(1986)*.

81. J. Vajda, A.G. Harrison, A. Hirota and F.W. McLafferty, *J. Amer.Chem. Soc.*, *103*, *38*, *(1981)*.

82. C. Wesdemiotis, R. Csencsits and F.W. McLafferty, *Org. Mass Spectrom.*, *20*, *98*, *(1985)*.

83. R.E. Johnson and J.W. Boring in R.G. Cooks, Ed., "Collision Spectroscopy", Plenum Press, New York, (1978).

84. J.A. Laramee, D. Cameron and R.G. Cooks, *J. Amer. Chem. Soc.*, *103*, *12*, *(1981)*.

85. B.F. Yates, W.J. Bouma and L. Radom, *J. Amer. Chem. Soc.*, *106*, *5805*, *(1984)*.

86. B.F. Yates, W.J. Bouma and L. Radom, *J. Am. Chem. Soc., (in press), (1987)*.

87. C.E.C.A. Hop, J. Bordas-Nagy, J.L. Holmes and J.K. Terlouw, *J. Am. Chem. Soc. (submitted)*

88. P.C. Burgers, J.L. Holmes, J.E. Szulejko, A.A. Mommers and J.K. Terlouw, *Org. Mass Spectrom.*, *18*, *254*, *(1983)*.

89. R.H. Nobes, W.J. Bouma and L. Radom, *J. Am. Chem. Soc.*, *105*, *309*, *(1983)*.

90a. W.J. Bouma, J.K. MacLeod and L. Radom, *J. Am. Chem. Soc.*, *104*, *2930*, *(1982)*. b. J.L. Holmes, F.P. Lossing, J.K. Terlouw and P.C. Burgers, *Ibid.*, *104*, *2931*, *(1982)*.

91. W.J. Bouma, R.H. Nobes and L. Radom, *J. Am. Chem. Soc.*, *105*, *1743*, *(1983)*.

92. R. Postma, P.J.A. Ruttink, B. van Baar, J.K. Terlouw, J.L. Holmes and P.C. Burgers, *Chem. Phys. Lett.*, *123*, *409*, *(1986)*.

93. R. Postma, P.J.A. Ruttink, F.B. van Duijneveldt, J.K. Terlouw and J.L. Holmes, *Can. J. Chem.*, *63*, *2798*, *(1985)*.

94. M.C. Blanchette, J.L. Holmes, C.E.C.A. Hop, F.P. Lossing, R. Postma, P.J.A. Ruttink and J.K. Terlouw, *J. Am. Chem. Soc.*, *108*, *7589*, *(1986)*.

95. P.C. Burgers, J.L. Holmes and A.A. Mommers, *Int. J. Mass Spectrom. Ion Proc.*, *54*, *283*, *(1983)*.

96. S. Petitjean, D. Dehareng, M.Th. Praet and J.C. Lorquet, *Adv. Mass Spectrom.*, *1129*, *(1986)*.

97. A. Cornu and R. Massot, "Compilation of Mass Spectral Data" Heyden & Sons, London, (1966).

98. M.M. Bursey, D.J. Harvan, C.E. Parker, L.G. Pedersen and J.R. Hass, *J. Am. Chem. Soc.*, *101*, *5489*, *(1979)*.

99. P.R. Briggs and T.W. Shannon, *J. Am. Chem. Soc.*, *91*, *4307, (1969).*

100. M.T. Reetz and W.F. Maier, *Theor. Chim. Acta*, *35*, *167, (1974).*

101. W.F. Maier and M.T. Reetz, *J. Am. Chem. Soc.*, *96*, *3687, (1975).*

102. D. van Raalte and A.G. Harrison, *Can. J. Chem.*, *41*, *2054, (1963).*

103. GAMESS was originally derived by M. Dupuis et. al. and modified by M.F. Guest, J. Kendrick and S. Pope.

104. C.C.J. Roothaan, *Rev. Mod. Phys.*, *23*, *69, (1951).*

105. J.S. Binkley, J.A. Pople and P.A. Dobosh, *Mol. Phys.*, *28*, *1423, (1974).*

106a W.J. Hehre, R.F. Stewart and J.A. Pople, *J. Chem. Phys.*, *51*, *2657, (1969).* b. R. Ditchfield, W.J. Hehre and J.A. Pople, *J. Chem. Phys.*, *54*, *724, (1971).* c. P.C. Hariharan and J.A. Pople, *Chem. Phys. Lett.*, *16*, *217, (1972).*

107. W.J. Bouma, P.M.W. Gill and L. Radom, *Org. Mass Spectrom.*, *19*, *610, (1984).*

108. B.P. Roos, P.R. Taylor and P.E.M. Siegbahn, *Chem. Phys.*, *48*, *157, (1980).*

109. J.K. Terlouw, W. Heerma and J.L. Holmes, *Org. Mass Spectrom.*, *16*, *306, (1981).*

110. $\Delta H_f°[ICH_2COOH]$ estimated by adding 82±4 kJ mol^{-1} to $\Delta H_f°[CH_3COOH]$=-432 kJ mol^{-1}. From Benson's additivity scheme (38) the effect of $-CH_3$ to $-CH_2I$ $=^{+}76$ kJ mol^{-1};the difference in the $\Delta H_f°$ for $[CH_3COOH]$ and $[CH_3COCH_2I]$ =87 kJ mol^{-1}, mean difference =82±4 kJ mol^{-1}.

111. J.C. Traeger, R.G. McLoughlin and A.J.C. Nicholson, *J. Am. Chem. Soc.*, *104*, *5318, (1982).*

112. J.L. Holmes, F.P. Lossing and P.C. Burgers, *Int. J. Mass Spectrom. Ion Phys.*, *47*, *133, (1983).*

113. M. Meot-Ner (Mautner), M.M. Ross and J.E. Campana, *J. Am. Chem. Soc.*, *107*, *4839, (1985).*

114. R. Postma, P.J.A. Ruttink, J.K. Terlouw and J.L. Holmes, in preparation.

115. R. Postma, P.J.A. Ruttink, J.K. Terlouw and J.L. Holmes, *J. Chem. Soc., Chem. Commun.*, *683, (1986).*

116. E.W. Godbole and P. Kebarle, *Trans. Faraday Soc.*, *58*, *1897, (1962).*

117. D.F. McMillen and D.M.Golden, *Ann. Rev. Phys. Chem.*, *33*, *493, (1982).*

118. W.J. Bouma, R.H. Nobes and L. Radom, *J. Amer. Chem. Soc.*, *104*, *2929, (1982)*

119. a. B.F. Yates, W.J. Bouma and L. Radom, *J. Amer. Chem. Soc.*, *106*, *5805, (1984)* b. L. Radom, W.J. Bouma, R.H. Nobes and B.F. Yates, *Pure & Appl. Chem.*, *56*, *1831, (1984)*

120. B.F. Yates, W.J. Bouma and L. Radom, *J. Am. Chem. Soc.*, *109*, *(in press)*, *(1987)*.

121. F. Maquin, D. Stahl, A. Sawaryn, P.von R. Schleyer, W. Koch, G. Frenking and H. Schwarz, *J. Chem. Soc., Chem. Commun.*, *504*, *(1984)*

122. B.F. Yates, W.J. Bouma and L. Radom, *J. Am. Chem. Soc.*, *108*, *6545*, *(1986)*

123. S. Hammerum, *Mass Spec. Rev.*, *(in press)*, *(1987)*

124. H. Halim, B. Ciommer and H. Schwarz, *Angew. Chem. Int. Ed. Engl.*, *21*, *528*, *(1982)*

125. J.L. Holmes, F.P. Lossing, J.K. Terlouw and P.C. Burgers, *Can. J. Chem.*, *61*, *2305*, *(1983)*

126. D.A. Dixon, T.H. Dunning, Jr., R.A. Eades and P.G. Gassman, *J. Am. Chem. Soc.*, *105*, *7011*, *(1983)*

127. Y. Apeloig, B. Ciommer, G. Frenking, M. Karni, A. Mandelbaum, H. Schwarz and A. Weisz, *J. Am. Chem. Soc.*, *105*, *2186*, *(1983)*

128. A. Lorenzi-Riatsch, N. Bild and M. Hesse, *Helv. Chim. Acta*, *64*, *1563*, *(1981)*

129. B. Ciommer, G. Frenking and H. Schwarz, *Int. J. Mass Spectrom. Ion Proc.*, *57*, *135*, *(1984)*

130. T. Clark and M.C.R. Symons, *J. Chem. Soc., Chem. Commun.*, *96*, *(1986)*

131. G. Frenking and H. Schwarz, *Croatica Chem. Acta*, *56*, *185*, *(1983)*

132. B.F. Yates, W.J. Bouma and L. Radom, *Tetrahedron*, *22*, *6225*, *(1986)*

133 a. G.A. Olah, Y. Yamada and R.J. Spear, *J. Am. Chem. Soc.*, *97*, *680*, *(1975)*
b. G.A. Olah, H. Doggweiler and J.D. Felberg, *J. Am. Chem. Soc.*, *107*, *4975*, *(1985)*

134. T. Yamazaki, S. Katsumata and K. Kimura, *J. Electron Spectrosc. Relat. Phenom.*, *2*, *335*, *(1973)*

135. S.S. Chen, A.S.Rogers, J. Chao, R.S. Wilhoit and B.J. Zwolinski, *J. Phys. Chem. Ref. Data*, *4*, *441*, *(1975)*

136. P. Sauvageau, J. Doucet, R. Gilbert and C. Sandorfy, *J. Chem. Phys.*, *61*, *391*, *(1974)*

137. V.P. Kolesov and T.S. Papina, Russ. *J. Phys. Chem.*, *(Engl. Transl.)*, *44*, *611*, *(1970)*

138. J.B. Pedley, R.D. Naylor and S.P. Kirby, Thermochem. Data of Org. Compds, 2nd Ed., (1986)

139. $\Delta H_f°[CH_2Cl]$=-81 kJ mol^{-1}, AE of CH_2Cl^+=12.96±0.05eV, with $\Delta H_f°[H\cdot]$=218 kJ mol^{-1}, $\Delta H_f°[CH_2Cl^+]$ is calculated to be 950 kJ mol^{-1}

140. From $\Delta H_f°[CH_2^+]$=344 kcal mol^{-1}, extrapolation for the heat of formation of the methyl substituted species $[CH_3\text{-}CH]^+$ via the technique and graph in Reference 55, J.L. Holmes, F.P. Lossing, *Can. J. Chem.*, *60*, *2365*, *(1982)*.

141. $H_f°[CH_2Br]$=-35 kJ mol^{-1}, AE of CH_2Br^+=12.98±0.05eV, with $\Delta H_f°[H\cdot]$=218 kJ mol^{-1}, $\Delta H_f°[CH_2Br^+]$=999 kJ mol^{-1}. Also, $\Delta H_f°[CH_2Br_2]$=-4 kJ mol^{-1}, AE for CH_2Br^+=11.31±0.05ev, giving a value of $\Delta H_f°[CH_2Br^+]$=975 kJ mol^{-1}. The average of these values, 987 kJ mol^{-1} is used.

142. M.J.S. Dewar and W. Thiel, *J. Am. Chem. Soc.*, *99*, *4899*, *& 4907*, *(1977)*

143. P.J. Derrick and S. Hammerum, *Can. J. Chem.*, *64*, *33*, *(1986)*.

144. A. Maccoll, *Chem. Rev.*, *69*, *33*, *(1969)*.

145. J.L Holmes and F.P. Lossing, *Int. J. Mass Spectrom. Ion Proc.*, *58*, *113*, *(1984)*.

146. C.E.C.A. Hop, J. Bordas-Nagy, J.L. Holmes J.K. Terlouw, *J. Am. Chem. Soc.*, *109*, *(in press)*, *(1987)*

147. R. Weber, K. Levsen, P.C. Burgers and J.K. Terlouw, *Org. Mass Spectrom.*, *16*, *514*, *(1981)*.

UNIVERSITÉ D'OTTAWA
UNIVERSITY OF OTTAWA